(12) INTERNATIONAL APPLICATION PUBLISHED UNDER THE PATENT COOPERATION TREATY (PCT)

(19) World Intellectual Property Organization
International Bureau

(43) International Publication Date
17 July 2003 (17.07.2003)

PCT

(10) International Publication Number
WO 03/057258 A2

(51) International Patent Classification[7]: A61K 49/00

(21) International Application Number: PCT/CA03/00014

(22) International Filing Date: 10 January 2003 (10.01.2003)

(25) Filing Language: English

(26) Publication Language: English

(30) Priority Data:
60/346,894 11 January 2002 (11.01.2002) US

(71) Applicant *(for all designated States except US)*: **NATIONAL RESEARCH COUNCIL OF CANADA** [CA/CA]; 1200 Montreal Road, Building M-58, Room EG-12, Ottawa, Ontario K1A 0R6 (CA).

(72) Inventors; and
(75) Inventors/Applicants *(for US only)*: **NI, Feng** [CA/CA]; 4507 Maplewood, Pierrefonds, Québec H9A 1B2 (CA). **SU, Zhengding** [CA/CA]; 1445 Ouimet, Apt. 45, St. Laurent, Québec H4L 3R2 (CA). **XU, Ping** [CA/CA]; 4830 Queen Mary, Apt. 405, Montreal, Québec H3W 3G3 (CA). **TOLKATCHEV, Dmitri** [CA/CA]; 4891 Bourret, Apt. 306, Montreal, Québec H3W 1L2 (CA). **OSBORNE, Michael, J.** [GB/CA]; 4892 Saint-Urbain, Montreal, Québec H2T 2W2 (CA). **KOUTYCHENKO, Anatol** [CA/CA]; 3765 St. Kevin, Apt. 17, Montreal, Québec H3T 1H8 (CA).

(74) Agent: **OGILVY RENAULT**; Suite 1600, 1981 McGill College Avenue, Montreal, Québec H3A 2Y3 (CA).

(81) Designated States *(national)*: AE, AG, AL, AM, AT, AU, AZ, BA, BB, BG, BR, BY, BZ, CA, CH, CN, CO, CR, CU, CZ, DE, DK, DM, DZ, EC, EE, ES, FI, GB, GD, GE, GH, GM, HR, HU, ID, IL, IN, IS, JP, KE, KG, KP, KR, KZ, LC, LK, LR, LS, LT, LU, LV, MA, MD, MG, MK, MN, MW, MX, MZ, NO, NZ, OM, PH, PL, PT, RO, RU, SC, SD, SE, SG, SK, SL, TJ, TM, TN, TR, TT, TZ, UA, UG, US, UZ, VC, VN, YU, ZA, ZM, ZW.

(84) Designated States *(regional)*: ARIPO patent (GH, GM, KE, LS, MW, MZ, SD, SL, SZ, TZ, UG, ZM, ZW), Eurasian patent (AM, AZ, BY, KG, KZ, MD, RU, TJ, TM), European patent (AT, BE, BG, CH, CY, CZ, DE, DK, EE, ES, FI, FR, GB, GR, HU, IE, IT, LU, MC, NL, PT, SE, SI, SK, TR), OAPI patent (BF, BJ, CF, CG, CI, CM, GA, GN, GQ, GW, ML, MR, NE, SN, TD, TG).

**Published:**
— *without international search report and to be republished upon receipt of that report*

*For two-letter codes and other abbreviations, refer to the "Guidance Notes on Codes and Abbreviations" appearing at the beginning of each regular issue of the PCT Gazette.*

WO 03/057258 A2

(54) Title: QUANTITATIVE RANKING OF TRANSIENT LIGAND BINDING TO TARGET BIOMOLECULES BY USE OF NUCLEAR MAGNETIC RESONANCE

(57) Abstract: The present invention relates to a new use of NMR for quantitatively ranking transient ligand binding to target biomolecules. The present invention also relates to a new method to identify ligand site obeying two-state and more complex binding behavior in a transient complex of a ligand with a target molecule, still with the use of NMR. There is also provided an efficient method to quantitate fast dissociation rates of ligands containing at least one magnetic nuclei by performing NMR relaxation dispersion experiments at different protein concentrations, enabling the evaluation of populations and exchange rates, and extending the practical applicability of the NMR relaxation dispersion experiments.

# QUANTITATIVE RANKING OF TRANSIENT LIGAND BINDING TO TARGET BIOMOLECULES BY USE OF NUCLEAR MAGNETIC RESONANCE

## TECHNICAL FIELD

**[0001]** The present invention relates to a new use of NMR for quantitatively ranking transient ligand binding to target biomolecules.

## BACKGROUND OF THE INVENTION

**[0002]** The molecular nature of protein-ligand associations is a subject of tremendous interest in chemistry, biochemistry and pharmaceutical drug discovery research (Kuntz, I. D., Chen, K., Sharp, K. A., and Kollman, P. A. (1999) *Proc.Natl.Acad.Sci.U.S.A 96,* 9997-10002; and Brooijmans, N., Sharp, K. A., and Kuntz, I. D. (2002) *Proteins 48,* 645-653). Targeting enzymes and protein surfaces involved in molecular regulatory pathways by low-molecular-weight molecules leads to various means of maintaining human health and treating diseases. Thermodynamic analyses of complex formation, such as equilibrium binding experiments and enzyme inhibition assays, have provided valuable information regarding the molecular/atomic forces that dictate the structural stability of protein-ligand complexes (Kuntz, I. D., Chen, K., Sharp, K. A., and Kollman, P. A. (1999) *Proc.Natl.Acad.Sci.U.S.A 96,* 9997-10002; and Brooijmans, N., Sharp, K. A., and Kuntz, I. D. (2002) *Proteins 48,* 645-653). In general, however, it is still difficult if not impossible to explain quantitatively the exact correlations between molecular structures and the binding affinity of protein-ligand complexes (Kuntz, I. D., Chen, K., Sharp, K. A., and Kollman, P. A. (1999) *Proc.Natl.Acad.Sci.U.S.A 96,* 9997-10002). In most cases, the difficulties are related to the failure to account for even subtle molecular motions in the otherwise very exact dimensions of microscopic protein-ligand interactions captured by high-resolution molecular structures (Kuntz, I. D., Chen, K., Sharp, K. A., and Kollman, P. A. (1999) *Proc.Natl.Acad.Sci.U.S.A 96,* 9997-10002; and Nienaber, V. L., Mersinger, L. J., and Kettner, C. A. (1996) *Biochemistry 35,* 9690-9699; and Carlson, H. A. (2002) *Curr.Opin.Chem.Biol. 6,* 447-452). On top of all these, there is as yet

no clear understanding of the relationship between binding, kinetics and molecular structure of protein-ligand interactions (Van Regenmortel, M. H. (2001) *Cell Mol.Life Sci. 58,* 794-800; and Andersson, K., Choulier, L., Hamalainen, M. D., Van Regenmortel, M. H., Altschuh, D., and Malmqvist, M. (2001) *J.Mol.Recognit. 14,* 62-71; and Day, Y. S., Baird, C. L., Rich, R. L., and Myszka, D. G. (2002) *Protein Sci. 11,* 1017-1025). The significance of protein-ligand binding kinetics becomes particularly high *in vivo*, where transient complexes are formed and broken as a cause or in response to biomolecular regulatory mechanisms.

**[0003]** A number of techniques are already available for quantitating the kinetics of protein-protein and protein-ligand interactions, such as surface plasmon resonance (Van Regenmortel, M. H. (2001) *Cell Mol.Life Sci. 58,* 794-800; and Wilson, W. D. (2002) *Science 295,* 2103-2105) and analysis of the progress curves of enzyme inhibition by specific ligands (Pargellis, C. A., Morelock, M. M., Graham, E. T., Kinkade, P., Pav, S., Lubbe, K., Lamarre, D., and Anderson, P. C. (1994) *Biochemistry 33,* 12527-12534; and Day, Y. S., Baird, C. L., Rich, R. L., and Myszka, D. G. (2002) *Protein Sci. 11,* 1017-1025). All these methodologies are limited to the characterization of tight-binding or slow-dissociating protein-ligand complexes with lifetimes longer than at least several seconds (Van Regenmortel, M. H. (2001) *Cell Mol.Life Sci. 58,* 794-800; and Day, Y. S., Baird, C. L., Rich, R. L., and Myszka, D. G. (2002) *Protein Sci. 11,* 1017-1025). Another limitation of these methods is that they only provide a macroscopic description of binding kinetics, without details of the dynamic behavior of the interacting molecules at atomic resolution.

**[0004]** Short-lived or transient, but specific-binding, protein-ligand complexes represent a good starting point for the design of high affinity inhibitors or effectors (Wells, J. A. (1996) *Science 273,* 449-450; and Shuker, S. B., Hajduk, P. J., Meadows, R. P., and Fesik, S. W. (1996) *Science 274,* 1531-1534). These fast dissociating ligands are often derived from naturally occurring protein-protein interfaces (Song, J. and Ni, F. (1998) *Biochem.Cell Biol. 76,* 177-188) or discovered by screening against peptide and/or protein

libraries (Wells, J. A. (1996) *Science 273,* 449-450; and Mourez, M., Kane, R. S., Mogridge, J., Metallo, S., Deschatelets, P., Sellman, B. R., Whitesides, G. M., and Collier, R. J. (2001) *Nat.Biotechnol. 19,* 958-961). Even without affinity "maturation", these specific-binding ligands can be converted into bivalent and polyvalent molecules with a dramatic increase in affinity and decrease in the dissociation rates (Song, J. and Ni, F. (1998) *Biochem.Cell Biol. 76,* 177-188; and Mammen, M., Choi, S.-K., and Whitesides, G. M. (1998) *Angew.Chem.Int.Ed. 37,* 2754-2794; and Rao, J., Lahiri, J., Isaacs, L., Weis, R. M., and Whitesides, G. M. (1998) *Science 280,* 708-711; and Kramer, R. H. and Karpen, J. W. (1998) *Nature 395,* 710-713; and Kitov, P. I., Sadowska, J. M., Mulvey, G., Armstrong, G. D., Ling, H., Pannu, N. S., Read, R. J., and Bundle, D. R. (2000) *Nature 403,* 669-672; and Fan, E., Zhang, Z., Minke, W. E., Hou, Z., Verlinde, C. L. M. J., and Hol, W. G. J. (2000) *J.Am.Chem.Soc. 122,* 2663-2664; and Kiessling, L. L., Gestwicki, J. E., and Strong, L. E. (2000) *Curr.Opin.Chem.Biol. 4,* 696-703; and Mourez, M., Kane, R. S., Mogridge, J., Metallo, S., Deschatelets, P., Sellman, B. R., Whitesides, G. M., and Collier, R. J. (2001) *Nat.Biotechnol. 19,* 958-961).

**[0005]** Nuclear magnetic resonance (NMR) spectroscopy has been established as one of the most powerful tools for studying the kinetic processes in chemical systems. Fast chemical interconversions often lead to extensive broadening of the NMR signals, from which the underlining rate constants and energetic parameters can be derived (Sandstrom, J. (1982) *Dynamic NMR spectroscopy.* London: Academic Press; and Blackledge, M. J., Bruschweiler, R., Griesinger, C., Schmidt, J. M., Xu, P., and Ernst, R. R. (1993) *Biochemistry 32,* 10960-10974). In contrast, fast exchange processes in biological systems have very rarely been measured in the details needed for an adequate understanding of the underlying kinetic processes. The binding kinetics of large and transient enzyme-inhibitor and protein-ligand complexes were only estimated by use of NMR spectroscopy and other methods (Jardetzky, O. and Roberts, G. C. K. (1981) *NMR in molecular biology.* New York: Academic Press; and Hammes, G. G. (1982) *Enzyme catalysis and regulation.* New York: Academic Press). Some earlier attempts

at quantitative measurements utilized mostly $^{19}F$ NMR, including spin-lock ($T_{1\rho}$), $T_1/T_2$ and $T_2$ (CPMG) relaxation experiments (Sykes, B. D. (1969) *J.Am.Chem.Soc. 91,* 949-955; and Smallcombe, S. H., Ault, B., and Richards, J. H. (1972) *J.Am.Chem.Soc. 94,* 4585-4590; and Gerig, J. T. and Stock, A. D. (1975) *Org.Magn.Res. 7,* 249-255; and Gerig, J. T., Halley, B. A., and Ortiz, C. E. (1977) *J.Am.Chem.Soc. 99,* 6219-6226; and Dubois, B. W. and Evers, A. S. (1992) *Biochemistry 31,* 7069-7076) and spectral lineshape analysis (Jacobson, A. R. and Gerig, J. T. (1991) *J.Biomol.NMR 1,* 131-144). More recent developments include combined analyses of proton $T_1$, $T_{1\rho}$, $T_2$ and $T_2$ (CPMG) relaxation data (Davis, D. G., Perlman, M. E., and London, R. E. (1994) *J.Magn Reson.B 104,* 266-275) or the use of $^{19}F$ cross-correlated relaxation measurements (Peng, J. W. (2001) *J.Magn Reson. 153,* 32-47) to help deconvolute the relaxation dispersion curves of the ligand molecules. The NMR $T_2$ (CPMG) relaxation measurements in particular appeared to be a promising technique for quantitating the binding kinetics of rapidly-dissociating protein-ligand complexes (Carver, J. P. and Richards, R. E. (1972) *J.Magn.Reson. 6,* 89-105; and Gerig, J. T. and Stock, A. D. (1975) *Org.Magn.Res. 7,* 249-255; and Gerig, J. T., Halley, B. A., and Ortiz, C. E. (1977) *J.Am.Chem.Soc. 99,* 6219-6226; and Dubois, B. W. and Evers, A. S. (1992) *Biochemistry 31,* 7069-7076; and Davis, D. G., Perlman, M. E., and London, R. E. (1994) *J.Magn Reson.B 104,* 266-275).

**[0006]** The kinetics of transient protein-ligand interactions has been investigated recently in a few cases, one for a small protein-peptide complex (Hensmann, M., Booker, G. W., Panayotou, G., Boyd, J., Linacre, J., Waterfield, M., and Campbell, I. D. (1994) *Protein Sci. 3,* 1020-1030; and Gunther, U., Mittag, T., Schaffhausen, and B. (2002) *Biochemistry 41,* 11658-11669), and some for enzyme-substrate/inhibitor interactions (Deng, H., Zhadin, N., and Callender, R. (2001) *Biochemistry 40,* 3767-3773; and Gulotta, M., Deng, H., Deng, H., Dyer, R. B., and Callender, R. H. (2002) *Biochemistry 41,* 3353-3363; and Hammes, G. G. (2002) *Biochemistry 41,* 8221-8228). The studied protein-peptide complex in particular involves binding of a small protein (MW~12 kDa) with a phosphotyrosine-containing

peptide with equilibrium dissociation constant in the 30-100 nM range (Hensmann, M., Booker, G. W., Panayotou, G., Boyd, J., Linacre, J., Waterfield, M., and Campbell, I. D. (1994) *Protein Sci. 3,* 1020-1030). To characterize binding kinetics of the protein-peptide complex, the protein was recombinantly expressed, enriched uniformly with the $^{15}N$ isotope, and the NMR peak shapes in response to peptide titrations were analyzed. As a practical alternative, it is particularly attractive to deconvolute the kinetic contributions to protein-ligand interactions by following the NMR spectroscopic and relaxation behaviors of the small ligand molecules. This approach expands the capability of quantitating dissociation kinetics to systems where the binding proteins and other biomolecules are large or not perfectly folded, and therefore are not normally or easily accessible to direct NMR observation. In addition, the target proteins do not have to be isotopically labeled and therefore can be purified from the natural sources or from a wide range of recombinant expression systems. Small ligand molecules require considerably less amount of time for NMR signal identification, and can be observed and resolved spectroscopically when mixed with other molecules with comparable molecular weights. The challenge here lies in the difficulty or impossibility to observe the bound states of the ligands due to the high molecular weight of the protein-ligand complex, such that conclusions may depend on the kinetic mechanism chosen to explain the experimental data.

## SUMMARY OF THE INVENTION

**[0007]** One aim of the present invention is to provide a new use of the dissociation rates ($k_{off}$) of protein-ligand complexes as a measure of the potency of ligand molecules binding transiently to target proteins and other biomolecules.

**[0008]** Another aim of the present invention is to provide an efficient method for quantitating the fast dissociation rates of transient protein-ligand complexes with lifetimes ranging from a few milliseconds to hundreds of microseconds.

**[0009]** In accordance with the present invention there is provided an efficient method to quantitate fast dissociation rates of ligands containing one or more, and preferably at least two, magnetic nuclei by performing NMR relaxation dispersion experiments at different protein concentrations, enabling the evaluation of populations and exchange rates, and extending the practical applicability of the NMR relaxation dispersion experiments.

**[0010]** Nuclear magnetic resonance (NMR)-based tools have been developed for quantitating the binding kinetics of transient protein-ligand complexes. More specifically, it is shown herein that implementation of NMR relaxation dispersion spectroscopy in accordance with the present invention can be used to determine the dissociation rate constants or binding off-rates of protein-peptide complexes in the absence of an accurate knowledge of the concentrations of either the peptide or the binding protein.

**[0011]** It was found and detailed herein that the problem of discriminating two-state from multistate binding processes can be resolved by performing NMR relaxation dispersion experiments of only ligand NMR signals at a number of concentrations of the binding protein.

**[0012]** In accordance with the present invention, there is therefore provided a method to identify two or more ligand molecules that can be linked together to create high-affinity molecules. Specifically, it is proposed herein that bivalent or polyvalent molecules with enhanced binding capacity can be constructed from ligand molecules that bind non-competitively or cooperatively. Non-competitivity or positive coooperativity is to be measured by an unchanged or a decreased dissociation rate constant, $k_{off}$, of one ligand in the presence of other ligand molecules.

**[0013]** In accordance with the present invention, there is therefore provided a method to identify binding hotspots of high-affinity ligand-target interactions through chemical fragmentation of the ligand molecule.

**[0014]** In accordance with the present invention, there is provided a method to identify a ligand site obeying a two-state or more complex binding

behavior in a transient complex of a ligand with a target molecule, said method comprising the steps of:

a) preparing a ligand with at least one nucleus, and more preferably at least two nuclei, detectable by NMR;

b) collecting CPMG NMR relaxation dispersion profiles for free ligand at two or more magnetic fields;

c) determining apparent transverse relaxation rates for the nuclei detectable by NMR at two or more magnetic fields;

d) assigning resonance peaks to the specific NMR detectable nuclei of the ligand with one- and/or multi-dimensional NMR;

e) contacting the ligand with at least one, preferably at least two, and more preferably three concentrations of a target molecule;

f) collecting CPMG NMR relaxation dispersion profiles for the ligand with every concentration of the target molecule at two or more magnetic fields;

g) fitting the NMR relaxation dispersion profiles by a two-state exchange model independently for every nucleus, and independently or simultaneously for every concentration of the target molecule; and

h) determining a ligand site obeying a two-state binding behavior based on feasibility of extracted $R_{2b}$ and $p_b$ parameters or the quality of the fitting of step g).

**[0015]** In accordance with the present invention there is provided a method to determine quantitatively the dissociation rate constant ($k_{off}$) for a transient complex of a ligand with the target molecule comprising the steps of:

a) Identifying a ligand site obeying a two-state or more complex binding behavior in a transient complex of a ligand with a target molecule with the method as defined above; and

b) Extracting $k_{off}$ values for the ligand sites obeying two-site or more complex exchange mechanism, said $k_{off}$ values being a measure of the affinity of a transient complex of the ligand with the target molecule.

**[0016]** The ligand may be for example, without limitation a peptide, a $^{15}N$-enriched polypeptide, or a molecule binding to the target under study. The ligand may also be a mixture of any of the above

**[0017]** The target may be for example, without limitation a protein or a protein assembly.

**[0018]** In accordance with the present invention, there is provided the use of the method as defined above to determine amino acid residues with detectable NMR relaxation dispersion as a constituting binding hot-spot.

**[0019]** The method of the present invention may also be used to identify two or more ligands that can be linked together to create high-affinity molecules.

**[0020]** The method of the present invention may still be used to study high-affinity protein-protein interactions or slow-dissociating ligand-target complexes.

**[0021]** It is also proposed that structure-affinity relationships of protein-ligand complexes can be built using the dissociation rate constants alone instead of the commonly used binding equilibrium constants.

## BRIEF DESCRIPTION OF THE DRAWINGS

**[0022]** Fig. 1 illustrates a RF and field gradient pulse sequence for measuring the $^{15}N$ $R_2(1/\tau_{CPMG})$ dispersion profile with sensitivity enhancement and compensation of RF heating effects;

**[0023]** Fig. 2 illustrates a two-site and three-site exchange mechanisms for the interaction of N-acetyl-Hir(55-65) with human prothrombin;

**[0024]** Fig. 3 illustrates $^{15}N$ relaxation dispersion profiles for the residues Asp55 (■), Phe56 (x), Glu57 (●), Glu58 (□) and Ile59 (▲) of the free $^{15}N$-labeled N-acetyl-Hir(55-65) peptide at 298 K and 800 MHz;

**[0025]** Fig. 4 illustrates $^{15}N$ relaxation dispersion curves for the $^{15}N$-labeled peptide, N-acetyl-$^{*}D_{55}{}^{*}F{}^{*}E{}^{*}E{}^{*}IP_{60}EEYLQ_{65}$, in complex with human prothrombin;

**[0026]** Figs. 5A and 5B illustrate fits of $^{15}N$ relaxation dispersion curves for the peptide N-acetyl-Hir(55-65) in complex with human prothrombin to three-site exchange schemes in which eighteen curves were fitted simultaneously to experimental data using the "linear" (Fig. 5A) and the "full" (Fig. 5B) three-site exchange scheme shown in Fig. 2;

**[0027]** Fig. 6 illustrates the temperature dependence of the apparent $k_{off}$ values for residues $Phe_{56}$ (●), $Glu_{57}$ (■), $Glu_{58}$ (□), and $Ile_{59}$ (○) in the complex between the N-acetyl-Hir(55-65) peptide and human prothrombin;

**[0028]** Fig. 7 illustrates $^{15}N$ relaxation dispersion curves for the residues $Phe_{56}$ (◆), $Glu_{57}$ (ж), $Glu_{58}$ (○), $Ile_{59}$ (□), $Glu_{61}$ (△) and $Tyr_{63}$ (■) of the free uniformly $^{15}N$-labeled peptide Hir(54-65) at 288 K and 800 MHz;

**[0029]** Figs. 8A to 8F illustrate $^{15}N$ relaxation dispersion curves for selected amide nitrogen atoms of the uniformly $^{15}N$-labeled recombinant Hir(54-65) peptide in complex with human prothrombin at 288 K;

**[0030]** Figs. 9a to 9D illustrate $^{15}N$ relaxation dispersion data at 500 MHz (◇; $^{15}N$ frequency: 50.684 MHz) and 800 MHz (□; $^{15}N$ frequency: 81.076 MHz), and fitted profiles for selected amide nitrogen atoms of the $^{15}N$-labeled peptide, N-acetyl-Hir(55-65), in complex with human α-thrombin in 50 mM NaCl and 50 mM sodium phosphate at pH 5.5, and in the presence of 10% $D_2O$;

**[0031]** Figs. 10A and 10B illustrate [$^{1}$H-$^{15}$N]-HSQC spectra of a mixture of six uniformly $^{15}$N-labeled hexa/pentapeptides, GLDPRH$_L$, GVDPRH$_L$, GFNPRH$_L$, GPNPRH$_L$, GFSARH$_L$, GVSPR, where a one-letter code is used to define the amino acid sequence, and H$_L$ stands for homoserine lactone, in the absence (Fig. 10A), and presence (Fig. 10B) of the N-acetyl-Hir(55-65) peptide and human thrombin;

**[0032]** Figs. 11A and 11B illustrate $^{15}$N relaxation dispersion curves for the mixture of the N-acetyl-Hir(55-65) peptide with six uniformly $^{15}$N-labeled pentapeptides, GLDPR, GVDPR, GFNPR, GPNPR, GFSAR, and GVSPR, in complex with human thrombin;

**[0033]** Figs. 12A to 12H illustrate $^{15}$N relaxation dispersion curves for selected amide nitrogen atoms of the uniformly $^{15}$N-labeled FD22 thrombin-cleaved peptide in complex with human thrombin at a peptide concentration of ~0.9 mM in 60 mM sodium phosphate buffer, 0.2 mM EDTA, at pH 5.5, and at 288 K;

**[0034]** Figs. 13A and 13B illustrate titration experiments showing the effect of adding the mCRIB peptide to cCRIB in the presence of Cdc42;

**[0035]** Figs. 13C to 13F illustrate dispersion curves of the mCRIB peptides in the presence of (red) Cdc42and (black) Cdc42 and cognate cCRIB peptide;

**[0036]** Fig. 14 illustrates the CRIB containing peptides fragments used in Examples 5 and 7;

**[0037]** Figs. 15A and 15B illustrate [$^{1}$H-$^{15}$N] HSQC spectrum (Fig. 15A) and human prothrombin-induced $^{15}$N relaxation dispersion curves for the backbone $^{15}$N nuclei of residues Phe$_{56}$ (○), Glu$_{57}$ (▼), and Glu$_{58}$ (●) (Fig. 15B) of the peptide Hir(54-65) at 288 K;

**[0038]** Figs. 16A to 16D represent $^{15}$N relaxation dispersion curves for a mixture of mSte20 and mCla4 competing for the same binding site on Cdc42;

**[0039]** Figs. 17A to 17D illustrate perturbations of Cla4 and Ste20 peptide fragments ($^{15}$N-mCla4+Cdc42 [Fig. 17A], $^{15}$N-cCla4+Cdc42 [Fig. 17B], $^{15}$N-mSte20+Cdc42 [Fig. 17C], and $^{15}$N-cSte20+Cdc42 [Fig. 17D] by Cdc42;

**[0040]** Figs. 18A to 18D represent $^{15}$N relaxation dispersion curves for $^{15}$N-mCla4 free (red) and in complex with Cdc42 (ratio ~10:1)(black)(Figs. 18A and 18B) and best fit curves generated from simultaneous fits to data recorded at two magnetic field strengths (800 MHz and 500 MHz) on the mCla4-Cdc42 complex (Figs. 18C and 18D);

**[0041]** Figs. 19A to 19D represent $^{15}$N relaxation dispersion curves for $^{15}$N-mSte20 free (red) and in complex with Cdc42 (ratio ~10:1)(black)(Figs. 19A and 19B and best fit curves generated from simultaneous fits to data recorded at two magnetic field strengths (800 MHz and 500 MHz) on the mSte20:Cdc42 complex (Figs. 19C and 19D);

**[0042]** Fig. 20A illustrates the fragmentation of human cathepsin B propeptide producing the amino acid sequences of the wild-type full-length sequence (WT), methionine-introducing mutant (Mutant) and the CNBr-cleaved fragments (F1-F5) of the propeptide wherein $S^H$ indicates homoserine lactone; and

**[0043]** Figs. 20b and 20C illustrate the [$^1$H-$^{15}$N]-HSQC spectrum of the $^{15}$N-labeled recombinant propeptide with the wild-type amino acid sequence (Fig. 20B and of the F1-F5 peptide mixture (Fig. 20C).

## DETAILED DESCRIPTION OF THE PREFERRED EMBODIMENT

**[0044]** The following analysis of $^{15}$N NMR relaxation dispersion reveals that it is possible to determine the dissociation rate constant $k_{off}$ of protein-ligand complexes from the NMR relaxation dispersion curves obtained with two or more external magnetic fields and at one or more protein concentrations. More importantly, it is found that the accuracy of the ligand or protein concentrations is not critical for the data analysis, as only the increases in the protein/ligand ratio, measured by the volumes of the titrated protein solution,

need to be included in the data fitting process. In particular, it can be shown that if $[L_{free}] >> K_D$ and $[L_0] >> [E_0]$,

$$k_{on}'(\text{second}) = [(V_{stock}^1 + V_{stock}^2)/V_{stock}^1] \times k_{on}'(\text{first})$$

where $V_{stock}^1$ is the volume of the protein stock solution used in the first addition, $V_{stock}^2$ is the volume of the protein stock solution used in the second addition, etc. Any other method of titration allowing determination of the proportionality between the $k_{on}'$ values at different protein concentrations is also valid.

**[0045]** Simultaneous fitting of the dispersion curves obtained at multiple protein concentrations makes it possible to identify ligand moieties involving more complex exchange mechanisms (including one free and two or more bound states). The nuclei (or ligand moieties) following a two-state binding-dissociation mechanism behave similarly to each other and display reasonable physical parameters, such as $k_{off}$, $p_b$ (apparent fraction of the bound peptide), $R_{2b}(500)$, $R_{2b}(800)$(apparent $R_2$ relaxation rate of the peptide $^{15}N$ nuclei in the bound stateat either 500 or 800 MHz), and $\delta\omega_{bf}$ (frequency separation of a peptide $^{15}N$ signal in the free and bound states: $\delta\omega_b$-$\delta\omega_f$), allowing a more accurate determination of the dissociation rate constants through combined data fitting.

**[0046]** The data analysis procedure can be easily automated, including input of the relaxation dispersion data, model fitting, identification of the sites with two-state binding behavior and calculation of the $k_{off}$ values at multiple protein titrations. In practical implementations it should be kept in mind that the CPMG NMR relaxation dispersion experiments, including $^{15}N$ relaxation as illustrated here as well as NMR relaxation of other nuclei, such as $^{1}H$, $^{19}F$, $^{13}C$, $^{31}P$, etc., have a limited sensitivity to the time scales of the ligand dissociating process, i.e. from tens of milliseconds to hundreds of microseconds. As well, quantitative analysis using the proposed titration procedure without precise knowledge of the ligand and protein concentrations requires the large excess of the ligand over the binding protein and that the ligand concentration be

much larger than the dissociation constant of the protein complex (see Eqn 3). In some cases, faster ligand off-rates may be quantitated by the NMR $T_{1\rho}$ experiments (Mulder, F. A., van Tilborg, P. J., Kaptein, R., and Boelens, R. (1999) *J.Biomol.NMR 13,* 275-288; and Trott, O. and Palmer, A. G., III (2002) *J.Magn Reson. 154,* 157-160) and multiple quantum relaxations (Wang, C. and Palmer, A. G. (2002) *J.Biomol.NMR 24,* 263-268).

**[0047]** The new NMR techniques according to the present invention have now also been applied to a mixture of peptides either binding to distinct sites or competing for one site on a target protein (Figs. 11-16).

## Materials and Methods

### Protein preparation

**[0048]** Stock solutions of human prothrombin and thrombin were prepared as described previously (Carlisle, T. L., Bock, P. E., and Jackson, C. M. (1990) *J.Biol.Chem. 265,* 22044-22055; and Fenton, J. W., Fasco, M. J., and Stackrow, A. B. (1977) *J.Biol.Chem. 252,* 3587-3598; and Ni, F., Ning, Q., Jackson, C. M., and Fenton, J. W. (1993) *J.Biol.Chem. 268,* 16899-16902). Immediately before use, human thrombin was thawed on ice and concentrated to ~8 mg/ml using Centricon-10 concentrator (Amicon).

**[0049]** Recombinant Cdc42 (residues 1-178) from *Candida Albicans* (CaCdc42) was expressed as a $His_6$-tag protein in *Escherichia coli* BL21(DE3) (Novagen) using a pET15b-CaCdc42 expression plasmid engineered with a thrombin cleavage site. Uniform enrichment of CaCdc42 with $^{15}N$ and/or $^{13}C$ was achieved by growing the bacteria in minimal medium supplemented with $^{15}(NH_4)_2SO_4$ and/or $^{13}C_6$-glucose as the sole nitrogen and carbon sources. $His_6$-CaCdc42 was purified from bacterial lysate by absorption onto a Ni-NTA column (Qiagen) under native conditions (20 mM Tris-HCl, 500 mM NaCl and 2 mM $MgCl_2$ at pH 8.0, 15 mM immidazole) and eluted with a 30 mM to 300 mM immidazole gradient. Following buffer exchange into 20 mM Tris-HCl, 2 mM $MgCl_2$ at pH 8.0, the $His_6$-tag was removed with thrombin and the thrombin inhibitor PPACK added to halt the cleavage reaction. CaCdc42 was

obtained after application to a Q-Sepharose™ column and eluted with a 0 to 400 mM NaCl gradient. An activated form of Cdc42 was generated using the non-hydrolysable GTP analogue, β,γ-methyleneguanosine 5'-triphosphate, or GMPPCP (SIGMA). Due to the similar affinity of GDP and GMPPCP for Cdc42, alkaline phosphatase beads were used to degrade GDP as follows. The GDP-loaded form of CaCdc42 was exchanged into a buffer that was 20 mM in Tris, 2 mM $MgCl_2$, at pH 8.0. Ammonium sulfate was added to a final concentration of 0.2 M. Excess $Mg^{2+}$ was removed by adding 20 mM EDTA. GMPPCP was then added to a 10-fold molar excess of Cdc42 and the mixture added to alkaline phosphatase beads (~ 100 units) and shaken gently for 2 hours. The beads were then removed by low speed centrifugation and 25 mM $MgCl_2$ were added. NMR samples were obtained after exchange into a buffer containing 50 mM phosphate, 2 mM $MgCl_2$, 50 mM NaCl, pH 6.15 using a PD-10 column.

Peptide preparation

**[0050]** The peptide N-acetyl-$^{*}D_{55}{}^{*}F{}^{*}E{}^{*}E{}^{*}IP_{60}EEYLQ_{65}$ (N-acetyl-Hir(55-65)) was enriched selectively with $^{15}N$ isotopes at the amides of five residues $Asp_{55}$, $Phe_{56}$, $Glu_{57}$, $Glu_{58}$ and $Ile_{59}$ as described previously (Carpenter, K. A. and Ni, F. (1992) *J.Magn.Reson. 99,* 192-197). Dried powder of the purified peptide was weighed using a Sartorius Supermicro S4™ balance and dissolved at ~1.5 mM in an aqueous solution (10% $D_2O$) that was 50 mM in NaCl and 50 mM in sodium phosphate at pH 5.5. Carefully measured volume aliquots of human prothrombin at a stock concentration of 0.3 mM were added to the peptide solution to produce molar ratios of ~1:45, ~1:35, and ~1:30 for the prothrombin and peptide concentrations, respectively.

**[0051]** A small fusion sequence, termed SFC120, was used as the carrier protein to express all the $^{15}N$-labeled peptides used in this application. SFC120 was adopted for peptide production from the N-terminal oligonucleotide binding domain of *M. ribonuclease HL* which comprises 120 amino acid residues. The cDNA was amplified by standard PCR methods while the restriction enzyme site of *Nco I* was generated in the 5'-end and the

two restriction enzyme sites of *EcoR I* and *BamH I* were generated in the 3'-end. The PCR product was double-digested by *Nco I* and *BamH I* and ligated into the pET15M vector, which was modified from the pET-15b vector (Novagen) by removing the *EcoR I* site. The constructed fusion protein expression vector was termed as *pTSN-6A*.

**[0052]** The DNA fragments encoding the peptides were amplified from a cDNA library by PCR or synthesized as oligonucleotides using the codon preference of *E. coli*. The DNA fragments were digested with *EcoR I* and *BamH I*, and subcloned into the *pTSN-6A* vector. The expression constructs were transformed into the BL21(DE3) expression host and confirmed by DNA sequencing. A single methionine residue was inserted between the fusion protein and the desired peptide sequence to facilitate release of the peptides by CNBr cleavage. A His-tag with six histidines can be placed at the N-terminus of SFC120 to allow purification of the fusion protein by adsorption onto a Ni-NTA agarose column (QIAGEN). In the present case, the His-tagged SFC120 vector was used to express the peptide FD22 (see Examples 4 and 7). Non-His-tagged SFC120 was used to express the rest of the peptides.

**[0053]** Expression of the peptide fragments was achieved by transformation of the appropriate plasmid into *E. coli* BL21(DE3) competent cells. An overnight culture grown in 2YT containing 100 µg/ml ampicillin (25 ml) was used to inoculate 1 L of M9 minimal media (100 µg/ml ampicillin) supplemented with BME vitamins solution (10 ml/L of 100x stock – SIGMA). $^{15}$N-labeled peptides were expressed using $^{15}(NH_4)_2SO_4$ (2 g/L) as the sole nitrogen source. The cells were grown at 37°C to a cell density of $OD_{600}$ = 0.8 and induced by adding IPTG to a final concentration of 1 mM. The cells were incubated for 4-12 hours at 37°C and collected by centrifugation (8000*g* for 20 minutes).

**[0054]** Cell pellets were resuspended in 6 M urea in 20 mM Tris, 100 mM NaCl buffer, pH 8.0 for 4 hours and then sonicated for 45 seconds on ice. The solution was then centrifuged at 7 K rpm for 20 minutes. An equivolume of 100% cold ethanol was added to the supernatant and the solution allowed to

stand at 4°C for two hours. After centrifugation, another equivolume of cold ethanol was added to the supernatant and allowed to stand overnight. The solution was centrifuged at 8,500 rpm and the pellet containing the pure fusion-peptide fragment subjected to SDS-page analysis. If necessary the pellet was further resuspended in 6 M urea and applied to a Sep-Pak™ column (Waters) to remove any impurities. The fusion protein was then lyophilized.

**[0055]** An additional step of purification on a Ni-NTA agarose column for His-tagged fusion peptides was performed as follows. Cell pellets were resuspended in 6 M urea in Tris-HCL buffer at pH 8.0 by gentle shaking for ~4 hours and briefly sonicated on ice. After centrifugation at 7 K rpm for 20 minutes the supernatant was applied to a Ni-NTA agarose column (QIAGEN) previously equilibrated with the lysis buffer. The column was then washed with ~ 20 column volumes of 6 M urea in Tris buffer at pH 6.3 to eliminate non-specific binding to the column. The His-tagged fusion protein was then eluted with 6 M urea in 20 mM Tris buffer at pH 4.5. The solubilized fusion protein was then lyophilized to dryness.

**[0056]** CNBr cleavage was used to release the target peptide from the fusion protein as follows. The fusion protein was dissolved in 70% TFA, CNBr added to a final molar ratio of 100:1 and the solution allowed to stand for ~ 24 hours. The samples were then diluted with water (x10) and lyophilized to dryness and purified by RP-HPLC on a C18 column using an acetonitrile-water gradient containing 0.1% TFA. The peptides were lyophilized and there identity was confirmed by electrospray mass spectrometry. Free peptides were prepared for NMR analysis by resuspending the lyophilized peptides into the appropriate NMR buffer solution.

**[0057]** The mixture of the fragments F1, F2, F3, F4, and F5 of human cathepsin B were prepared as follows. The fusion protein was purified by GST affinity chromatography followed by the proteolytic removal of the carrier protein using thrombin as the cleavage enzyme. The intact mutant propeptide was further purified by HPLC and cleaved by CNBr in the solution of 50%

formic acid for 24 hours at room temperature. The peptide mixture was desalted either by dialysis or by a Sep-Pak™ reversed-phase $C_{18}$ column. The peptide mixture was then lyophilized and dissolved in 50 mM sodium acetate-$d_3$ buffer, pH 5.5-6.0.

**[0058]** Titration of the thrombin-cleaved FD22 peptide was carried out as follows. The sample of FD22 was concentrated by Speed-Vac to 40 µl and 180 µl of a concentrated thrombin solution were added to give a final thrombin:peptide ratio of approximately ~1:20 in 60 mM sodium phosphate buffer, 0.2 mM EDTA, 10% $D_2O$, at pH 5.5. Additional steps of thrombin titrations were carried out by the addition of the human □-thrombin concentrated to ~8 mg/ml.

NMR Signal Assignments of the $^{15}N$-labeled Peptides

**[0059]** Proton resonance assignment for the N-acetyl-Hir(55-65) peptide was achieved by using 2D NOESY-[$^1H$,$^{15}N$]-HSQC with an NOE mixing time of 250 ms and 2D TOCSY-[$^1H$,$^{15}N$]-HSQC with a TOCSY mixing time of 56.6 ms (Cavanagh, J., Fairbrother, W. J., Palmer, A. G., and Skelton, N. J. (1995) Protein NMR Spectroscopy: Principles and Practice. Academic Press, San Diego) spectra recorded at 288 K and 500 MHz. Amino acid residues were identified on the basis of the cross-peak patterns from the TOCSY spectrum, and assigned through sequential NOE connectivities. $^{15}N$ resonances were assigned using a [$^1H$-$^{15}N$] HSQC (Cavanagh, J., Fairbrother, W. J., Palmer, A. G., and Skelton, N. J. (1995) Protein NMR Spectroscopy: Principles and Practice. Academic Press, San Diego) spectrum acquired at 288 K and 500 MHz.

**[0060]** Proton resonance assignment for the recombinantly expressed $^{15}N$-labeled Hir(54-65) peptide was achieved by using 2D NOESY-[$^1H$,$^{15}N$]-HSQC with an NOE mixing time of 250 ms and 2D TOCSY-[$^1H$,$^{15}N$]-HSQC with a TOCSY mixing time of 60.48 ms spectra recorded at 288 K and 800 MHz. Amino acid residues were identified on the basis of the cross-peak patterns from the TOCSY spectrum, and assigned through sequential NOE

connectivities. $^{15}N$ resonances were assigned by using a 2D [$^{1}H$,$^{15}N$]-HSQC-TOCSY spectrum with a TOCSY mixing time of 55.76 ms (Cavanagh, J., Fairbrother, W. J., Palmer, A. G., and Skelton, N. J. (1995) Protein NMR Spectroscopy: Principles and Practice. Academic Press, San Diego) acquired at 288 K and 800 MHz.

**[0061]** Resonances of the thrombin-cleaved $^{15}N$-labeled FD22 peptide were assigned by use of two homonuclear experiments, NOESY with an NOE mixing time of 250 ms and TOCSY with a TOCSY mixing time of 58.32 ms, were recorded at 288 K and 500 MHz. In both experiments, $^{15}N$ decoupling was applied during the t1 and t2 periods, and the water resonance was flipped-back to the +Z axis prior to data acquisition (Lippens, G., Dhalluin, C., and Wieruszeski, J.-M. (1995) J.Biomol.NMR 5, 327-331; and Fulton, D. B., Hrabal, R., and Ni, F. (1996) J.Biomol.NMR 8, 213-218; and Fulton, D. B. and Ni, F. (1997) J.Magn Reson. 129, 93-97). Amino acid residues were identified on the basis of the cross-peak patterns from the TOCSY spectrum, and assigned through sequential NOE connectivities. $^{15}N$ resonances were assigned by using 2D [$^{1}H$,$^{15}N$]-HSQC-TOCSY with a TOCSY mixing time of 55.44 ms acquired at 288 K and 800 MHz.

**[0062]** Assignments for the $^{15}N$ labeled CRIB peptides were obtained in a sequential manner from homonuclear $^{1}H$-$^{1}H$ 2D and 3D $^{15}N$-edited TOCSY and NOESY spectra.

<u>Measurements of the $^{15}N$ NMR Relaxation Dispersion Profiles</u>

**[0063]** The sample temperatures were calibrated using methanol (Cavanagh, J., Fairbrother, W. J., Palmer, A. G., and Skelton, N. J. (1995) *Protein NMR Spectroscopy: Principles and Practice.* Academic Press, San Diego). The core of the NMR relaxation dispersion measurements is the relaxation-compensated CPMG pulse scheme (Fig. 1) (Millet, O., Loria, J. P., Kroenke, C. D., Pons, M., and Palmer, A. G. (2000) *J.Am.Chem.Soc. 122,* 2867-2877; and Loria, J. P., Rance, M., and Palmer, A. G. (1999) *J.Am.Chem.Soc. 121,* 2331-2332). A train of $^{15}N$ 180° pulses with a separation of 1 ms is applied at

100 ppm off the center of the HSQC spectrum at the beginning of the recycle delay $d_1$ such that the total number of $^{15}N$ 180° pulses, 4N, is kept the same for all experiments with different CPMG pulse repetition rates. An XY-16 180° pulse train (Gullion, T., Baker, D. B., and Conradi, M. S. (1990) *J.Magn.Reson. 89,* 479-484) is also applied to both the $^{1}H$ and $^{15}N$ nuclei during the two INEPT periods, which limits the decay of exchange-broadened ligand resonances. Further enhancement in sensitivity was achieved by using the 3919 WATERGATE sequence for water suppression (Piotto, M., Saudek, V., and Sklenar, V. (1992) *J.Biomol.NMR 2,* 661-665). The 90° and 180° RF pulses are represented by narrow and wide bars, respectively, applied along the +X axis unless specified otherwise. The open rectangles are water-selective soft pulses with duration of 2 ms. During data acquisition, $^{15}N$ decoupling is achieved using a GARP sequence (Shaka, A. J., Barker, P. B., and Freeman, R. (1985) *J.Magn.Reson. 64,* 547-552) with an RF field of 1.0 kHz (at 500 MHz) or 1.2 kHz (at 800 MHz). The delays are: $\Delta$ = 2.7 ms, $\tau$ = 1 ms, $d_2 = d_1-4(N-n)\tau$ and $\tau_{CPMG} = (T/4n - pw180_N)$, where T is the total duration of the $^{15}N$ CPMG pulse train and $pw180_N$ is the width of the $^{15}N$ 180° pulse. Sinebell-shaped gradient pulses with a duration of 1 ms are used with gradient strengths of $g_1$=5G/cm, $g_2$=-6G/cm, $g_3$=1.2G/cm, $g_4$=6G/cm, and $g_5$=10G/cm. The phases of some RF pulses are the same as those reported previously with $\phi1$ = +X –X, $\phi2$= 4(+X) 4(-X) and $\phi3$= 2(+X) 2(+Y) 2(-X) 2(-Y) (Millet, O., Loria, J. P., Kroenke, C. D., Pons, M., and Palmer, A. G. (2000) *J.Am.Chem.Soc. 122,* 2867-2877), except that the phases for the last $^{15}N$ 90° pulse, the WATERGATE sequence and the RF receiver are cycled as $\phi4$= 4(+X) 4(-X), $\phi5$=8(+X) 8(+Y), $\phi6$=8(-X) 8(-Y) and receiver=(+X –X –X +X) 2(–X +X +X –X) (+X –X –X +X). Phase-sensitive $^{1}H$-$^{15}N$ HSQC spectra were obtained by incrementing $\phi4$, according to the States-TPPI scheme (Marion, D., Ikura, M., Tschudin, R., and Bax, A. (1989) *J.Magn.Reson. 85,* 393-). The relaxation dispersion profile is derived from the spectral peak intensities at different effective $B_1$ fields (Blackledge, M. J., Bruschweiler, R., Griesinger, C., Schmidt, J. M., Xu, P., and Ernst, R. R. (1993) *Biochemistry 32,* 10960-10974), expressed by the equation $R_2(1/\tau_{CPMG}) = -\ln[I(1/\tau_{CPMG})/I(0)]/T$ (Mulder,

F. A. A., Skrynnikov, N. R., Hon, B., Dahlquist, F. W., and Kay, L. E. (2001) *J.Am.Chem.Soc. 123,* 967-975), where $I(1/\tau_{CPMG})$ is the intensity of an HSQC peak with varying n, hence the $\tau_{CPMG}$ delay, and I(0) is the intensity of the same HSQC peak in the absence of the $^{15}N$ CPMG pulse trains (i.e. n=0 in periods a-b and c-d). NMR data were collected at $^{15}N$ frequencies of 50.684 and 81.076 MHz using Bruker Avance/DRX 500 and 800 MHz NMR spectrometers. The total length of the $^{15}N$ CPMG pulse train, T (Fig. 1), is kept at a constant value of 40 ms and the total number (4N) of the $^{15}N$ CPMG 180° pulses was set to 100.

Fitting of the NMR Relaxation Dispersion Profiles and Derivation of the Dissociation Rate Constants $k_{off}$

**[0064]** Under the experimental conditions, the NMR magnetization ***M*** in the rotating frame was assumed to evolve between the 180° refocusing pulses according to the following equations:

$$d\boldsymbol{M}/dt=(\boldsymbol{R}+\boldsymbol{R}_{EX})\boldsymbol{M}; \quad (1)$$

where $$\boldsymbol{R} = \begin{bmatrix} -R_{2b}-i\delta\omega_b & 0 \\ 0 & -R_{2f}-i\delta\omega_f \end{bmatrix}; \quad (1a)$$

$$\boldsymbol{R}_{EX} = \begin{bmatrix} -k_{off} & k_{on}' \\ k_{off} & -k_{on}' \end{bmatrix};$$

(1b)

for a two-state exchange model, and

$$\boldsymbol{R} = \begin{pmatrix} -R_{2b}-i\delta\omega_{b2} & 0 & 0 \\ 0 & -R_{2b}-i\delta\omega_{b1} & 0 \\ 0 & 0 & -R_{2f}-i\delta\omega_{f} \end{pmatrix}; \qquad (1c)$$

$$\boldsymbol{R}_{EX} = \begin{pmatrix} -k_1-k_{off}^{2} & k_2 & k_{on}'^{2} \\ k_1 & -k_2-k_{off}^{1} & k_{on}'^{1} \\ k_{off}^{2} & k_{off}^{1} & -k_{on}'^{1}-k_{on}'^{2} \end{pmatrix}; \qquad (1d)$$

for a three-state exchange model (Jen, J. (1978) *J.Magn Reson. 30,* 111-128).

**[0065]** The notation for the exchange rate constants is shown in Fig. 2. In Fig. 2, addition of an extra bound state to the two-state exchange model (pathway A) produces a "full" three-site exchange model (pathway B) with two additional exchange pathways. "Full" three-site exchange scheme turns into "linear" (pathway C) and "forked" (pathway D), if the corresponding absent exchange pathways are too slow to be sensed by NMR. In the cases of "linear" (pathway C) or "forked" (pathway D) three-state exchange schemes, rate constants between non-exchanging species ($k_{on}'^{2}$, $k_{off}^{2}$ or $k_1$, $k_2$, respectively) were set to zero. $R_{2b}$ and $R_{2f}$ are the intrinsic transverse relaxation rates for the peptide $^{15}N$ nuclei in the bound and free states, respectively. The transverse relaxation rates for the bound peptide in the two possible complexes were assumed to be equal. Variables $\delta\omega_b$, $\delta\omega_{b2}$ and $\delta\omega_{b1}$ are the resonance frequency offsets ($\omega$-$\omega_0$) for the corresponding bound states, $\delta\omega_f$ is the resonance frequency offset for the free peptide, and $\omega_0$ is the angular frequency of the CPMG RF pulse train.

**[0066]** The two-state exchange model can be fit to the experimental relaxation dispersion curves by use of a single exponential approximation, which is valid for all exchange conditions when the concentration of the free ligand is in large excess over that of the bound states (Carver, J. P. and Richards, R. E. (1972) *J.Magn.Reson. 6,* 89-105; and Jen, J. (1978) *J.Magn Reson. 30,* 111-128; and Davis, D. G., Perlman, M. E., and London, R. E. (1994) *J.Magn*

*Reson.B 104,* 266-275; and Ni, F. (1994) *Progress in NMR spectroscopy 26,* 517-606). In this case the following equations relate the NMR relaxation dispersion profiles to the underlying physical parameters (Carver, J. P. and Richards, R. E. (1972) *J.Magn.Reson. 6,* 89-105; and Jen, J. (1978) *J.Magn Reson. 30,* 111-128; and Davis, D. G., Perlman, M. E., and London, R. E. (1994) *J.Magn Reson.B 104,* 266-275),

$$R_2^{eff}=-\ln[I(1/\tau_{CPMG})/I(0)]/T=(R_{2f}+R_{2b}+k_{off}+k_{on}')/2-(1/\tau_{CPMG})\ln\lambda+ \quad (2)$$

where

$$\ln\lambda+=1/2\cosh^{-1}[D_+\cosh 2\xi-D_-\cos 2\eta]; \quad (2a)$$

$$D_\pm=1/2[\pm 1+(\psi+2\delta\omega_{bf}^2)/(\psi^2+\zeta^2)^{1/2}]; \quad (2b)$$

$$\xi=(\tau_{CPMG}/\sqrt{8})[+\psi+(\psi^2+\zeta^2)^{1/2}]^{1/2}; \quad (2c)$$

$$\eta=(\tau_{CPMG}/\sqrt{8})[-\psi+(\psi^2+\zeta^2)^{1/2}]^{1/2}; \quad (2d)$$

$$\psi=(R_{2f}-R_{2b}+k_{on}'-k_{off})^2-\delta\omega_{bf}^2+4k_{on}'k_{off} \quad (2e)$$

$$\zeta=2\delta\omega_{bf}(R_{2f}-R_{2b}+k_{on}'-k_{off}) \quad (2f)$$

$$\delta\omega_{bf}=\delta\omega_b-\delta\omega_f. \quad (2g)$$

**[0067]** For three-site exchange situation, the magnetization evolution can be obtained by numeric integration of the equations (1) and fit to the experimental NMR relaxation data (Jen, J. (1978) *J.Magn Reson. 30,* 111-128; and Tollinger, M., Skrynnikov, N. R., Mulder, F. A., Forman-Kay, J. D., and Kay, L. E. (2001) *J.Am:Chem.Soc. 123,* 11341-11352). For the specific application herein, values for $k_{off}$, $k_{on}'$, $k_{off}^1$, $k_{off}^2$, $k_{on}'^1$, $k_1$, $k_2$, $R_{2b}$(500 MHz), $R_{2b}$(800 MHz), $\delta\omega_b$, $\delta\omega_{b1}$ and $\delta\omega_{b2}$ (Fig. 2) were fitted as independent variables. Values $k_{on}'^2$, $p_b$, $p_{b1}$, $p_{b2}$, and $p_f=(1-p_{b1}-p_{b2})$, with p standing for the population of the corresponding species, were derived using the condition of microscopic reversibility $k_{ij}p_i=k_{ji}p_j$, where $k_{ij}$ denotes the exchange rate constant for the transformation of species *i* into species *j*. $R_{2f}$, or the intrinsic

$R_2$ relaxation rate of the peptide $^{15}N$ nuclei in the free state, and $\delta\omega_f$ are determined experimentally for a sample of the peptide alone under the same experimental conditions.

Error evaluation

**[0068]** The errors of fitting the kinetic and NMR relaxation parameters using Equations 1 and 1a to 1d were estimated through Monte-Carlo sampling as follows. Random deviations of the measured peak integral intensities were generated for each of the 200 Monte-Carlo samples. The absolute value of the deviation was set to 1% of the intensity corresponding to zero relaxation delay, which was a justifiable uncertainty based on a few independent experiments. Error analysis for curve fitting using Equations 2 and 2a to 2g was carried out in a slightly different manner. The standard deviations of the fitted parameters were estimated through (bootstrap) Monte Carlo simulations (Press, W. H., Teukolsky, S. A., Vetterling, W. T., and Flannery, B. P. (1992) *Numerical Recipes in Fortran.* Cambridge University Press) using a maximum deviation of ±10% for all experimental $R_2$ values.

**Quantitative analysis of ligand NMR relaxation dispersion profiles of transient protein-ligand complexes**

$^{15}N$ NMR relaxation dispersion profiles of an anti-thrombin peptide interacting with human prothrombin.

**[0069]** The anti-thrombin peptide N-acetyl-*Asp-*Phe-*Glu-*Glu-*Ile-Pro-Glu-Glu-Tyr-Leu-Gln (SEQ ID NO:15)(to be referred to as N-acetyl-Hir(55-65) in the subsequent descriptions), contains five $^{15}N$-labeled residues $Asp_{55}$, $Phe_{56}$, $Glu_{57}$, $Glu_{58}$ and $Ile_{59}$ at their backbone amide nitrogens. The peptide free in solution displays slowly relaxing (sharp) NMR signals with no detectable response (Fig. 3) of the $^{15}N$ transverse relaxation rate to the changes in CPMG pulse rate using the NMR pulse sequence in Fig. 1. In Fig. 3, the peptide was ~1.5 mM in an aqueous solution (10% $D_2O$) that was 50 mM in NaCl and 50 mM in sodium phosphate at pH 5.5. Upon addition of a small

amount of prothrombin (less than 1:50 protein/ligand molar ratio), four of the five {$^{1}$H-$^{15}$N}-HSQC peaks were found to significantly shift and broaden. For all exchange regimes, excess ligand over a large protein-ligand complex guarantees that the NMR spectrum is dominated by the slowly decaying signals resulting from the free ligand (Ni, F. (1994) *Progress in NMR spectroscopy 26,* 517-606). The $^{15}$N transverse relaxation dispersion data (Fig. 4) were collected using the implementation illustrated in (Fig. 1) of the constant-time $^{15}$N CPMG experiment (Mulder, F. A. A., Skrynnikov, N. R., Hon, B., Dahlquist, F. W., and Kay, L. E. (2001) *J.Am.Chem.Soc. 123,* 967-975) along with additional CPMG elements for sensitivity enhancement of exchange-broadened signals (Mulder, F. A. A., Spronk, C. A. E. M., Slijper, M., Kaptein, R., and Boelens, R. (1996) *J.Biomol.NMR 8,* 223-228) and for the compensation of heating effects (Wang, A. C. and Bax, A. (1993) *J.Biomol.NMR 3,* 715-720) caused by the CPMG pulses (Mulder, F. A., van Tilborg, P. J., Kaptein, R., and Boelens, R. (1999) *J.Biomol.NMR 13,* 275-288). The use of compensating $^{15}$N CPMG pulses was found to be critical for running the relaxation dispersion experiments on a very high field NMR spectrometer (such as at 800 MHz) that may be very sensitive to small temperature fluctuations.

**[0070]** Fig. 4 shows the $^{15}$N relaxation dispersion of the backbone amide nitrogen atoms of residues $Phe_{56}$, $Glu_{57}$, $Glu_{58}$ and $Ile_{59}$ of N-acetyl-Hir(55-65) in the presence of human prothrombin. The amide nitrogen of $Asp_{55}$ had a rather sharp $^{15}$N NMR signal and showed very little relaxation dispersion, in agreement with the very little binding-induced line broadening of its amide proton resonance (Ni, F., Ning, Q., Jackson, C. M., and Fenton, J. W. (1993) *J.Biol.Chem. 268,* 16899-16902), and therefore was not included in further analysis. Three prothrombin/peptide molar ratios were used, namely ~1:45, ~1:35, and ~1:30. The accuracy of the absolute peptide or prothrombin concentrations was not critical for the data analysis, as only the increases in the prothrombin/peptide ratio, measured by the volume of the added prothrombin stock solution, need to be included in the data fitting process (*vide infra*). The approximate prothrombin concentrations were used only to

discriminate physically reasonable from unreasonable fits. In the course of the titration the volumes of the added prothrombin solution after the second and third additions were 1.29 and 1.5 times that of the first addition, respectively. The relaxation dispersion data were fitted using numerical calculation of the magnetization evolution (Equations 1 and 1a to 1d) or the single-exponential approximation (Equations 2 and 2a to 2g) during the ($\tau_{CPMG}/2$-180°-$\tau_{CPMG}$-180°-$\tau_{CPMG}/2$) element of CPMG sequence (Jen, J. (1978) *J.Magn Reson. 30,* 111-128). In Fig. 4, the peptide was ~1.5 mM in an aqueous solution (10% $D_2O$) that was 50 mM in NaCl and 50 mM in sodium phosphate at pH 5.5, and at 298 K. The dispersion curves were recorded at three prothrombin:peptide ratios, 1:45 (○, ●), 1:35 (□, ■), and 1:30 (◇, ◆), and at two $^{15}N$ frequencies, 50.684 MHz (○,□, and ◇) and 81.076 MHz (●,■ , and ◆). The $^{15}N$ dispersion curves were fitted to a two-site exchange scheme separately for each residue, but simultaneously for all three prothrombin:peptide ratios. The fitted curves are shown as solid line at 1:45, dotted line at 1:35, and dash-dot line at 1:30 prothrombin:peptide ratios.

Data analysis using a two-site exchange model

**[0071]** A two-site exchange model was fitted independently for every $^1H/^{15}N$ cross-peak either at each prothrombin concentration or by combining the data for all three prothrombin concentrations. In this scheme, $p_b$ is the bound population of the peptide, $\delta\omega_{bf}$ is the $^{15}N$ resonance peak separation ($\delta\omega_b$-$\delta\omega_f$) between the bound and the free states, $R_{2f}$ is the transverse relaxation rate for the free peptide, $R_{2b}$ is the transverse relaxation rate for the bound peptide, $k_{off}$ is the dissociation rate constant, $k_{on}'=k_{on}\times[E_f]$ is a pseudo-first order binding rate constant, where $k_{on}$ is the association rate constant, and $[E_f]$ is the concentration of the free prothrombin. In turn, the concentration of the free prothrombin $[E_f]$ is defined by the concentration of the free peptide $[L_{free}]$, the total concentration of added prothrombin $[E_0]$, and an equilibrium dissociation constant $K_D$ (which in the case of a two-state exchange is equal to $k_{off}/k_{on}$) as

$$[E_f] = [E_0]K_D/(K_D+[L_{free}]), \quad (3)$$

which in the case of $[L_{free}]>>K_D$, and $[L_0]>>[E_0]$, is proportional to the $[E_0]/[L_0]$ ratio. A least squares fitting procedure was used to extract the values of $R_{2b}$ at the two magnetic fields, $k_{off}$, $p_b$, and $\delta\omega_{bf}$. The values of $R_{2f}$, the transverse relaxation rate for the $^{15}N$-labeled sites of the free peptide, were derived from the CPMG relaxation dispersion profile of the free peptide (Fig. 3).

**[0072]** The results of the fits are presented in Table 1. It is seen that the behavior of residues $Phe_{56}$ and $Ile_{59}$ is consistent with a two-site exchange model. Both residues display highly similar $k_{off}$ and $R_{2b}$ values independent of the peptide/prothrombin ratio, and $p_b$ is growing roughly proportionally to the added prothrombin. $Glu_{58}$, on the other hand, has a noticeably different behavior: the calculated $k_{off}$ value decreases with the addition of prothrombin, while $R_{2b}$ increases, and $p_b$ is not changing. $Glu_{57}$ displays some growth of $k_{off}$ and only slight increase in $p_b$ upon the incremental growth of the prothrombin concentration. In addition, $R_{2b}$ values for $Glu_{57}$ at both fields appear to be unusually high, almost doubling the values calculated for other $^{15}N$ sites. Regardless, fitting results with residues $Phe_{56}$ and $Ile_{59}$ indicate that $^{15}N$-relaxation dispersion data at two magnetic fields and at a single prothrombin concentration can uniquely determine the five unknown parameters, $R_{2b}(500)$, $R_{2b}(800)$, $k_{off}$, $p_b$ and $\delta\omega_{bf}$ describing two-state binding.

**Table 1**

**Kinetic and $^{15}N$ Relaxation Dispersion Parameters of the N-acetyl-Hir(55-65) Peptide in Complex with Human Prothrombin for a Two-Site Exchange Scheme at 298 K[1]**

| Residue | $k_{off}$, $s^{-1}$ | $\delta\omega_{bf}$, ppm | $p_b$, % | $R_{2b}$ [$R_{2b}$(800)], $s^{-1}$ | $R_{2f}$ [$R_{2f}$(800)], $s^{-1}$ |
|---|---|---|---|---|---|
| Phe56/1 | 2030±110 | 3.7±0.2 | 2.01±0.14 | 161±8 [319±22] | 1.38 [0.95] |
| Phe56/* | 2050±146 | 3.6±0.2 | 2.0±0.2 | 155±11 [308±30] | |
| Phe56/2 | 2015±110 | 3.9±0.2 | 2.40±0.21 | 199±10 [304±21] | |
| Phe56/3 | 2150±105 | 4.2±0.2 | 2.53±0.15 | 190±7 [304±18] | |
| Phe56 | 2080±60 | 4.0±0.1 | 1.80±0.06 | 188±5 [308±11] | |
| Glu57/1 | 1540±180 | -2.6±0.3 | 1.74±0.20 | 310±35 [460±60] | 1.60 [1.44] |
| Glu57/* | 1570±209 | -2.6±0.4 | 1.7±0.3 | 310±46 [454±78] | |
| Glu57/2 | 1820±190 | -3.4±0.3 | 1.74±0.16 | 410±40 [514±54] | |
| Glu57/3 | 2030±200 | -3.5±0.4 | 1.92±0.21 | 400±40 [513±58] | |
| Glu57 | 1850±110 | -3.2±0.2 | 1.36±0.08 | 390±20 [510±35] | |
| Glu58/1 | 2260±100 | 4.2±0.2 | 3.42±0.20 | 136±6 [255±17] | 2.14 [2.53] |
| Glu58/* | 2437±153 | 4.3±0.3 | 3.2±0.3 | 132±9 [245±24] | |
| Glu58/2 | 1790±80 | 5.4±0.2 | 3.09±0.12 | 233±7 [339±14] | |
| Glu58/3 | 1680±80 | 5.3±0.2 | 3.34±0.14 | 259±7 [367±14] | |
| Ile59/1 | 2060±90 | -4.4±0.2 | 3.04±0.15 | 209±7 [361±18] | 0.71 [1.03] |
| Ile59/* | 2165±153 | -4.5±0.3 | 3.0±0.2 | 206±11 [351±27] | |
| Ile59/2 | 2020±80 | -4.9±0.2 | 3.55±0.15 | 260±8 [340±15] | |
| Ile59/3 | 2260±100 | -4.5±0.2 | 4.41±0.28 | 193±8 [312±18] | |
| Ile59 | 2160±60 | -4.6±0.1 | 2.90±0.10 | 221±5 [330±10] | |
| 56/57/59[2] | 2470±40 | | 2.40±0.05 | 193±4 [245±6] | |

[1] The fitted parameters $k_{off}$, $\delta\omega_{bf}$, $p_b$ and $R_{2b}$ represent, respectively, the dissociation rate constant of the protein-peptide complex, the frequency separation for a peptide $^{15}N$ signal in the free and bound states ($\delta\omega_b$-$\delta\omega_f$), the apparent fraction of the bound peptide, and the apparent $R_2$ relaxation rate of the peptide $^{15}N$ nuclei in the bound state. Signs of the $\delta\omega_{bf}$ values are derived from the signs of the prothrombin-induced chemical shifts for the corresponding [$^1H$-$^{15}N$]-HSQC cross-peaks. The listed values $R_{2b}$ are those at 500 MHz (with an $^{15}N$ frequency of 50.684 MHz) and the values in the square brackets are those at 800 MHz ($^{15}N$ frequency: 81.076 MHz). The values of $R_{2f}$, or the intrinsic $R_2$ relaxation rate of the peptide $^{15}N$ nuclei in the free state, were determined experimentally for a sample of the peptide in the absence of prothrombin under the same experimental conditions, and were found independent of the CPMG pulse rate. Residues were fitted independently except for the last row designated as 56/57/59. For every amino acid residue, rows denoted /1, /2, and /3 correspond to data sets at prothrombin:ligand ratios of 1:45, 1:35, and 1:30, respectively. Rows denoted /* show the results of the fitting of the data in rows denoted /1 (~1:45 prothrombin/peptide ratio) with a single-exponential approximation (Carver, J. P. and Richards, R. E. (1972) *J.Magn.Reson. 6,* 89-105; and Jen, J. (1978) *J.Magn Reson. 30,* 111-128; and Davis, D. G., Perlman, M. E., and London, R. E. (1994) *J.Magn Reson.B 104,* 266-275). The last row for every residue, except for $Glu_{58}$ which strongly deviates from the concentration dependence implied in a two-site model, lists parameters obtained by a simultaneous fit to dispersion data at all three concentrations, with the value in $p_b$ column corresponding to the prothrombin:ligand ratio of 1:45. The row 56/57/59 displays parameters for the simultaneous fit to the relaxation dispersion of three residues $Phe_{56}$, $Glu_{57}$ and $Ile_{59}$ at three prothrombin concentrations.

[2] Fitted values of $\delta\omega_{bf}$ were 3.1±0.1, (-1.2)±1.8, and (-5.5)±0.1 ppm, for residues $Phe_{56}$, $Glu_{57}$ and $Ile_{59}$, respectively.

**[0073]** A simultaneous fit of the dispersion curves was then carried out at all three prothrombin concentrations, using the fact, that $k_{on}'$ is proportional to $[E_f]$, hence to $[E_0]$ (Equation 3). Three matrices $\boldsymbol{R}_{EX}$(1:45), $\boldsymbol{R}_{EX}$(1:35), and $\boldsymbol{R}_{EX}$(1:30) for each prothrombin:peptide ratio were used to fit simultaneously

relaxation dispersion curves from three prothrombin concentrations. Matrices $R_{EX}$(1:35) and $R_{EX}$(1:30) are produced from $R_{EX}$(1:45) by substituting exchange rates $k_{on}'$ (or $k_{on}'^{1}$ and $k_{on}'^{2}$ in the models with two dissociation routes) with 1.29×$k_{on}'$ (or 1.29×$k_{on}'^{1}$ and 1.29×$k_{on}'^{2}$) and 1.5×$k_{on}'$ (or 1.5×$k_{on}'^{1}$ and 1.5×$k_{on}'^{2}$), respectively. The ratios 1.29 and 1.5 for $R_{EX}$(1:35) and $R_{EX}$(1:30) reflect the increase of prothrombin/ligand ratio in the relationship $k_{on}' \sim K_D[E_0]/[L_0]$ under the assumptions of $[L_{free}] >> K_D$ and $[L_0] >> [E_0]$ (see equations (3) and (4)), and are obtained using the volumes of the added prothrombin solution in the titration. The populations of different species with increased prothrombin concentrations were recalculated in accordance with the modified $k_{on}'$ (or $k_{on}'^{1}$ and $k_{on}'^{2}$) values. The fit was performed independently for each $^{1}H/^{15}N$ cross-peak (Fig. 4 and Table 1). As expected, the fitted dispersion curves for $Phe_{56}$ and $Ile_{59}$ were in a good agreement with the two-site exchange model. It was also possible to fit reasonably well the dispersion curves of $Glu_{57}$ using the same model. Again, for $Glu_{57}$ fitted $R_{2b}$ values were higher, while $p_b$ was smaller than expected (Table 1). It is important to emphasize that the apparent transverse relaxation rate was very sensitive to the increase of $[E_f]$ for every pair of the dispersion curves with the addition of prothrombin. It was therefore easy to verify the linearity of $[E_f]$ growth with protein addition simply by including it as a fitted parameter. For $Phe_{56}$, $Glu_{57}$ and $Ile_{59}$ $^{15}N$ sites, fitted $[E_f]_1/[E_f]_2$ values for every pair of prothrombin concentrations was in excellent agreement with the relative volumes of prothrombin solution added, or the $([E_0]/[L_0])_1/([E_0]/[L_0])_2$ ratio. This observation is consistent with the previous reports demonstrating that $K_D$ for the binding of N-acetyl-Hir(55-65) with prothrombin is of the order of ~100-300 μM (Ni, F., Ning, Q., Jackson, C. M., and Fenton, J. W. (1993) *J.Biol.Chem. 268,* 16899-16902; and Anderson, P. J., Nesset, A., Dharmawardana, K. R., and Bock, P. E. (2000) *J.Biol.Chem. 275,* 16428-16434), and therefore is significantly less than the peptide concentration (~1.5 mM).

**[0074]** Simultaneous fitting of eighteen dispersion curves at the three concentrations of prothrombin for all three residues $Phe_{56}$, $Glu_{57}$ and $Ile_{59}$ was

also performed and is listed in the last row of Table 1. For this particular fitting, equal $R_{2b}$ values were assumed for each residue in the bound state to simplify the calculations. Whereas parameters for $Phe_{56}$ and $Ile_{59}$ remained similar to those obtained independently for every residue, the fit forced poor convergence of the parameter $\delta\omega_{bf}$ (1.2±1.8 ppm) for $Glu_{57}$.

**[0075]** It was not possible to obtain a reasonable fit for residue $Glu_{58}$ using a two-site exchange model at the three prothrombin concentrations (Fig. 4). The apparent transverse relaxation rate of $Glu_{58}$ does not grow rapidly enough with the addition of prothrombin to be consistent with the two-site exchange model, thus indicating that $Glu_{58}$ may undergo more complex exchange processes.

Data analysis using a three-site exchange model

**[0076]** The relaxation behaviors of residues $Glu_{57}$ and particularly $Glu_{58}$ suggest the presence of other conformations for these residues in the bound state. Although the relaxation dispersion of $Glu_{57}$ is possible to be fitted by a two-site exchange model at all three prothrombin concentrations, the abnormally high values of $R_{2b}$ as well as comparatively low values of $p_b$, might be artifacts originating from the presence of additional exchange pathways. In fact, even residues $Phe_{56}$ and $Ile_{59}$ display $R_{2b}$ values somewhat higher than expected, if It is assumed that in the bound state it is the motions of the complex as a whole that define the transverse relaxation of the ligand. Theoretical values of $R_2$ for a protein with the molecular mass of prothrombin (72 kDa) and order parameter S=0.8 and 1.0 were estimated to be respectively 95/122 and 119/153 $s^{-1}$ at 500/800 MHz (Luginbuhl, P. and Wuthrich, K. (2002) *Progress in NMR spectroscopy 40,* 199-247).

**[0077]** In the most general case including additional bound state adds two kinetic pathways to the model (Fig. 2, pathway B). One pathway is the kinetic exchange on the surface of the protein, that can be a consequence of both protein and peptide conformational conversions. Another pathway is an alternative association-dissociation route of the distinct bound species,

formally producing an additional pair of $k_{off}$ and $k_{on}$ rate constants. If one of the two pathways is too slow to influence the relaxation, the system obeys either "linear" three-state behavior (Fig. 2, pathway C), or "forked" three-state behavior (Fig. 2, pathway D). In the present evaluation, it was assumed that the transverse relaxation rate $R_{2b}$ for both bound states are equal. This way, there are a total of nine independent parameters describing the general three-site exchange, while the total number of the degrees of freedom is reduced by one for the "linear" or "forked" three-site exchange mechanisms (Fig. 2 and Equation 1). The increment of the prothrombin concentration during the titration does not increase the total degrees of freedom as long as the volume ratios of the titrated prothrombin are known accurately. In principle, therefore, the nine kinetic and NMR relaxation parameters may be obtained from fitting of only two dispersion data sets at two different prothrombin concentrations. Equation (3) and the linear proportionality of $[E_f]$ to $[E_0]/[L_0]$, given $[L_{free}]>>K_D$ and $[L_0]>>[E_0]$, remains valid if an apparent $K_D$ value is defined as $[E_f][L_{free}]/[\{EL\}_{complex}]$. Here $\{EL\}_{complex}$ represents an ensemble of 1:1 protein-ligand complexes, but $K_D$ is not equal to $k_{off}/k_{on}$ for the three-site or more complex exchange situations.

**[0078]** In practice, it was found that the three-state system may be somewhat underdefined, and depending on the starting conditions, the calculation converged to a few clusters of fitted parameters. The clusters were filtered on the basis of physical feasibility, and parameter sets containing negative rate constants or relaxation times, as well as $p_b=p_{b1}+p_{b2}$ exceeding or comparable with $p_{free}=(1-p_b)$, were not considered. To fit the experimental dispersion curves of $Glu_{57}$ to a "linear" three-site model (Fig. 2, pathway C), it was necessary to use simultaneously the six dispersion curves for the three concentrations of prothrombin and at two different magnetic fields to obtain convergent results. Depending on the starting conditions for iterative fitting, the fitted parameters in the calculations converged either to the two-site exchange mechanism ($k_1\approx k_2\approx 0$), or to the actual linear three-site exchange mechanism ($k_1=50\pm30$ $s^{-1}$, $k_2=150\pm70$ $s^{-1}$). The resulting three-site exchange scheme was, in fact, not so much different from the two-site exchange

scheme, since the population of the dissociation-competent bound state, $p_{b1}$, was found to be 1.3±0.1%, close to that found for the two-site mechanism (Table 1). Part of the bound peptide was redistributed into the $(L_{bound})_2$ state ($p_{b2}$=4.0±1.8 %), thus increasing the total bound peptide population. Notably, the $k_{off}$ value (2090±230 $s^{-1}$) was close to that of residues $Phe_{56}$ and $Ile_{59}$ found in the two-site exchange analysis, while the apparent $R_{2b}$ of $Glu_{57}$ decreased (275±50 and 370±65 $s^{-1}$ at 500 and 800 MHz, respectively) as compared to that in two-site exchange model (Table 1). Treatment of $Glu_{57}$ as an independent association-dissociation site, undergoing conformational exchange on the protein surface (Fig. 2, pathway C), yields smaller apparent $R_{2b}$ and larger $p_b=p_{b1}+p_{b2}$ (~5.3%) values, but it is again not fully consistent with the behavior of $Phe_{56}$ and $Ile_{59}$ sites since the total bound population of $Glu_{57}$ becomes larger than the bound populations for the $Phe_{56}/Ile_{59}$ sites in the two-state analysis. In other words, $Glu_{57}$ appears to spend more time in "bound" state than $Phe_{56}$ and $Ile_{59}$, which is not consistent with the applied model. It is worthwhile to note that in the formal three-state exchange description (Fig. 2, pathway B) the actual separation of "bound" state from "free" state at the residue level is mainly reflected in the large difference between the intrinsic $R_{2b}$ and $R_{2f}$ values. In this respect, although it is easy to imagine a situation when a residue is not interacting (or interacting only weakly) with a prothrombin surface in one of the two bound states in the N-acetyl-Hir(55-65)-prothrombin complex, it would still be in the "bound" state, since its $R_{2b}$ would be closer to that dictated by the correlation time of the complex. Within the limits of this definition, dissociation and association of all residues in the peptide occurs simultaneously, regardless of their residue-specific behavior on the protein surface.

**[0079]** To "link" the process of binding-dissociation between different $^{15}N$ sites of the peptide, fitting of all eighteen dispersion curves was performed for the three residues $Phe_{56}$, $Glu_{57}$ and $Ile_{59}$ at three concentrations of prothrombin and at two magnetic fields (Fig. 5A). The experimental curves were in agreement with the "linear" three-site exchange model (Fig. 5A), and yielded $k_{off}$=2670±140 $s^{-1}$, $k_{off}^{app}$ = 1900±400 $s^{-1}$, $k_1$=560±510 $s^{-1}$, $k_2$=134±40 $s^{-1}$, $k_{ex}$=

$k_1$+ $k_2$ =700±500 $s^{-1}$, $p_{b1}$=2.30±0.14 %, $p_{b2}$=1.0±0.77 %, $p_b$= $p_{b1}$+$p_{b2}$ = 3.35±0.75 %, $R_{2b}$=150/200±16/18 $s^{-1}$ at 500/800 MHz. Here $k_{off}^{app}$=($p_{b1}$×$k_{off}^1$+$p_{b2}$×$k_{off}^2$)/($p_{b1}$+$p_{b2}$) is defined as an apparent population-weighted dissociation rate for a general three-state system. In the "linear" three-site exchange model $k_{off}^2$ is equal to zero, and the expression for $k_{off}^{app}$ becomes $p_{b1}$×$k_{off}$/($p_{b1}$+$p_{b2}$). Overall, the "linear" three-site exchange scheme is consistent with more realistic apparent $R_{2b}$ and $p_b$ values, than those found in the two-site exchange scheme. Importantly, the calculated $k_{off}$ value was not strongly compromised upon the addition of the second bound state to the model.

**[0080]** The "forked" three-site mechanism (Fig. 2, pathway D) did not give additional insights in the explanation of experimental results, even if $R_{2b}$ was presumed to be different in the two bound complexes. The fitted curves either did not produce physically meaningful parameters (for example, negative kinetic rate constants and populations were produced), or were similar to the two-site exchange treatment, if $k_{off}^1$ was assumed to be equal to $k_{off}^2$.

**[0081]** In a general three-site exchange mechanism, the presence of two dissociation pathways as well as an exchange between two complex conformers is presumed (Fig. 2, pathway B). Simultaneous fitting of all eighteen dispersion curves for the three residues $Phe_{56}$, $Glu_{57}$ and $Ile_{59}$ at three prothrombin concentrations assuming the same kinetic exchange parameters for every $^{15}N$ peak is shown in Fig. 5B. The fitting gave $k_{off}^1$=2400±1600 $s^{-1}$, $k_{off}^2$=2600±500 $s^{-1}$, $k_{off}^{app}$=2350±230 $s^{-1}$, $k_1$=66±57 $s^{-1}$, $k_2$=110±130 $s^{-1}$, $k_{ex}$= $k_1$+ $k_2$ =180±150 $s^{-1}$, $p_{b1}$=1.45±1.0 %, $p_{b2}$=1.5±0.5 %, $p_b$=$p_{b1}$+$p_{b2}$=3.0±0.7 %, $R_{2b}$=160/205±26/35 $s^{-1}$ at 500/800 MHz. The apparent dissociation rate constant $k_{off}^{app}$ has significantly less variability than each of the rate constants $k_{off}^1$ and $k_{off}^2$. It means that fitting of the experimental curves may allow a contribution of a state with $k_{off}$ values markedly different from the average, but its contribution to the total bound species is either small or compensated in the averaged dissociation rate. Some of the fits produced

results with $k_{off}^1$ or $k_{off}^2$ close to zero, which essentially corresponds to "linear" mechanism.

**[0082]** In Figs. 5A and 5B, experimental conditions and labeling are the same as in Fig. 4.

**[0083]** Interestingly, both the "linear" and "full" three-state models failed to describe the relaxation behavior of the backbone $^{15}N$ nucleus of $Glu_{58}$. Although they produce a somewhat closer fit than two-site model, reducing $\chi^2$ from ~4.8 $s^{-2}$ for two-site to ~1.2 $s^{-2}$ for three-site exchange, the calculated parameters are not physically reasonable.

**[0084]** The present invention will be more readily understood by referring to the following examples, which are given to illustrate the invention rather than to limit its scope.

## Example 1

**Quantitative determination of the dissociation rate constant $k_{off}$ of transient protein-ligand complexes without precise knowledge of the ligand and protein concentrations: binding of the N-acetyl-Hir(55-65) peptide to human prothrombin**

**[0085]** The changes in $^{15}N$ transverse relaxation dispersion of a selectively $^{15}N$-labeled N-acetyl-*$Asp_{55}$-*Phe-*Glu-*Glu-*Ile-$Pro_{60}$-Glu-Glu-Tyr-Leu-$Gln_{65}$-COOH (SEQ ID NO:15)(N-acetyl-Hir(55-65)) were followed as a function of the concentration of the binding protein, human prothrombin. The $^{15}N$ NMR transverse relaxation rate of the 11-residue peptide is not responsive to the CPMG pulse rate (Fig. 3). Interaction of the peptide with the fibrinogen recognition site of prothrombin (Ni, F., Ning, Q., Jackson, C. M., and Fenton, J. W. (1993) J.Biol.Chem. 268, 16899-16902; and Anderson, P. J., Nesset, A., Dharmawardana, K. R., and Bock, P. E. (2000) J.Biol.Chem. 275, 16428-16434) causes broadening of the peptide's amide proton resonances (Ni, F., Ning, Q., Jackson, C. M., and Fenton, J. W. (1993) J.Biol.Chem. 268, 16899-16902) and the {$^{15}N$-$^{1}H$}-HSQC peaks, so that the $^{15}N$ relaxation dispersion curves can be recorded in the presence of sub-equivalent amounts of the

large binding protein. Although the major exchange process in the system was presumed to be the association-dissociation of the peptide-prothrombin complex, it was interesting to see how well a simple two-site exchange model ("bound state-free state") describes the relaxation behavior of the peptide and whether the dissociation $k_{off}$ rate can be extracted from the experimental NMR relaxation dispersion curves.

**[0086]** In the course of the titration with human prothrombin, each $^{15}N$ labeled residue displayed slightly different relaxation behavior in response to increased prothrombin concentrations. Transverse relaxation of residue $Asp_{55}$ showed a very weak response to the complex formation, implying a small change in chemical shift upon binding. This is in agreement with the very little binding-induced line broadening of the amide proton resonance of $Asp_{55}$ reported previously (Ni, F., Ning, Q., Jackson, C. M., and Fenton, J. W. (1993) J.Biol.Chem. 268, 16899-16902). Contrary to $Asp_{55}$, there is a pronounced increase in the transverse relaxation of residues 56-59 induced by binding with prothrombin. Residues $Phe_{56}$ and $Ile_{59}$ followed a two-site exchange model fairly well and displayed the same concentration-independent $k_{off}$ and $R_{2b}$ values at both magnetic fields (Table 1). In addition, the calculated bound population for these two residues rose proportionally to the amount of prothrombin added, and were roughly comparable with the absolute concentration of prothrombin. The value of the calculated $k_{off}$ rate was also quite reasonable. One can estimate the $K_D$ for the interaction of Hir(55-65) and N-acetyl-Hir(55-65) peptides with human prothrombin to be approximately 100-300 μM (Krstenansky, J. L., Owen, T. J., Yates, M. T., and Mao, S. J. (1987) J.Med.Chem. 30, 1688-1691; and Ni, F., Ning, Q., Jackson, C. M., and Fenton, J. W. (1993) J.Biol.Chem. 268, 16899-16902; and Anderson, P. J., Nesset, A., Dharmawardana, K. R., and Bock, P. E. (2000) J.Biol.Chem. 275, 16428-16434). If one assumes the $k_{on}$ for N-acetyl-Hir(55-65) to be in the range of $10^7$-$10^8$ $M^{-1}s^{-1}$, as reported for hirudin-based peptides (Skordalakes, E., Elgendy, S., Goodwin, C. A., Green, D., Scully, M. F., Kakkar, V. V., Freyssinet, J. M., Dodson, G., and Deadman, J. J. (1998) Biochemistry 37, 14420-14427; and Myles, T., Le Bonniec, B. F., Betz, A., and Stone, S. R.

(2001) Biochemistry 40, 4972-4979; and Betz, A., Hofsteenge, J., and Stone, S. R. (1991) Biochem.J. 275 ( Pt 3), 801-803), $k_{off}=K_D k_{on}$ can be estimated as $10^3$-$10^4$ $s^{-1}$, in good agreement with the $k_{off}$ value determined here by use of $^{15}N$ NMR relaxation dispersion spectroscopy (Table 1).

**[0087]** Residues $Glu_{57}$ and $Glu_{58}$ displayed a complex NMR relaxation behavior suggesting the presence of other binding states. The most obvious deviation from a simple two-state binding was found for $Glu_{58}$. The transverse relaxation of $Glu_{58}$ was growing with the addition of prothrombin too slowly to be consistent with either two-state or even three-state exchange models, although the three-state model represented a slightly better description. Although the relaxation dispersion curves of $Glu_{57}$ were possible to be fitted to a two-state exchange model, the apparent values of $R_{2b}$ for $Glu_{57}$ were significantly higher, whereas $p_b$ was lower than those of $Phe_{56}$ and $Ile_{59}$. To establish if extension of the exchange model to a three-state process will produce more realistic values of $R_{2b}$ and $p_b$, the relaxation of the peptide was analyzed at all three prothrombin concentrations simultaneously. Since the rate constants of the conformational exchange between the bound states do not depend on the prothrombin concentration, whereas the pseudo-first order binding rate constant is proportional to $[E_f]$, titration by the binding protein may in principle help isolate the contributions of ligand association-dissociation and conformational change of the protein-ligand complex to the observed transverse relaxation. The fitted $k_1$ and $k_2$ rates for the conformational change were on the order of 100 $s^{-1}$ for the prothrombin-peptide complex which is comparable with those (~115 and ~185 $s^{-1}$, respectively) obtained with the stopped-flow fluorescence spectroscopy for thrombin-peptide interactions (Jackman, M. P., Parry, M. A., Hofsteenge, J., and Stone, S. R. (1992) J.Biol.Chem. 267, 15375-15383). At the same time, $R_{2b}$ and $p_b$ values turned out to be closer to the expected physically meaningful values, than those obtained by a two-state exchange scheme. It appears that the $k_{off}$ value obtained from the "linear" three-site exchange scheme might be underestimated by a two-site model, but not dramatically.

**[0088]** The contributions of multi-site exchanges or conformational changes of the protein-ligand complex can be assessed by a full three-state exchange scheme (Fig. 2, pathway B). Similarly to the "linear" three-site exchange scheme, full three-state exchange scheme (Fig. 2, pathway B) reduces $R_{2b}$ closer to physically reasonable values. The $k_{off}$ values for both bound states display larger variability than in the schemes with only one dissociation-competent species. It was, however, noticed that a state with $k_{off}$ rate constant significantly larger or smaller, than the average, might have only small contribution to the total bound population. The apparent $k_{off}$ rate constant has much smaller variation, which appears to be the consequence of the restraints imposed by the transverse relaxation dependence on the protein concentration. Overall, the full three-state exchange scheme did not explain the increased apparent $R_{2b}$ values any better than the "linear" three-state exchange scheme. The apparent dissociation rate constant $k_{off}^{app}$ is again rather close to the value obtained for residues $Glu_{57}$ and $Ile_{59}$ by means of a two-state exchange mechanism.

**[0089]** In summary, the dissociation rate $k_{off}$ can be obtained by fitting a two-state exchange model to the $^{15}N$ relaxation dispersion curves obtained for the N-acetyl-Hir(55-65) peptide at two external magnetic fields and at three prothrombin concentrations (Fig. 4 and Table 1). The accuracy of the absolute peptide or prothrombin concentrations was not critical, as only the increases in the prothrombin/peptide ratio, measured by the volume of the added prothrombin stock solution, need to be included in the data fitting process. This approach in addition makes it possible to separate ligand sites (i.e. residues $Phe_{56}$ and $Ile_{59}$) obeying a two-state binding mechanism (including one free and one bound ligand states) from more complex exchange mechanisms, including one free and two or more bound ligand states (i.e. residues $Glu_{57}$ and $Glu_{58}$). The nuclei following a two-state binding mechanism behave similarly to each other and display reasonable physical parameters, such as $k_{off}$, $p_b$, $R_{2b}(500)$, $R_{2b}(800)$, and $\delta\omega_{bf}$. The derived $k_{off}$ value is independent of protein concentration and can serve as a measure of the binding affinity of a transient protein-ligand complex.

**[0090]** The different binding behavior of ligand sites can be further verified by the temperature dependence of the dissociation rate constants of a protein-ligand complex. The peptide $^{15}N$ relaxation dispersion was collected at three different temperatures for the N-acetyl-Hir(55-65) peptide in complex with human prothrombin (Table 2 and Fig. 6), with an approximate prothrombin:peptide ratio of ~1:30. The $k_{off}$ values of the $^{15}N$ sites obeying a two-state binding behavior, namely $Phe_{56}$ and $Ile_{59}$, grow monotonously and are identical at each temperature within the experimental error. The apparent dissociation rates for the $^{15}N$ sites obeying a more complex exchange behavior (i.e. residues $Glu_{57}$ and $Glu_{58}$) differ from each other and from other $^{15}N$ sites, and have very different temperature dependence from two-state binding sites. For ligand sites obeying two-state binding, temperature dependence of the $k_{off}$ rates can be used to derive quantitative information on the energetic barriers of the complex dissociation, including the enthalpy and entropy of activation (Jardetzky, O. and Roberts, G. C. K. (1981) NMR in molecular biology. New York: Academic Press; and Sandstrom, J. (1982) Dynamic NMR spectroscopy. London: Academic Press). These energetic parameters can be used to assess the origins of fast dissociation for transient protein-ligand complexes, providing the physico-chemical basis for affinity enhancement and optimization.

**[0091]** In Fig. 6, the peptide/protein molar ratio is approximately 30:1. Calculation of the apparent $k_{off}$ was performed using a two-state exchange approximation. Other experimental conditions are as in Fig. 4.

**Table 2**

**Kinetic and $^{15}N$ Relaxation Dispersion Parameters of the N-acetyl-Hir(55-65) Peptide in Complex with Human Prothrombin for a Two-Site Exchange at different temperatures (protein:peptide ratio 1:30)**

| Residue/T | T, K | $k_{off}$, $s^{-1}$ | $\delta\omega_{bf}$, ppm | $p_b$, % | $R_{2b}$ [$R_{2b}(800)$], $s^{-1}$ |
|---|---|---|---|---|---|
| Phe56 | 298 | 2150±100 | 4.2±0.2 | 2.53±0.15 | 190±7 [303±18] |
| Phe56 | 288 | 1280±50 | 3.4±0.1 | 4.18±0.15 | 150±5 [226±9] |
| Phe56 | 278 | 930±40 | 3.1±0.1 | 4.92±0.17 | 171±5 [257±8] |
| Glu57 | 298 | 2030±200 | -3.5±0.4 | 1.92±0.21 | 400±40 [513±58] |
| Glu57 | 288 | 1200±90 | -1.9±0.2 | 5.02±0.21 | 194±26 [238±34] |
| Glu57 | 278 | 500±50 | -1.5±0.1 | 7.18±0.45 | 201±13 [259±19] |
| Glu58 | 298 | 1700±80 | 5.4±0.2 | 3.32±0.15 | 259±8 [367±15] |
| Glu58 | 288 | 690±50 | 5.0±0.1 | 5.57±0.29 | 195±8 [271±11] |
| Glu58 | 278 | 1030±50 | 4.2±0.1 | 5.27±0.19 | 214±6 [294±8] |
| Ile59 | 298 | 2260±100 | -4.5±0.2 | 4.41±0.28 | 193±8 [312±18] |
| Ile59 | 288 | 1170±50 | -4.0±0.1 | 6.01±0.20 | 189±5 [280±10] |
| Ile59 | 278 | 1020±50 | -3.6±0.1 | 5.86±0.22 | 260±9 [345±12] |

## Example 2

**Quantitative determination of the dissociation rate constant $k_{off}$ of transient protein-ligand complexes without precise knowledge of the ligand and protein concentrations: a uniformly $^{15}N$-labeled recombinant peptide interacting with human prothrombin.**

**[0092]** A peptide $Gly_{54}$-$Asp_{55}$-$Phe_{56}$-$Glu_{57}$-$Glu_{58}$-$Ile_{59}$-$Pro_{60}$-$Glu_{61}$-$Glu_{62}$-$Tyr_{63}$-$Leu_{64}$-$Gln_{65}$ (SEQ ID NO:19)(Hir(54-65)), related to the N-acetyl-Hir(55-65) peptide, was recombinantly expressed and uniformly labeled with the $^{15}N$ isotope. The Hir(54-65) peptide was dissolved at ~1.5 mM in an aqueous solution that was 50 mM in sodium phosphate at pH 5.5. NMR peak assignments were carried out as described hereinabove. The free peptide produces relaxation dispersion curves independent of the CPMG pulse rate (Fig. 7). Upon the addition of prothrombin, the peptide gives $^{15}N$ relaxation

dispersion curves and $k_{off}$ rates very similar to those obtained for its synthetic analog N-acetyl-Hir(55-65) (Figs. 4 and 8, Table 3).

**[0093]** In Fig. 7, the curves for every backbone $^{15}N$ site are flat and display no apparent CPMG pulse rate dependence. The peptide was ~1.0 mM in an aqueous solution (10% $D_2O$) that was 50 mM in sodium phosphate at pH 5.5.

**Table 3**

**Kinetic and $^{15}N$ Relaxation Dispersion Parameters of the Recombinant Hir(54-65)-Peptide in Complex with Human Prothrombin for a Two-Site Exchange Scheme at 288 K.**

| | $k_{off}$ ($s^{-1}$) | $\delta\omega_{bf}$, ppm | $p_b$, % | $R_{2b}$ [$R_{2b}(800)$] ($s^{-1}$) | $R_{2f}$ [$R_{2f}(800)$] ($s^{-1}$) |
|---|---|---|---|---|---|
| Phe56 | 980±50 | 4.3±0.1 | 4.5±0.1 | 200±5 [242±8] | 1.69 [2.88] |
| Glu57 | 990±80 | 2.2±0.2 | 4.9±0.3 | 265±20 [310±30] | 2.39 [2.40] |
| Glu58 | 610±45 | 4.7±0.1 | 6.5±0.4 | 232±10 [214±10] | 1.97 [4.38] |
| Ile59 | 550±60 | 5.5±0.2 | 6.0±0.5 | 270±20 [300±20] | 3.65 [5.27] |
| Glu62 | 740±60 | 1.8±0.1 | 6.9±0.5 | 140±9 [193±13] | 3.61 [3.81] |
| Tyr63 | 980±45 | 2.9±0.1 | 6.7±0.3 | 163±6 [263±12] | 3.69 [2.85] |

**[0094]** In Figs. 8A to 8F, the dispersion curves were recorded at two 15N frequencies, 50.684 MHz (o) and 81.076 MHz (•). Experimental values for every residue were fitted to a two-site model. Other experimental conditions are as in Fig. 7.

**Example 3**

**Quantitative determination of the dissociation rate constant $k_{off}$ of transient protein-ligand complexes without precise knowledge of the ligand and protein concentrations: the synthetic N-acetyl-Hir(55-65) peptide in complex with human thrombin**

**[0095]** The peptide N-acetyl-Hir(55-65) also binds to human thrombin with a higher affinity than for the same site on human prothrombin (Ni, F., Ning, Q., Jackson, C. M., and Fenton, J. W. (1993) J.Biol.Chem. 268, 16899-16902). Figs. 9A to 9D show the $^{15}N$ relaxation dispersion profiles for the residues of the peptide N-acetyl-Hir(55-65) in the presence of human thrombin at a

protein:peptide ratio of ~1:15. The dispersion curves show expected quantitative differences compared to those for the N-acetyl-Hir(55-65)-prothrombin complex. There were little differences in the lineshapes of the one-dimensional proton NMR spectra of the thrombin-peptide complex obtained at the two magnetic fields, namely at 500 and 800 MHz. On the other hand, the one-dimensional proton NMR spectra of the prothrombin-peptide complex were significantly more broadened at the higher magnetic field. This field dependence of the proton spectral lineshapes already indicate an intermediate to slow exchange situation for the thrombin-peptide complex. Fitting of the dispersion curves indeed shows a decreased dissociation rate for the thrombin-peptide complex (Table 4). Residue $Phe_{56}$ shows an elevated apparent $k_{off}$ (~650 $s^{-1}$), unreasonably large $R_{2b}$ at 800 MHz, and small $p_b$ values, which indicates that it may be involved in additional conformational exchange processes. Therefore, comparison of $k_{off}$ values for the N-acetyl-Hir(55-65)-thrombin complex and N-acetyl-Hir(55-65)-prothrombin complex reveal an expected acceleration for the dissociation of the weaker N-acetyl-Hir(55-65)-prothrombin complex.

**Table 4**

**Kinetic and $^{15}N$ Relaxation Dispersion Parameters of the N-acetyl-Hir(55-65) Peptide in Complex with Human α-Thrombin for a Two-Site Exchange Scheme (protein:peptide ratio ~1:15) at 298 K.[1]**

| | $k_{off}$ ($s^{-1}$) | $\delta\omega_{bf}$, ppm | $p_b$, % | $R_{2b}$ [$R_{2b}$(800)] ($s^{-1}$) | $R_{2f}$ [$R_{2f}$(800)] ($s^{-1}$) |
|---|---|---|---|---|---|
| Phe56 | 645±69 | 2.5±0.2 | 1.28±0.12 | 54±10 [276±23] | 1.38 [0.95] |
| Phe56* | 628±57 | 1.5±0.1 | 1.3±0.08 | 61±5 [264±17] | |
| Glu57 | 266±49 | -1.6±0.1 | 2.49±0.35 | 108±12 [81±8] | 1.60 [1.44] |
| Glu57* | 279±55 | -0.9±0.1 | 2.4±0.3 | 106±10 [79±7] | |
| Glu58 | 217±69 | 3.5±0.3 | 2.97±1.36 | 134±33 [58±20] | 2.14 [2.53] |
| Glu58* | 213±85 | 2.1±0.1 | 3.4±2.6 | 126±40 [56±20] | |
| Ile59 | 134±45 | -4.5±0.3 | 5.9±1.8 | 200±50 [88±26] | 0.71 [1.03] |
| Ile59* | 104±60 | -2.7±0.1 | 6.7±4.4 | 132±67 [60±30] | |

[1] Rows denoted with asterisk show the results of the fitting with a single-exponential approximation.

**[0096]** In Figs. 9A to 9D, the concentration of the peptide was ~2 mM with a concentration ratio of ~ 15:1 for the peptide and thrombin. For the dispersion profiles at 500 MHz, a total of 15 HSQC spectra were recorded with effective B1 fields (or 1/τCPMG) of 50, 100, 150, 200, 250, 300, 400, 500, 600, 700, 800, 1000, 1200, 1600 and 2000 Hz. For the dispersion profiles at 800 MHz, a total of 15 HSQC spectra were recorded with effective $B_1$ fields of 50, 100(2), 150, 200, 250, 300, 400, 500, 600, 700, 800, 1000(2), and 1200 Hz, of which the experiments were repeated twice for the 100 and 1000 Hz points. The total length of the $^{15}N$ CPMG pulse train, T (Fig. 1), was set to 80 ms, 53.336 ms and 48 ms for the CPMG fields of 50, 150 and 250 Hz, respectively, and kept at a constant value of 40 ms for the rest of the experiments. The total number (4N) of $^{15}N$ CPMG 180° pulses was 48 at 800 MHz and 80 at 500 MHz. As with Fig. 4, the calculated curves based on the fitted parameters (Table 4) are plotted as solid lines for the amide $^{15}N$ resonances of residues Phe56 (Fig. 9A), Glu57 (Fig. 9B), Glu58 (Fig. 9C) and Ile59 (Fig. 9D).

## Example 4

### Quantitative $k_{off}$ determination with ligand mixtures: the synthetic N-acetyl-Hir(55-65) and a mixture of peptides targeting different binding sites on human thrombin

**[0097]** A special procedure was used to express six uniformly $^{15}N$-labeled hexa/penta-peptides, GLDPR$H_L$ (SEQ ID NO:1), GVDPR$H_L$ (SEQ ID NO:2), GFNPR$H_L$ (SEQ ID NO:3), GPNPR$H_L$ (SEQ ID NO:4), GFSAR$H_L$ (SEQ ID NO:5), and GVSPR (SEQ ID NO:6), where a one-letter code is used to define the amino acid sequence, and $H_L$ stands for homoserine lactone. The six short peptides were expressed in tandem as a linear sequence GLDPRMGVDPRMGFNPRMGPNPRMGFSARMGVSPR (SEQ ID NO:16). The individual peptides were released by CNBr cleavage at the methionine residues, producing the homoserine lactone ($H_L$) derivatives of the pentapeptides. Upon introduction of the hexa/pentapeptides in the sample of the N-acetyl-Hir(55-65)-thrombin complex (see Example 3), the five $^1H$-$^{15}N$ HSQC cross-peaks of the N-acetyl-Hir(55-65) peptide were still easily

resolved and identifiable (Figs. 10A and 10B). The N-acetyl-Hir(55-65) peptide and the hexa/pentapeptides target the anion-binding exosite and the catalytic active site of human thrombin, respectively. The hexa/pentapeptides are proteolytically cleaved after the arginine residues in the presence of the human thrombin to produce the GLDPR (SEQ ID NO:7), GVDPR (SEQ ID NO:8), GFNPR (SEQ ID NO:9), GPNPR (SEQ ID NO:10), GFSAR (SEQ ID NO:11), and GVSPR (SEQ ID NO:6) pentapeptides targeting the thrombin active site. In Figs. 10A and 10B, NMR spectra are recorded in 50 mM sodium phosphate buffer (10% $D_2O$), pH 5.5, at 288K, and at 800 MHz. The $^{15}N$-labeled residues of the N-acetyl-Hir(55-65) peptide are well resolved and assigned. Arrows 1 to 4 indicate some of the unassigned [$^1H$-$^{15}N$]-HSQC cross-peaks of the pentapeptides GLDPR (SEQ ID NO:7), GVDPR (SEQ ID NO:8), GFNPR (SEQ ID NO:9), GPNPR (SEQ ID NO:10), GFSAR (SEQ ID NO:11), and GVSPR (SEQ ID NO:6). $^{15}N$ relaxation dispersion curves of the N-acetyl-Hir(55-65) peptide (Fig. 11A) and some resonances of the pentapeptides (Fig. 11B) can still be recorded, which demonstrate that $k_{off}$ values for the N-acetyl-Hir(55-65) peptide/human α-thrombin complex can be derived in the presence of other peptides. Fig. 11A represents $^{15}N$ relaxation dispersion curves displayed by residues Asp55 (○), Phe56 (ж), Glu57 (□), Glu58 (◇) and Ile59 (△) of the N-acetyl-Hir(55-65) peptide. Fig. 11B represents relaxation dispersion curves of peaks 1 (ж), 2 (●), 3 (■), and 4 (◆) (Fig. 10B) of the pentapeptides. Other experimental conditions are as in Figs. 10A and 10B.

**[0098]** Quantitative $k_{off}$ determination was carried out for the mixture of a short peptide Phe-$Asp_{45}$-Pro-Arg (FD22-N)(SEQ ID NO:17) with Pro-Gln-$Ser_{50}$-His-Asn-Asp-Gly-$Asp_{55}$-Phe-Glu-Glu-Ile-$Pro_{60}$-Glu-Glu-Tyr-Leu-$Gln_{65}$ (FD22-C) (SEQ ID NO:18), which contain the sequence of the N-acetyl-Hir(55-65) peptide. Calculated apparent $k_{off}$ values for the peptides FD22-N and FD22-C are presented in Table 5. Experimental values for every residue (Figs. 12A to 12H), except for $Phe_{56}$ and $Arg_{47}$, were fitted to a two-site model using $k_{on}'$, $1.52 \times k_{on}'$, and $2.78 \times k_{on}'$ for the pseudo-first-order association rate constants.

Residues $Phe_{56}$ and $Arg_{47}$ displayed very little response to the CPMG pulse rate at the two lower thrombin concentrations, and were therefore fitted to a two-state exchange scheme using the dispersion data obtained at the highest thrombin concentration. Residue $Tyr_{63}$ obey well the two-site exchange mechanism within the error of the experiment, with $k_{off}$ being approximately equal to 100 $s^{-1}$. Residues $Phe_{56}$ and $Leu_{64}$ display the most profound deviation from the two-state exchange behavior. They show elevated apparent $k_{off}$ values (~400 $s^{-1}$), unreasonably large $R_{2b}$ and small $p_b$ values. This behavior is typical of residues experiencing extensive conformational exchange in the bound state. Observation of relaxation dispersion for the $Arg_{47}$ residue of the FD22-N peptide confirms the possibility to measure $k_{off}$ rates for a number of peptides targeting the same protein non-competitively.

**[0099]** In Figs. 12A to 12H, the dispersion curves were recorded at two $^{15}N$ frequencies, 50.684 MHz (○,□, and ◇) and 81.076 MHz (●,■ , and ◆), and at three increasing thrombin:peptide ratios. Experimental values for every residue, except for $Phe_{56}$ and $Arg_{47}$, were fitted to a two-site model using $k_{on}'$ (○, ●, solid lines), $1.52 \times k_{on}'$ (□, ■, dotted lines), and $2.78 \times k_{on}'$ (◇, ◆, dash-dot lines) for the pseudo-first-order association rate constants at these thrombin concentrations. Residues $Phe_{56}$ and $Arg_{47}$ displayed very little response to the CPMG pulse rate at the two lower thrombin concentrations, and were therefore fitted to a two-state exchange scheme using the dispersion data obtained at the highest thrombin concentration. Open and filled circles for $Phe_{56}$ and $Arg_{47}$ correspond to data obtained at 50.684 MHz and 81.076 MHz, respectively. Values shown at the right lower corners represent r.m.s.d. of the fitted curves with respect to the experimental values.

**Table 5**

**Kinetic and $^{15}N$ Relaxation Dispersion Parameters of the thrombin-cleaved FD22-Peptide in Complex with Human Thrombin for a Two-Site Exchange Scheme at 288 K.[1]**

| | $k_{off}$ ($s^{-1}$) | $\delta\omega_{bf}$, ppm | $p_b$, % | $R_{2b}$ [$R_{2b}(800)$] ($s^{-1}$) | $R_{2f}$ [$R_{2f}(800)$] ($s^{-1}$) |
|---|---|---|---|---|---|
| Phe56 | 390±40 | 3.0±0.1 | 3.3±0.3 | 170±10 [330±20] | 2.15 [2.46] |
| Glu57 | 106±110 | 1.1±0.2 | 5.0±1.2 | 84±7 [31±2] | 2.86 [3.67] |
| Glu58 | 107±23 | 3.0±0.1 | 3.9±0.8 | 92±12 [79±10] | 2.52 [2.12] |
| Ile59 | 53±27 | 4.9±0.5 | 7.9±3.8 | 84±24 [18±5] | 3.23 [4.96] |
| Tyr63 | 103±11 | 4.2±0.1 | 3.5±0.4 | 79±6 [48±4] | 2.93 [3.49] |
| Leu64 | 394±54 | 6.1±0.1 | 1.1±0.2 | 208±21 [294±30] | 2.06 [4.50] |
| Gln65 | 85±14 | 2.7±0.1 | 4.9±0.7 | 52±5 [70±7] | 0.57 [0.63] |
| Arg47 | 310±40 | 1.3±0.2 | 3.2±0.4 | 110±10 [145±20] | 1.0 [1.2] |

[1] Every residue, except for $Phe_{56}$ and $Arg_{47}$, lists parameters obtained by a simultaneous fit to dispersion data at three α-thrombin concentrations using $k_{on}'$, $1.52\times k_{on}'$, and $2.78\times k_{on}'$ for the pseudo-first-order association rate constants. Values in $p_b$ column for these residues correspond to the lowest thrombin:ligand ratio. Residues $Phe_{56}$ and $Arg_{47}$ displayed very little response to the CPMG pulse rate at the two lower α-thrombin concentrations, and were fitted to a two-state exchange scheme at the highest α-thrombin concentration. Values in $p_b$ column for the residues $Phe_{56}$ and $Arg_{47}$ correspond to the highest thrombin:ligand ratio.

## Example 5

### Quantitative $k_{off}$ determination with ligand mixtures: identification of cooperative effects between two peptides targeting distinctive sites on the Cdc42 protein from Candida Albicans

**[00100]** The NMR relaxation dispersion technique can also be used to detect co-operative binding between two peptide ligands as shown in Figs. 13C to 13E. In this experiment, the dispersion profile for the Cdc42-peptide complexes was monitored with either mCla4 or mSte20 (see Fig. 14 for the identities of these peptides) in the absence and presence of the cognate cCRIB fragments (Fig. 14). Changes in the dispersion profiles indicate perturbation of the binding kinetics at the mCRIB:Cdc42 interface induced by binding at a distal site. The results indicate a co-operative binding to Cdc42 in the Ste20 system but not with the Cla4 peptides (Figs. 13C to 13E). These results were substantiated by titrating mCRIBs into $^{15}N$-labeled cCRIB saturated with Cdc42 (Figs. 13A and 13B). However, the advantage of the

approximately 1:30. The spectra were recorded at a $^{15}N$ frequency of 81.076 MHz.

**[00104]** $^{15}N$ relaxation dispersion curves were collected for the two $^{15}N$ labeled CRIB peptides, mSte20 and mCla4 (Figs. 13A to 13F and 14), mixed together in an approximately equal concentration. The peptide mixture did not show responses to the CPMG pulse rates, indicating lack of binding effects between the two peptides. Figs. 16A to 16D shows the $^{15}N$ relaxation dispersion of two sets of resonance peaks in the peptide mixture, assigned to residues 13 and 15 of the mSte20 and mCla4 peptides, respectively, after the addition of Cdc42. It is seen that only residues of the mSte20 peptide exhibit relaxation dispersion, suggesting a stronger binding affinity for this peptide. The dissociation rate constants for each of the peptides can be quantitated by further titration of the peptide mixture with Cdc42 and collection of $^{15}N$ relaxation dispersion curves of the peptide NMR signals at each Cdc42 concentrations (see Example 1). In Figs. 16A to 16D, Cdc42 was added to $^{15}N$-labeled mSte20 and mCla4 peptides in ~ 1:20 molar ratio. The data indicate a CPMG response from the mSte20 peptide (Figs. 16A and 16B) and not from mCla4 (Figs. 16C and 16D) suggesting mSte20 has higher affinity for the site on Cdc42 (in agreement with our previous observations). Due to the potentially complicated nature of binding at the Cdc42 surface, quantitative analysis will require a titration series as proposed in Example 1.

## Example 7

### Applications to high-affinity protein-protein interactions: identification of binding "hotspots" through peptide fragmentation

**[00105]** A peptide named FD22 has been discovered as a potent bivalent inhibitor of human thrombin with $IC_{50}\approx20$ nM. FD22 has the sequence of Phe-$Asp_{45}$-Pro-Arg-Pro-Gln-$Ser_{50}$-His-Asn-Asp-Gly-$Asp_{55}$-Phe-Glu-Glu-Ile-$Pro_{60}$-Glu-Glu-Tyr-Leu-$Gln_{65}$ (SEQ ID NO:20) and binds to thrombin via both the anion-binding exosite-I and the catalytic active site. The addition of active thrombin to the peptide FD22 (dissolved at a concentration of ~0.9 mM in 50 mM sodium phosphate buffer, 10% $D_2O$, 0.2 mM EDTA, at pH 5.5), caused

slow and specific proteolytic cleavage at the $Arg_{47}$-$Pro_{48}$ peptide bond (taking >60 hours for the cleavage to complete). Upon completion of the cleavage, the sample contains a mixture of two peptides, Phe-$Asp_{45}$-Pro-Arg (FD22-N) (SEQ ID NO:17) and Pro-Gln-$Ser_{50}$-His-Asn-Asp-Gly-$Asp_{55}$-Phe-Glu-Glu-Ile-$Pro_{60}$-Glu-Glu-Tyr-Leu-$Gln_{65}$ (FD22-C) (SEQ ID NO:18) that should bind separately to the active site and the anion-binding exosite I of thrombin. Residues $Phe_{56}$, $Glu_{57}$, $Glu_{58}$, $Ile_{59}$, $Tyr_{63}$, $Leu_{64}$ and $Gln_{65}$ of the 55-65 region of the FD22-C fragment displayed pronounced resonance line broadening and $^{15}N$ NMR relaxation dispersion (Figs. 12A to 12H), while residues $Gly_{54}$-$Asp_{55}$ had slowly relaxing $^{15}N$ signals and lack of relaxation dispersion. These data indicate that residues $Glu_{56}$-$Gln_{65}$ constitute a binding hotspot for the high affinity full-length FD22 peptide, in agreement with previous findings (Ni, F., Konishi, Y., and Scheraga, H. A. (1990) Biochemistry 29, 4479-4489). In addition, specific relaxation dispersion of the backbone $^{15}N$ atom of $Arg_{47}$ (Figs. 12A to 12H) shows that the small tetrapeptide Phe-$Asp_{45}$-Pro-Arg (or FDPR) (SEQ ID NO:17) may bind to thrombin with a decreased off-rate in the presence of the FD22-C peptide in contrast to other related pentapeptides, GLDPR (SEQ ID NO:7), GVDPR (SEQ ID NO:8), GFNPR (SEQ ID NO:9), GPNPR (SEQ ID NO:10), GFSAR (SEQ ID NO:11), and GVSPR (SEQ ID NO:6) (see Example 4).

**[00106]** The results obtained with the FD22 peptide indicate that the present techniques can also provide binding information for tight and essentially irreversible protein-protein complexes. This is exquisitely illustrated for the complexes of the Cdc42 protein with peptide fragments derived from two signaling kinases (Figs. 13A to 13F and 14). Cdc42 binds tightly with the 40-residue CRIB domains of Candida Cla4 and Ste20 ($K_D$ ~ 0.5 nM). When subjected to the relaxation dispersion techniques, these complexes exhibit no response, as expected for a tight binding complex. The full-length CRIB domains were dissected into two peptide fragments (Fig. 14). When subjected to the relaxation dispersion analysis the peptide fragments exhibit different binding preferences for Cdc42 (outlined below), which is unlikely to be determined from normal NMR or other analyses of the full-length peptides.

$^{15}N$ relaxation dispersion spectroscopy coupled with peptide fragmentation can therefore be used for the identification of binding 'hotspots' for complexes involving Cdc42 and the two CRIB (Cdc42/Rac interactive binding) proteins, Ste20 and Cla4 from Candida albicans.

**[00107]** For these experiments, two peptide fragments of the extended CRIB region from the Cla4 kinase (Fig. 14): (i) mCla4 (22 residues) including the CRIB motif, and (ii) cCla4 which comprises residues directly to the C-terminus of the CRIB motif were over-expressed. Figs. 17A and 17B shows the perturbations to the $^{1}H$-$^{15}N$ HSQC spectra of $^{15}N$-labeled mCla4 (Fig. 17A) and $^{15}N$-labeled cCla4 (Fig. 17B) upon addition of unlabeled Cdc42. The cCla4 spectrum undergoes minor peaks shifts indicating that the cCla4-Cdc42 complex may be in the fast-exchange regime, hence weak binding. In contrast, the mCla4 peptide may bind tighter to Cdc42, as shown by the extensive broadening and eventual disappearance of resonances. Different results were obtained when titration experiments were performed on the analogous peptide fragments from Ste20: mSte20 and cSte20 (Fig. 14). The cSte20 peptide showed no visible interaction with Cdc42 (Fig. 17D), whereas the HSQC signals of the mSte20 fragment broaden more easily than the analogous mCla4 peptide (Fig. 17C), suggesting that mSte20 may bind tighter or in a different mode to mCla4. In Figs. 17A to 17D, identical protein and peptide concentrations were in all titrations. Spectra are colored from black (free peptide) to red (Cdc42 in 10-fold excess). Differential binding properties between the two kinase fragments are seen.

**[00108]** $^{15}N$ relaxation dispersion spectroscopy was then used to probe the kinetics (specifically the off-rates), of the transient mCRIB complexes with Cdc42 in order to rank the relative affinities of similar peptide fragments. Figs. 18A to 18D and 19A to 19D show representative curves for selected residues of the mSte20 and mCla4 peptides in complex with Cdc42. The free mSte20 and mCla4 peptides show no response to the CPMG pulses (Figs. 18A and 19A red datasets), whereas addition of Cdc42 in ~ $1/10^{th}$ the concentration of the peptide induces significant responses, indicating the formation of a transient complex (black dataset). Acquiring data at two magnetic field

strengths can potentially yield more accurate $k_{off}$ values (Figs. 18B and 19B). Unfortunately, the simple two-state binding model employed may not be applicable to all residues in this system. However, it is noted that the fits do indicate generally lower off-rates for mSte20 (Figs. 18B, and 19B), in agreement with titration data.

**[00109]** In Figs. 18A to 18D and 19A to 19D, apparent values for $k_{off}$, based on a two-site exchange model are shown.

**[00110]** A large and tight-binding protein or peptide can also be fragmented into more than two subfragments for use in NMR relaxation dispersion studies. This is illustrated with the propeptide of human cathepsin B (Fig. 20A), which is a 62 amino acid protein fragment binding tightly to cathepsin B ($K_I$=0.4 nM at pH 6.0 (Fox, T., de Miguel, E., Mort, J. S., and Storer, A. C. (1992) Biochemistry 31, 12571-12576)). The propeptide has been found to contain two important binding motifs, labeled as the NT motif and the CG motif (Chen, Y., Plouffe, C., Menard, R., and Storer, A. C. (1996) FEBS Lett. 393, 24-26). Methionine residues were inserted into the propeptide sequence by site-directed mutagenesis in order to prepare a mixture of essentially equimolar concentrations of the individual peptide fragments F1, F2, F3, F4, and F5 (Fig. 20A). Fig. 20B shows the [$^{1}$H-$^{15}$N]-HSQC spectrum of the full-length propeptide, which was assigned through NMR experiments including 3D [$^{1}$H-$^{15}$N]-HSQC-TOCSY and [$^{1}$H-$^{15}$N]-HSQC-NOESY. The [$^{1}$H-$^{15}$N]-HSQC peaks of the fragmented propeptide are much sharper (Fig. 20C), and can be utilized for $^{15}$N relaxation dispersion experiments.

**[00111]** In Figs. 20B and 20C, the spectra were recorded in 50 mM sodium acetate-$d_3$ buffer, pH 5.5, at 500 MHz, and at 288 K.

**[00112]** While the invention has been described in connection with specific embodiments thereof, it will be understood that it is capable of further modifications and this application is intended to cover any variations, uses, or adaptations of the invention following, in general, the principles of the

invention and including such departures from the present disclosure as come within known or customary practice within the art to which the invention pertains and as may be applied to the essential features hereinbefore set forth, and as follows in the scope of the appended claims.

**WHAT IS CLAIMED IS:**

1. A method to identify a ligand site obeying a two-state or more complex binding behavior in a transient complex of a ligand with a target molecule, said method comprising the steps of:

a) preparing a ligand with at least one nucleus detectable by NMR;

b) collecting NMR relaxation dispersion profiles for free ligand at two or more magnetic fields;

c) determining apparent transverse relaxation rates for the nuclei detectable by NMR at two or more magnetic fields;

d) assigning resonance peaks to the specific NMR detectable nuclei of the ligand with one- and/or multi-dimensional NMR;

e) contacting the ligand with at least one concentration of a target molecule;

f) collecting NMR relaxation dispersion profiles for the ligand with every concentration of the target molecule at two or more magnetic fields;

g) fitting the NMR relaxation dispersion profiles by a two-state exchange model independently for every nucleus, and independently or simultaneously for every concentration of the target molecule; and

h) determining a ligand site obeying a two-state binding behavior based on feasibility of extracted $R_{2b}$ and $p_b$ parameters or the quality of the fitting of step g).

2. The method of claim 1, wherein the ligand of step a) has at least two detectable nuclei.

3. The method of claim 1 or 2, wherein the ligand in step e) is contacted with at least two concentrations of a target molecule.

4. The method of claim 3, wherein the ligand is contacted with three concentrations of target molecules.

5. A method to determine quantitatively the dissociation rate constant ($k_{off}$) for a transient complex of a ligand with the target molecule comprising the steps of:

a) Identifying a ligand site obeying a two-state or more complex binding behavior in a transient complex of a ligand with a target molecule with the method as defined in claim 1, 2, 3 or 4; and

b) Extracting $k_{off}$ values for the ligand sites obeying two-site or more complex exchange mechanism, said $k_{off}$ values being a measure of the affinity of a transient complex of the ligand with the target molecule.

6. A method according to claim 1, 2, 3, 4, or 5, wherein the ligand is a polypeptide.

7. A method according to claim 1, 2, 3, 4, 5 or 6, wherein the ligand is a $^{15}N$-enriched polypeptide.

8. A method according to claim 1, 2, 3, 4, 5, 6 or 7, wherein the ligand is a mixture of polypeptides and/or molecules.

9. A method according to claim 1, 2, 3, 4, 5, 6, 7 or 8, wherein the target molecule is a protein or a protein assembly.

10. Use of the method as defined in claim 1, 2, 3, 4, 5, 6, 7, 8 or 9 to determine amino acid residues with detectable NMR relaxation dispersion as a constituting binding hot-spot.

11. Use of the method as defined in claim 1, 2, 3, 4, 5, 6, 7, 8, 9 or 10 to identify two or more ligands that can be linked together to create high-affinity molecules.

12. Use of the method of claim 1, 2, 3, 4, 5, 6 7, 8 or 9 to study high-affinity protein-protein interactions or slow-dissociating ligand-target complexes.

13. The use of claim 10, 11 or 12, wherein the ligand is a polypeptide or a protein.

14. The use of claim 10, 11, 12 or 13, wherein the ligand is $^{15}N$-enriched.

15. The method of any one of claims 1 to 9, wherein in step b) said NMR relaxation dispersion profiles is CPMG.

16. The method of any one of claims 1 to 9, wherein in step f) said NMR relaxation dispersion profiles is CPMG.

17. The method of any one of claims 1 to 9, where the NMR relaxation dispersion profiles are collected by a CPMG method.

18. The use of claims 10 to 14 where the NMR relaxation dispersion profiles are collected by a CPMG method.

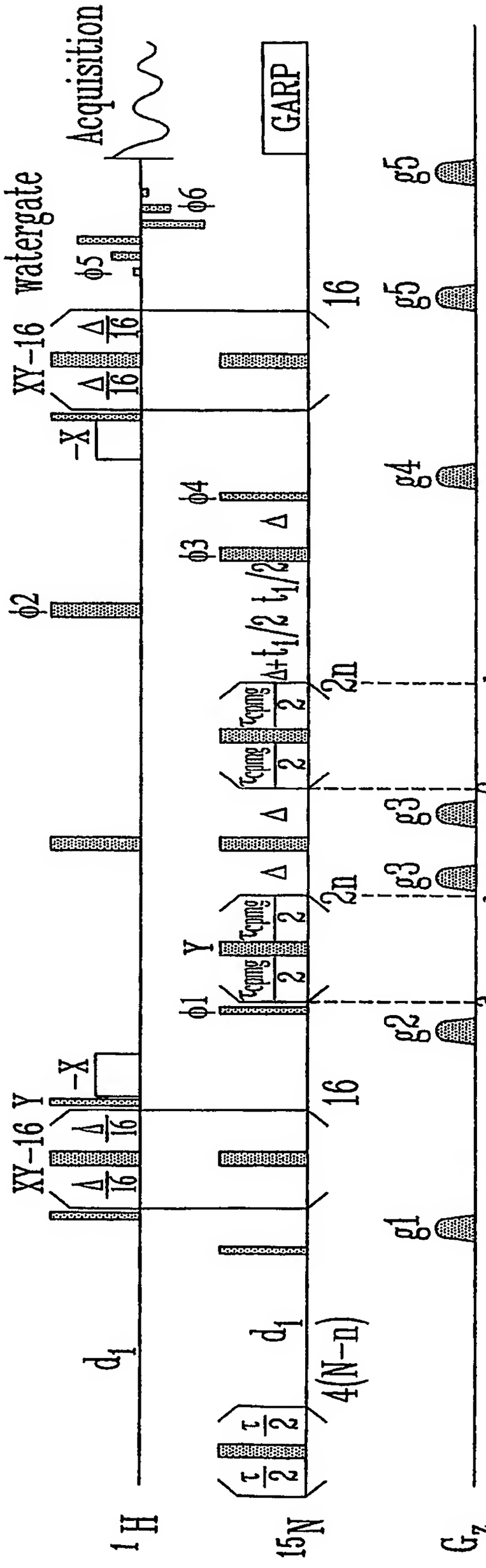
Acquisition
GARP
watergate
XY-16
$\frac{\Delta}{16}$
$\phi 5$
$\phi 6$
16
g5
g5
$\phi 2$
$\phi 4$
$\phi 3$
$\Delta$
$\Delta+t_1/2$ $t_1/2$
g4
$\tau_{comp}$
2
2n
d
c
g3
$\phi 1$
Y
b
g2
-X
XY-16
$d_1$
$d_1$
4(N-n)
$\frac{\tau}{2}$
$^1H$
$^{15}N$
$G_z$
g1

FIG. 1

FIG - 2A

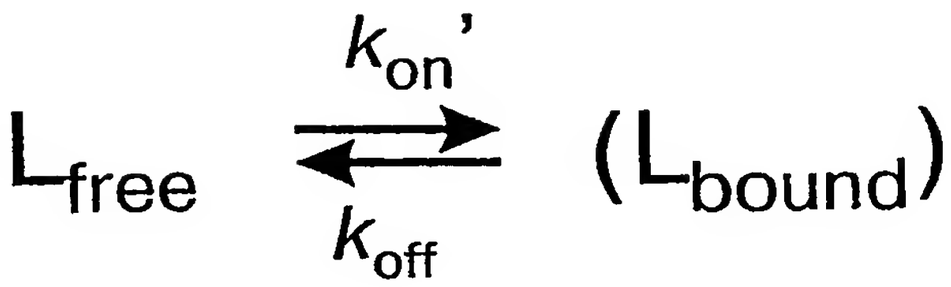


FIG - 2B

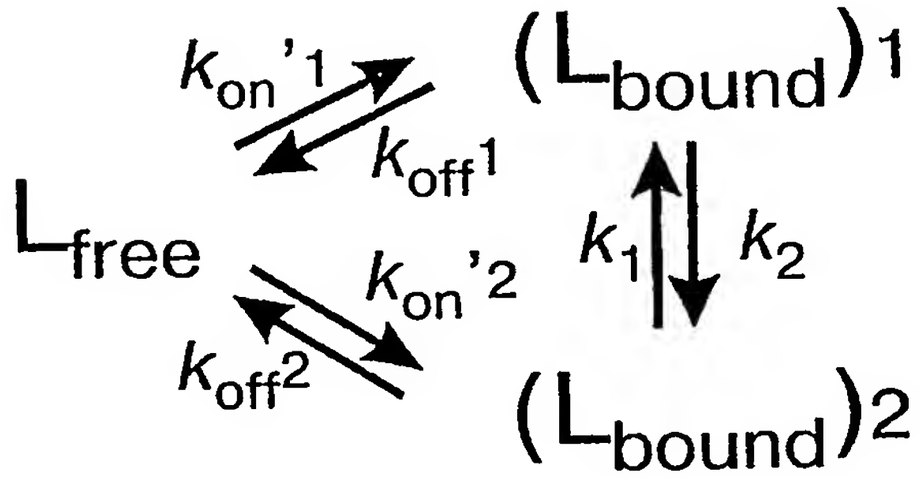


FIG - 2C

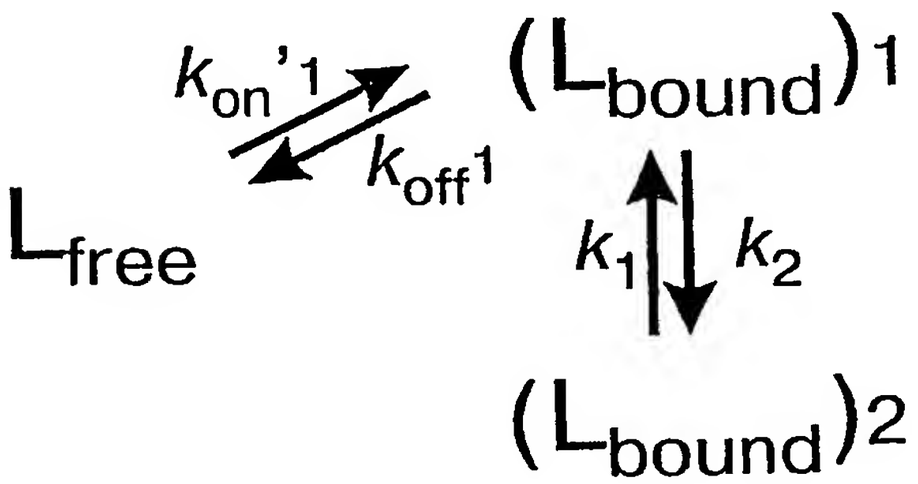


FIG - 2D

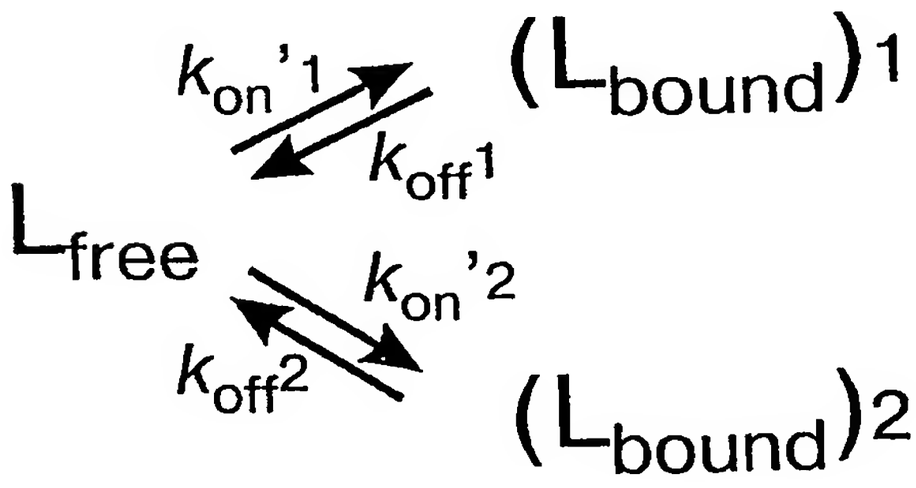

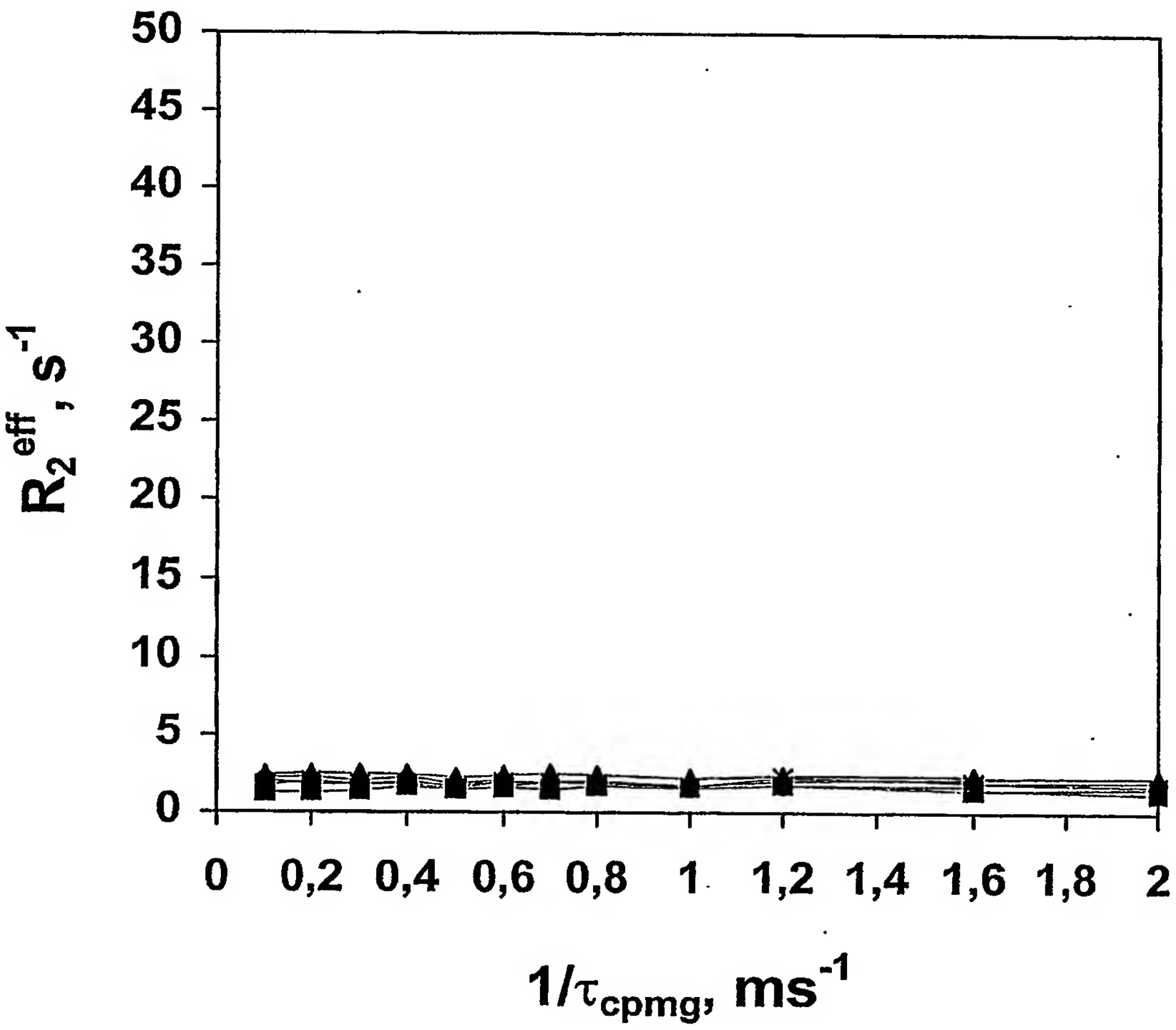
50
45
40
35
30
25
20
15
10
5
0
$R_2^{eff}$, $s^{-1}$
0
0,2
0,4
0,6
0,8
1
1,2
1,4
1,6
1,8
2
$1/\tau_{cpmg}$, $ms^{-1}$

Fig. 3

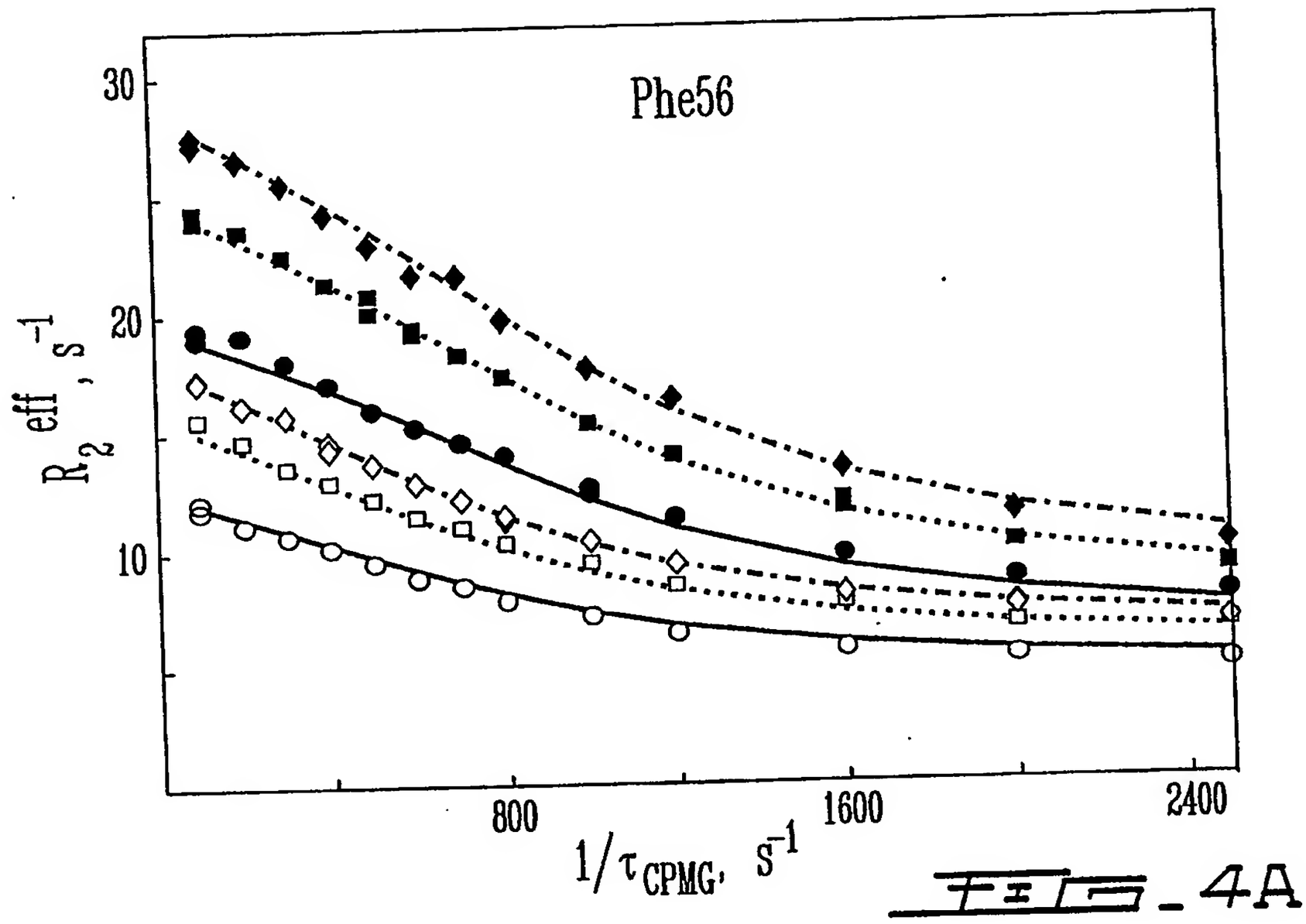
Phe56
30
20
10
800
1600
2400
$R_2$ eff, $s^{-1}$
$1/\tau_{CPMG}$, $s^{-1}$

FIG_4A

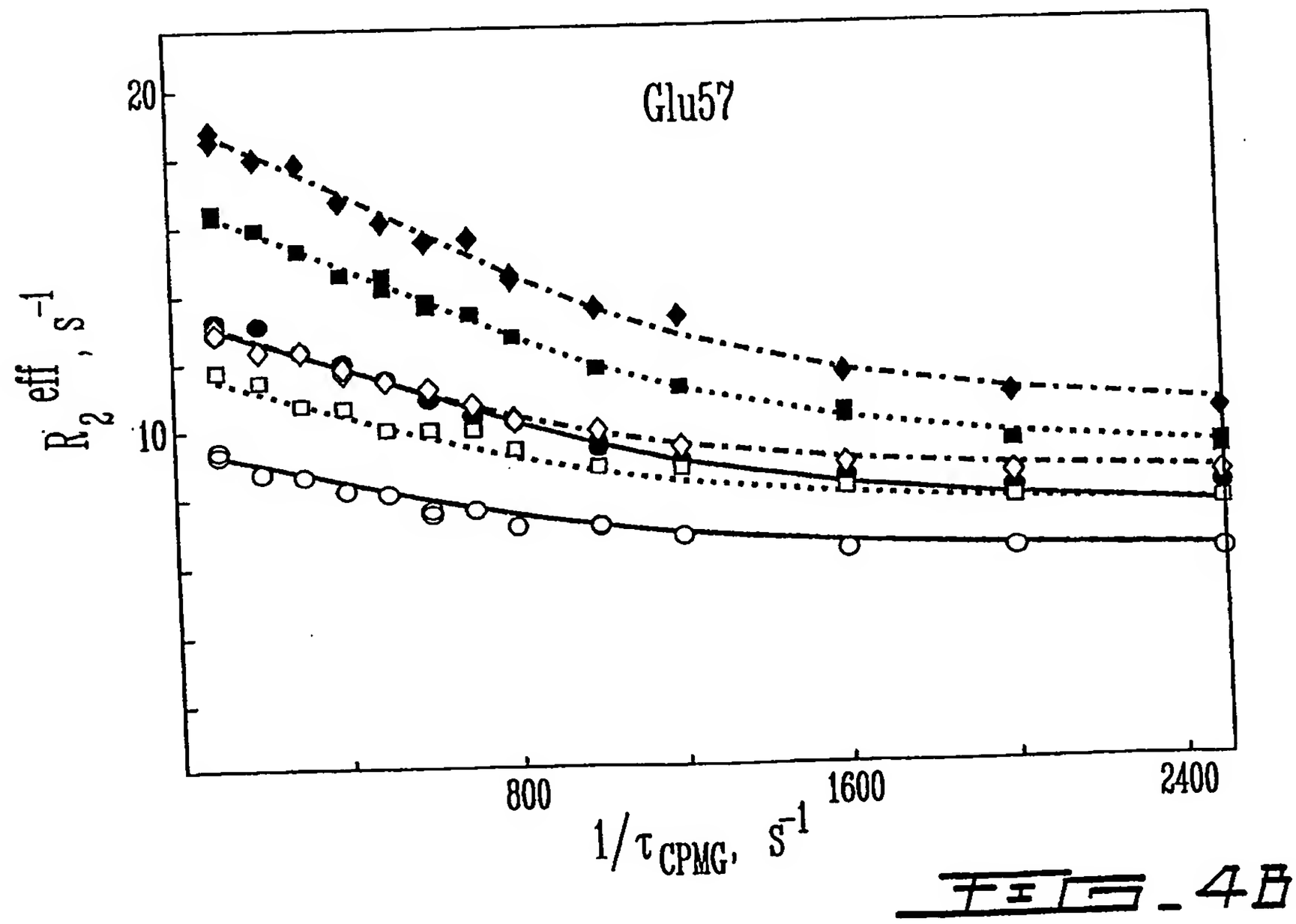
Glu57
20
10
800
1600
2400
$R_2$ eff, $s^{-1}$
$1/\tau_{CPMG}$, $s^{-1}$

FIG_4B

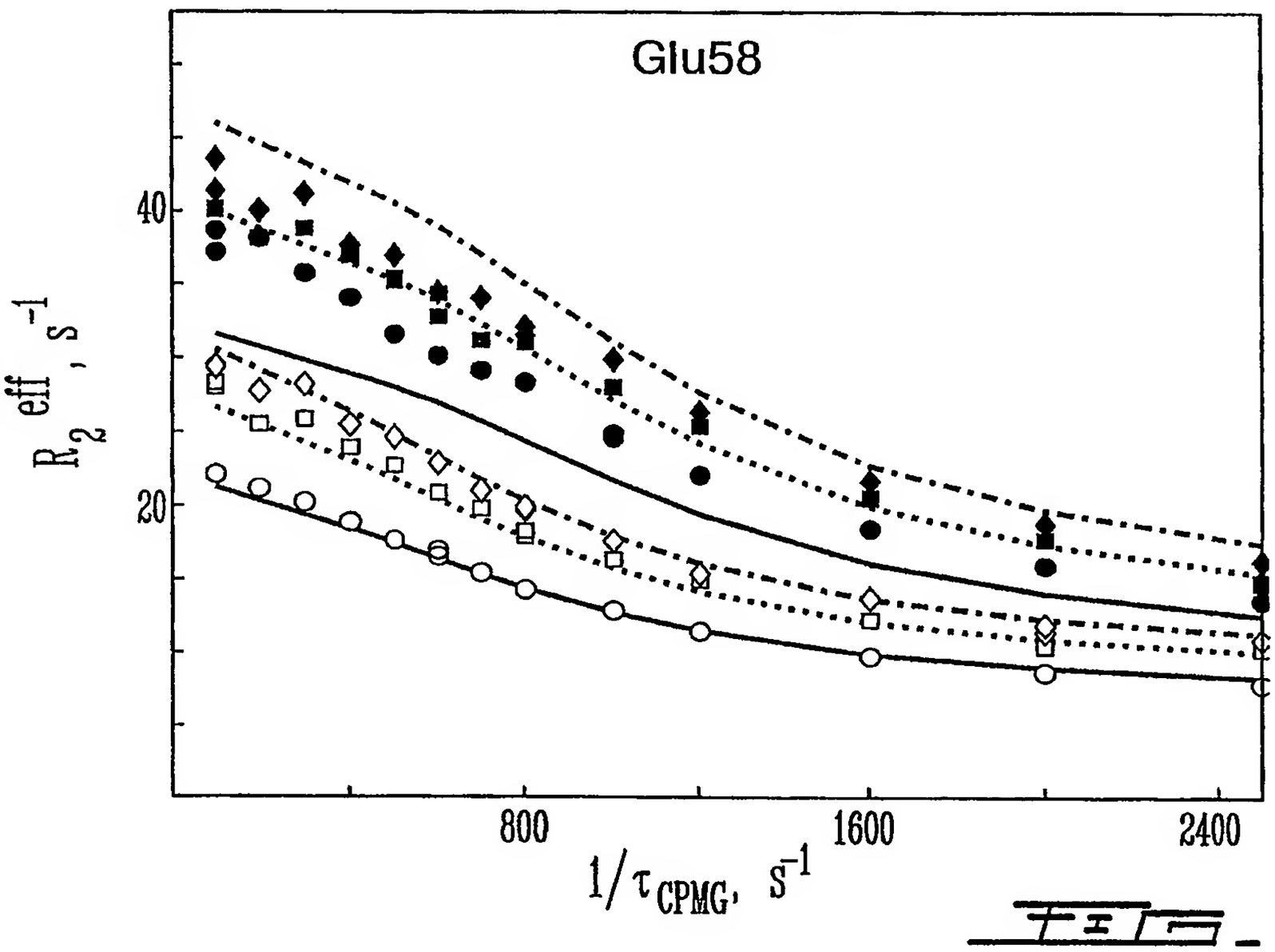
Glu58
40
20
$R_2$ eff , $s^{-1}$
800
1600
2400
$1/\tau_{CPMG}$, $s^{-1}$

FIG_4C

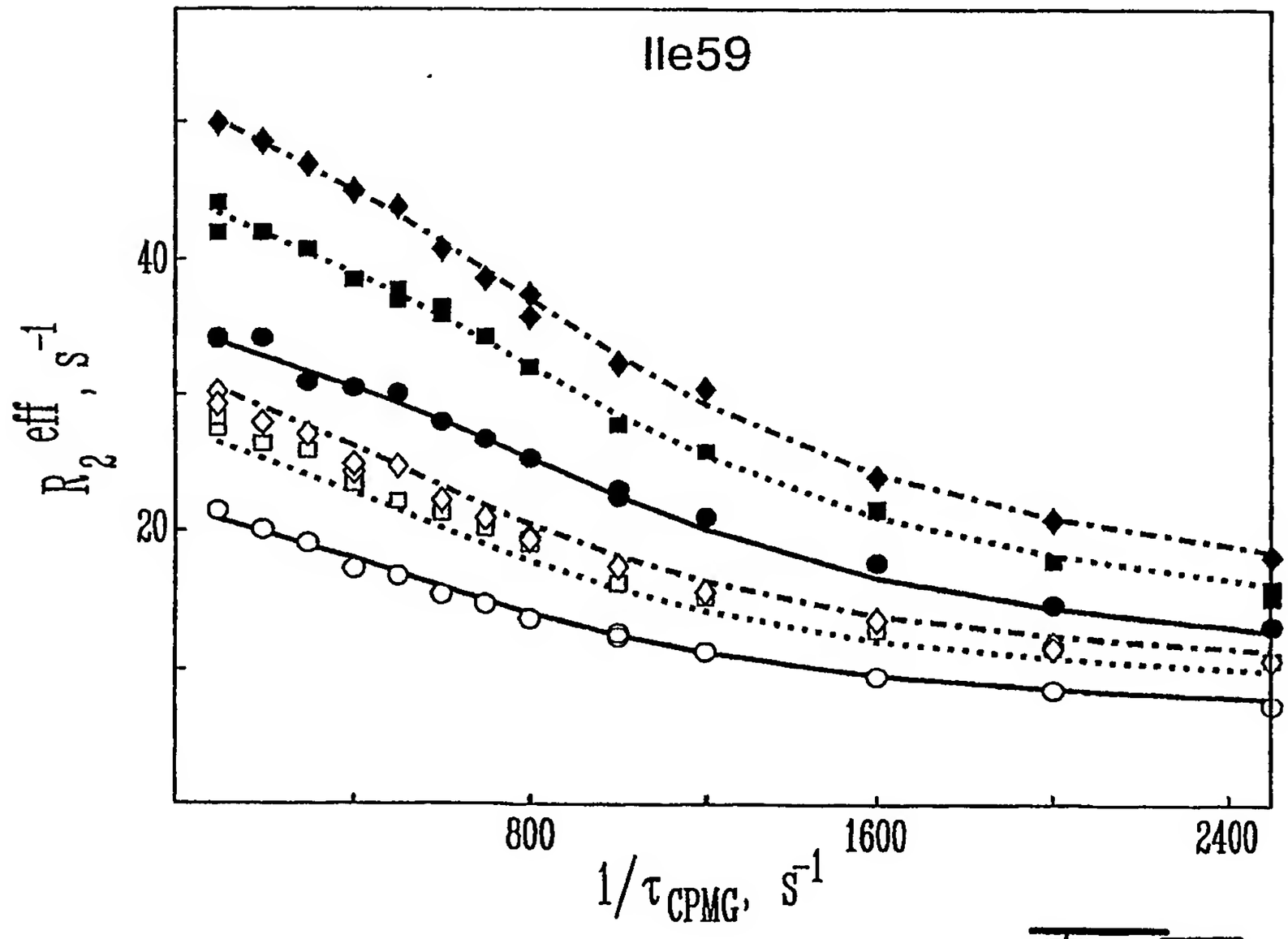
Ile59
40
20
$R_2$ eff , $s^{-1}$
800
1600
2400
$1/\tau_{CPMG}$, $s^{-1}$

FIG_4D

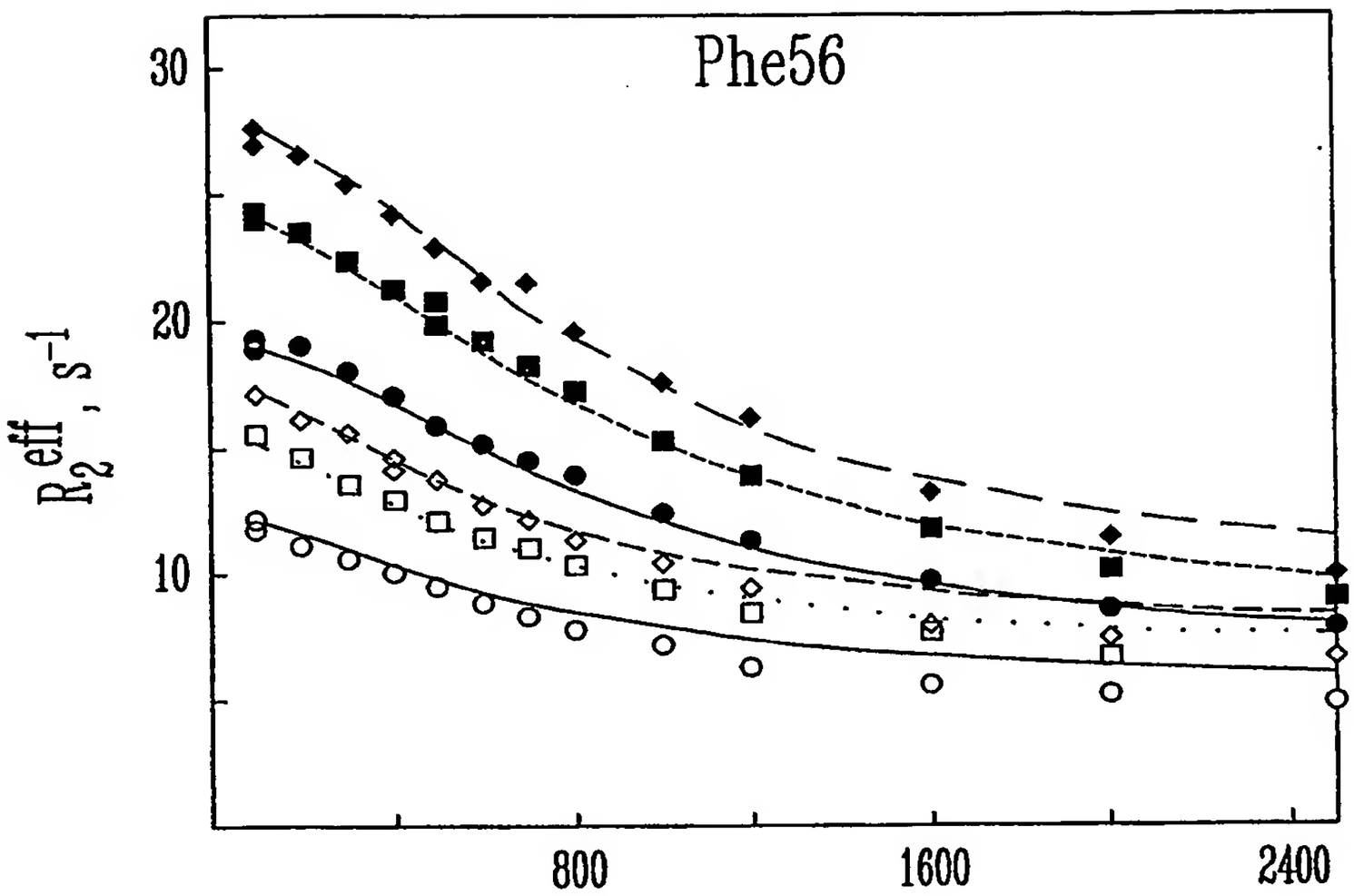
Phe56
30
20
10
800
1600
2400
$R_2^{eff}$, $s^{-1}$
$1/\tau_{CPMG}$, $s^{-1}$

FIG_5A

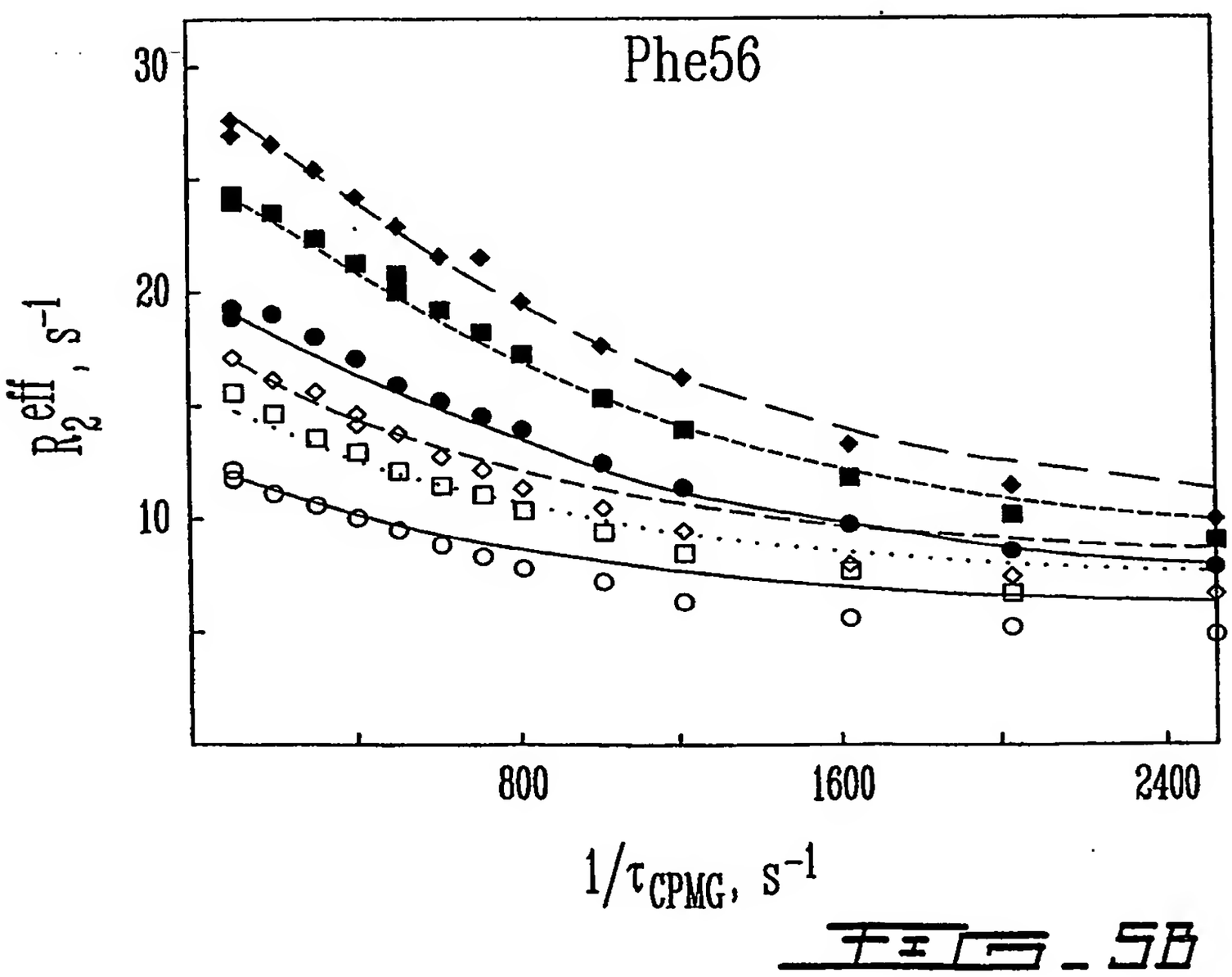
Phe56
30
20
10
800
1600
2400
$R_2^{eff}$, $s^{-1}$
$1/\tau_{CPMG}$, $s^{-1}$

FIG_5B

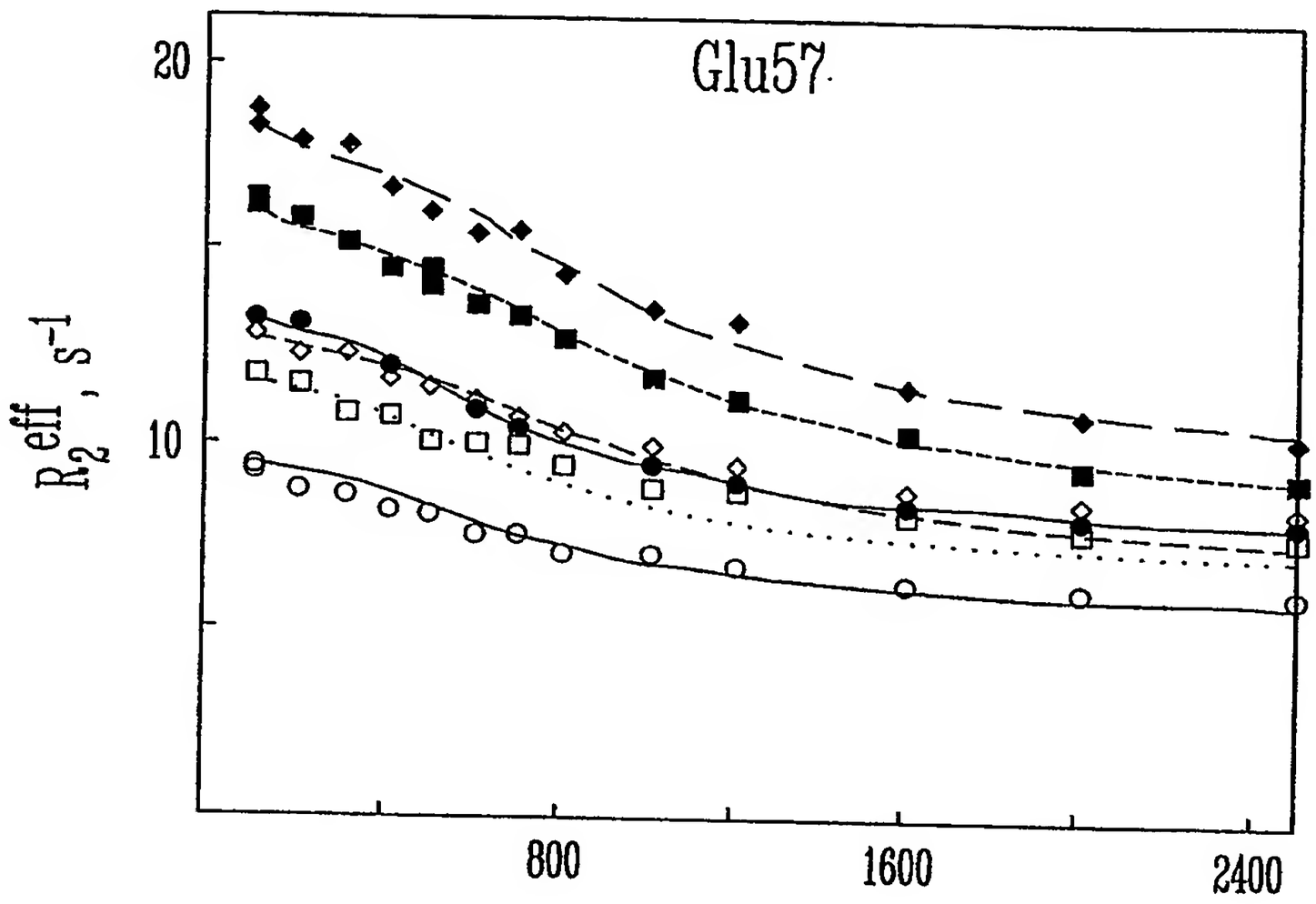
Glu57
20
10
$R_2^{eff}$, $s^{-1}$
800
1600
2400
$1/\tau_{CPMG}$, $s^{-1}$

Fig_5C

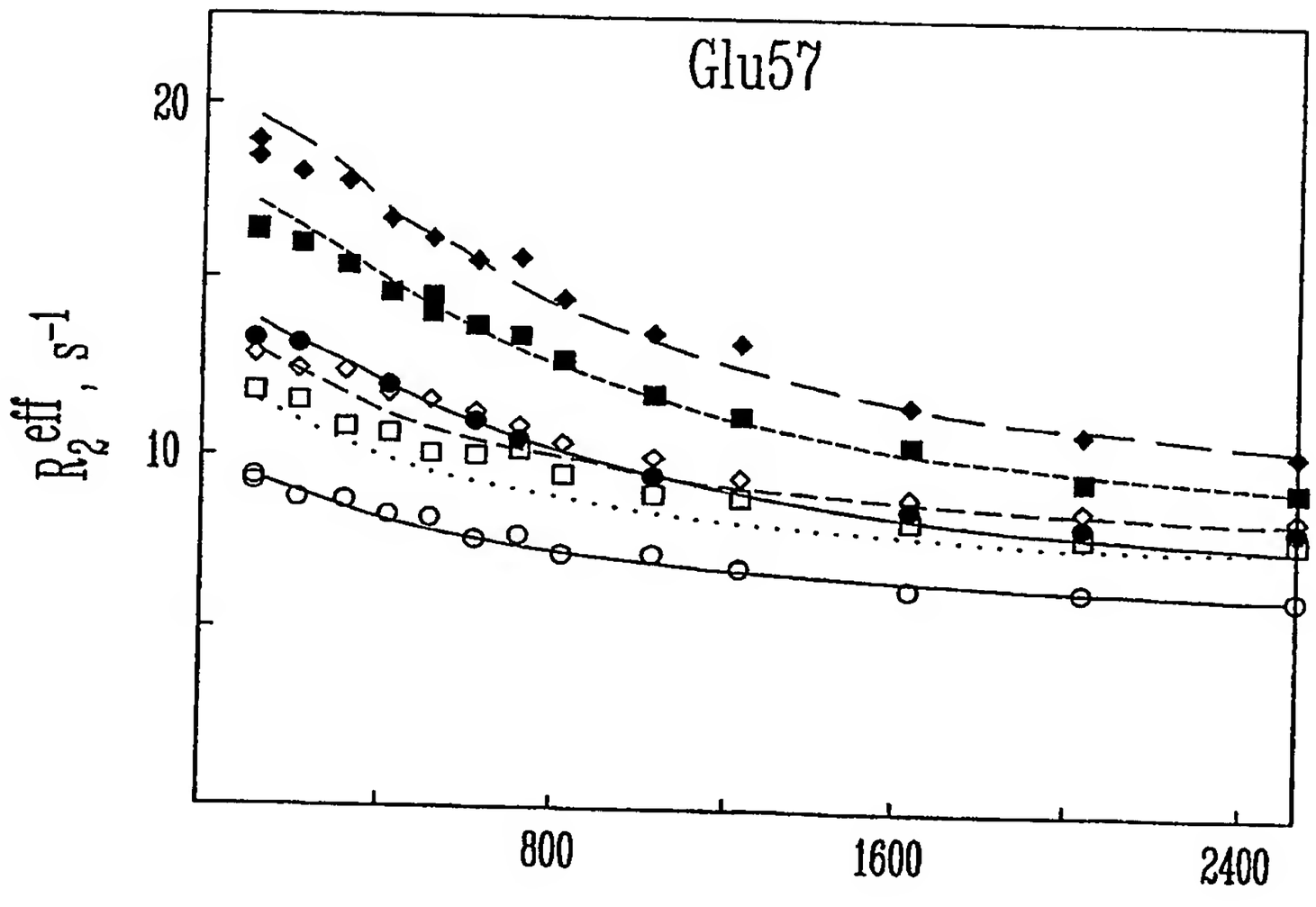
Glu57
20
10
$R_2^{eff}$, $s^{-1}$
800
1600
2400
$1/\tau_{CPMG}$, $s^{-1}$

Fig_5D

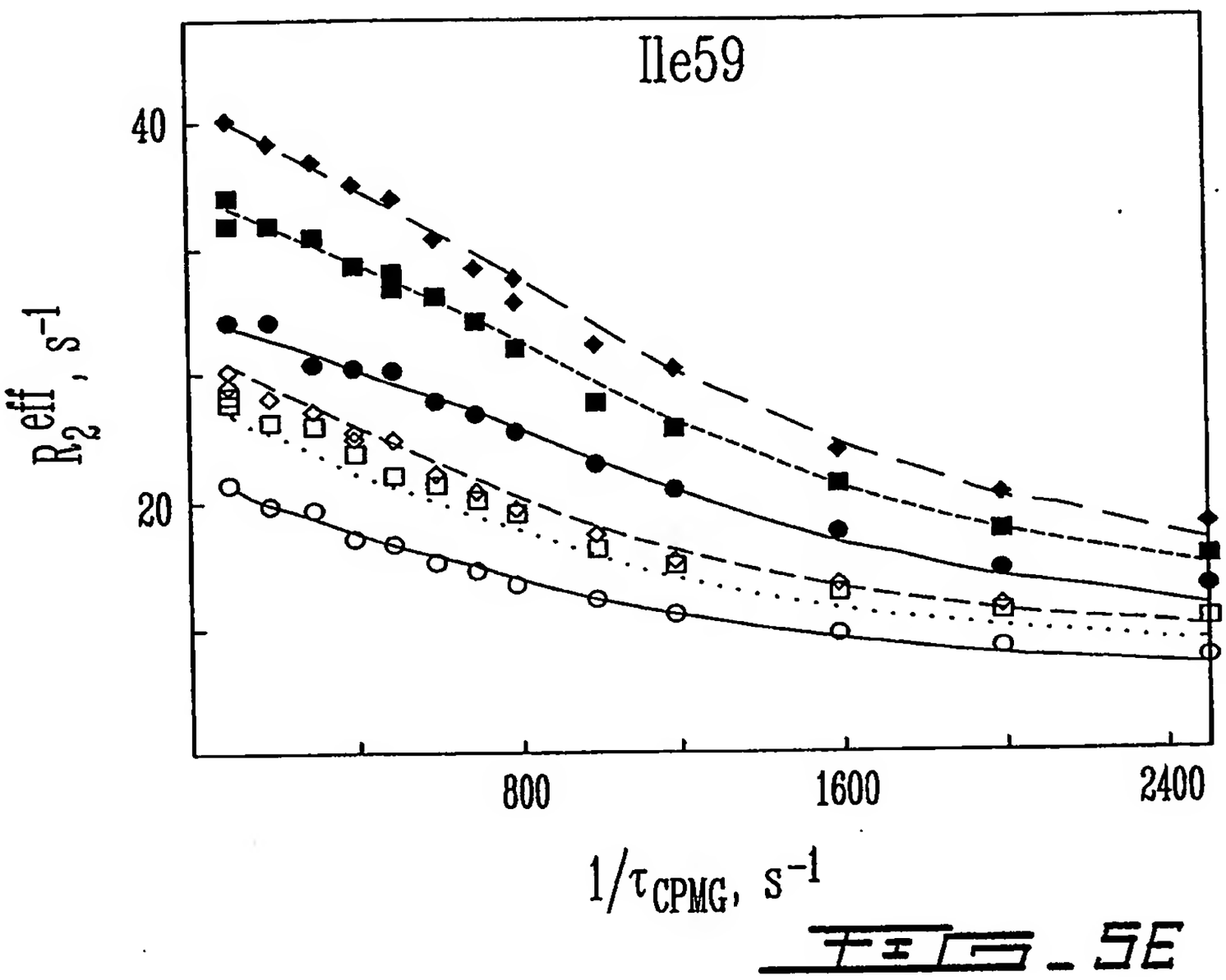
Ile59
40
20
800
1600
2400
$R_2^{eff}$, $s^{-1}$
$1/\tau_{CPMG}$, $s^{-1}$

FIG_5E

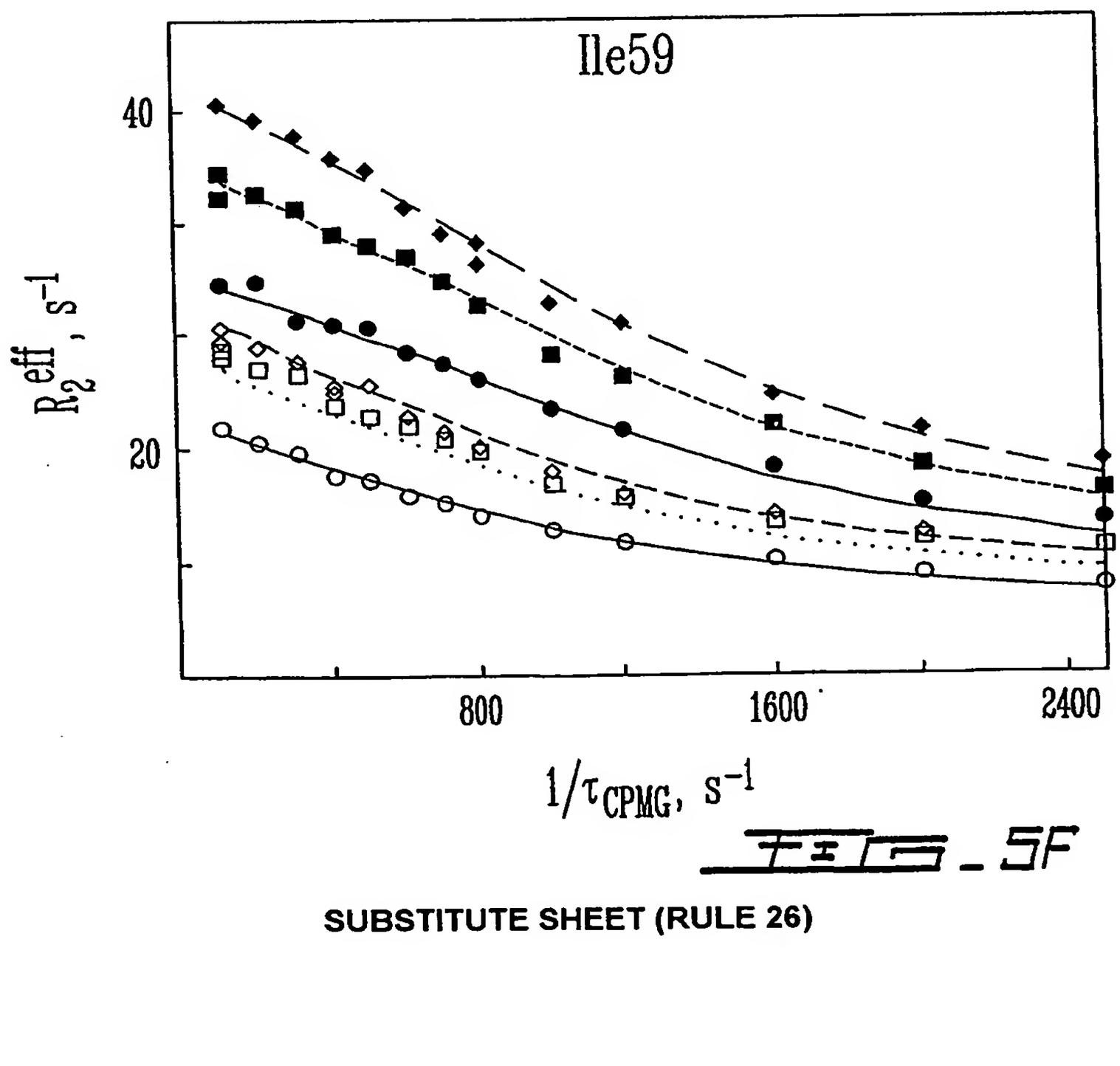
Ile59
40
20
800
1600
2400
$R_2^{eff}$, $s^{-1}$
$1/\tau_{CPMG}$, $s^{-1}$

FIG_5F

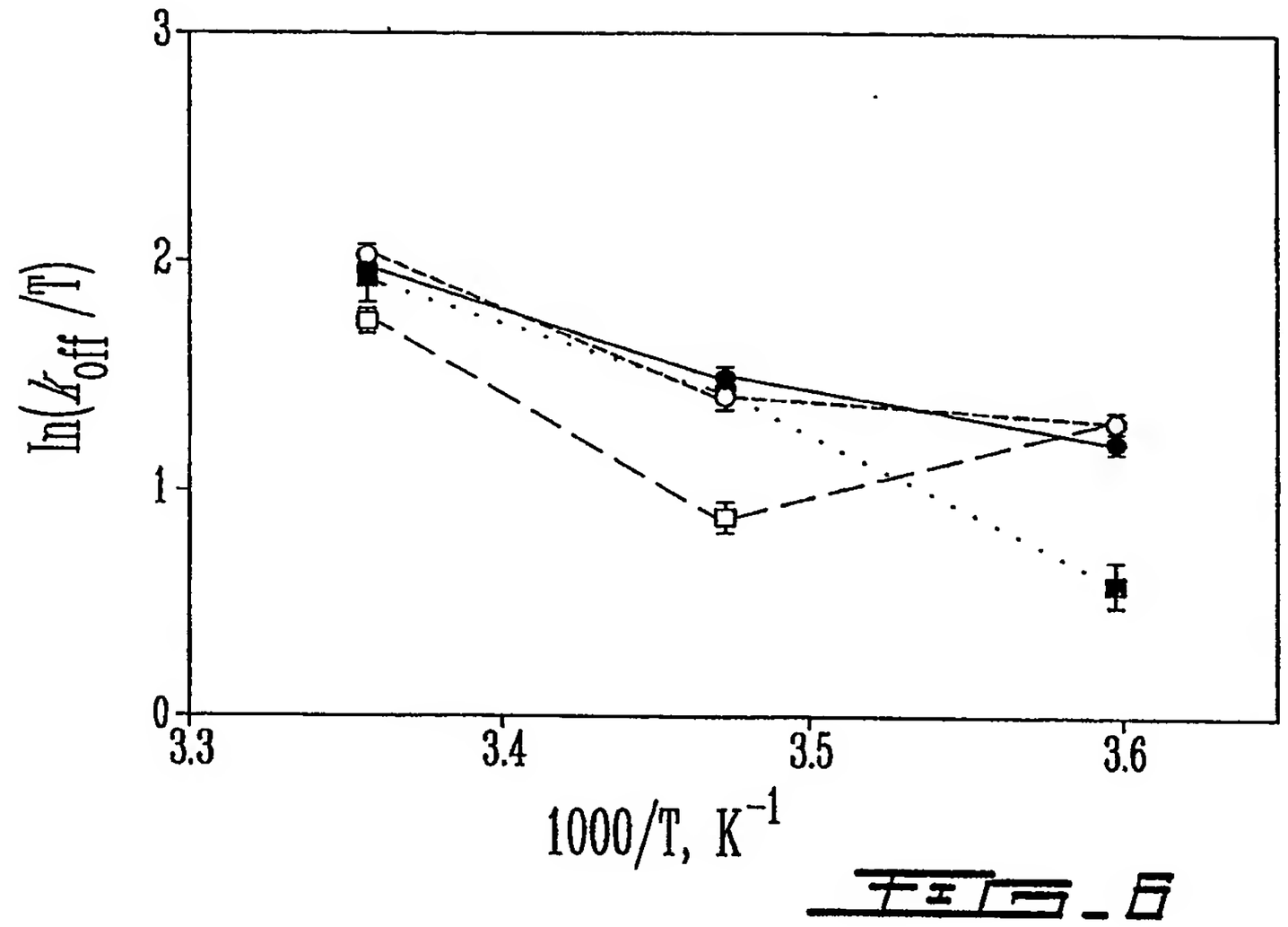
3
2
1
0
3.3
3.4
3.5
3.6
ln(k_off /T)
1000/T, K^-1

Fig_6

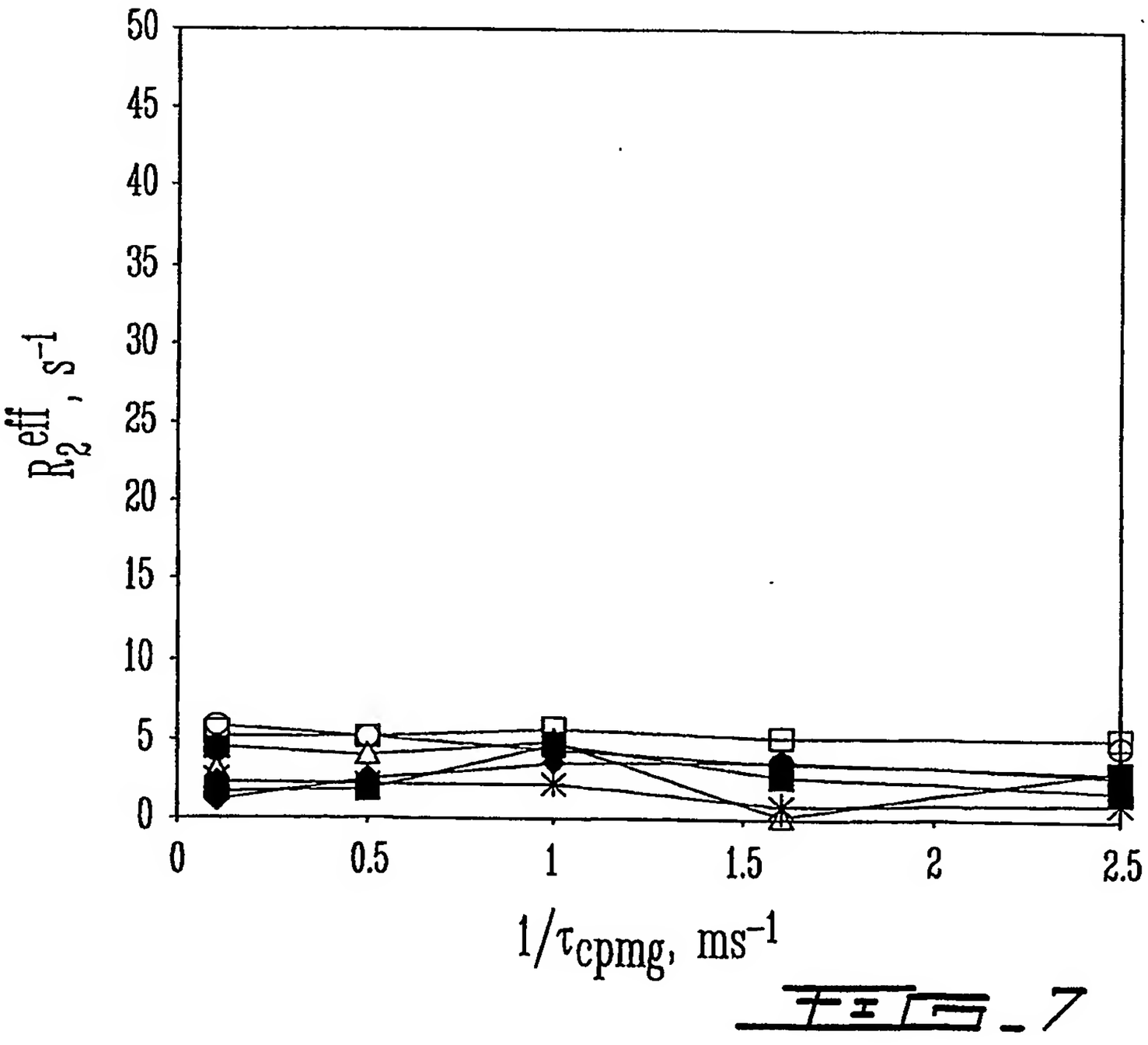
50
45
40
35
30
25
20
15
10
5
0
0
0.5
1
1.5
2
2.5
R2eff, s-1
1/τcpmg, ms-1

Fig_7

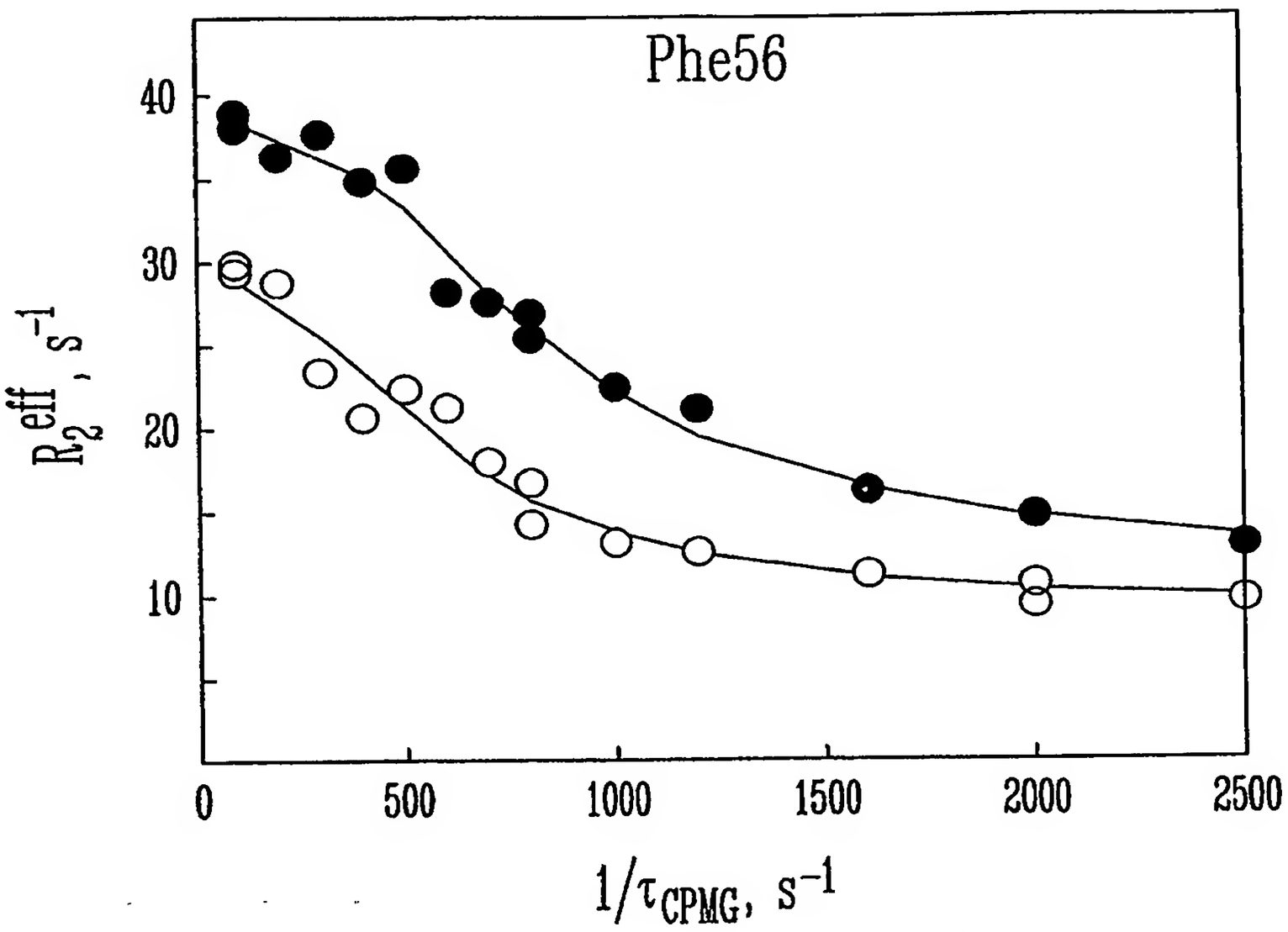
Phe56
40
30
20
10
0
500
1000
1500
2000
2500
$R_2^{eff}$, $s^{-1}$
$1/\tau_{CPMG}$, $s^{-1}$

FIG_8A

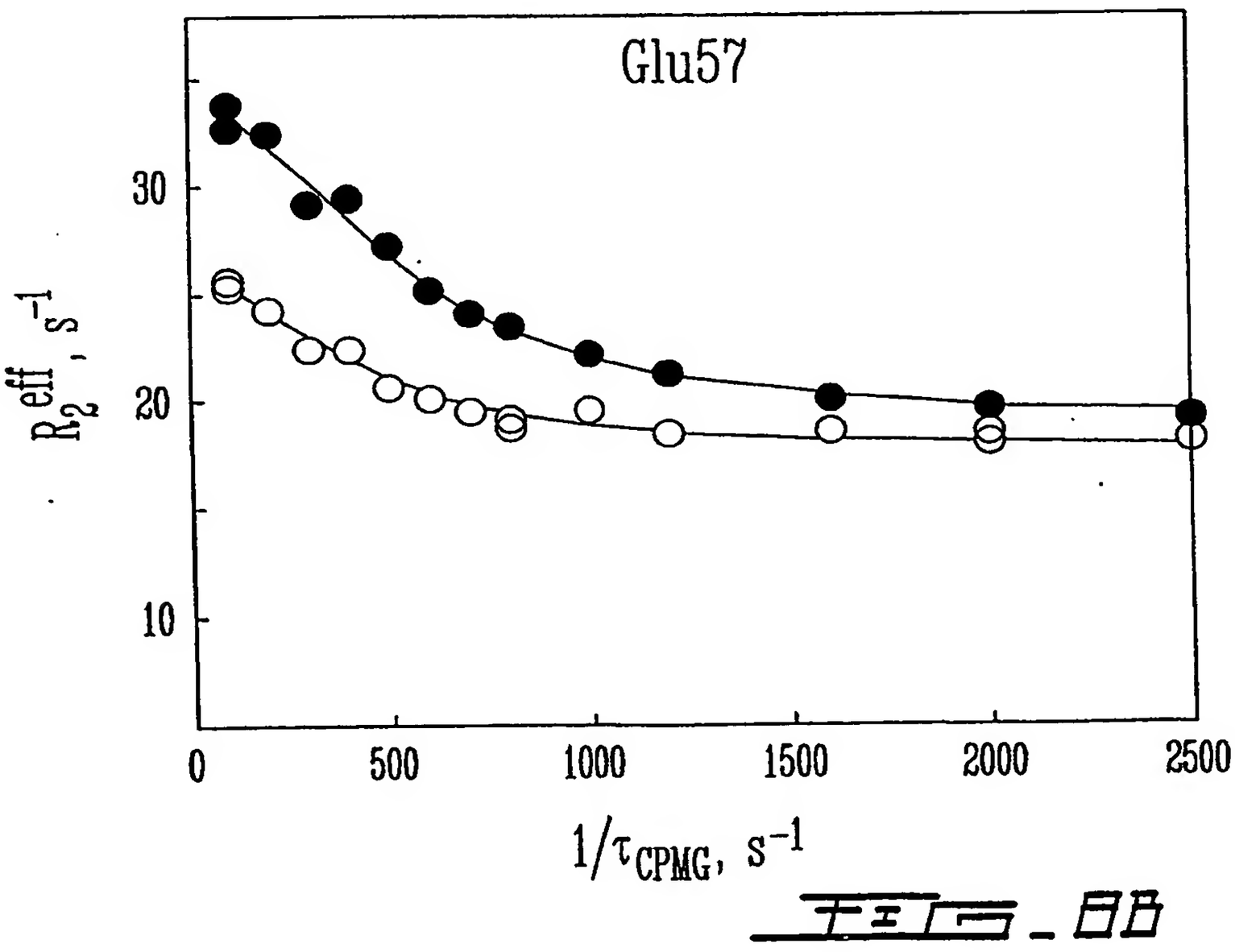
Glu57
30
20
10
0
500
1000
1500
2000
2500
$R_2^{eff}$, $s^{-1}$
$1/\tau_{CPMG}$, $s^{-1}$

FIG_8B

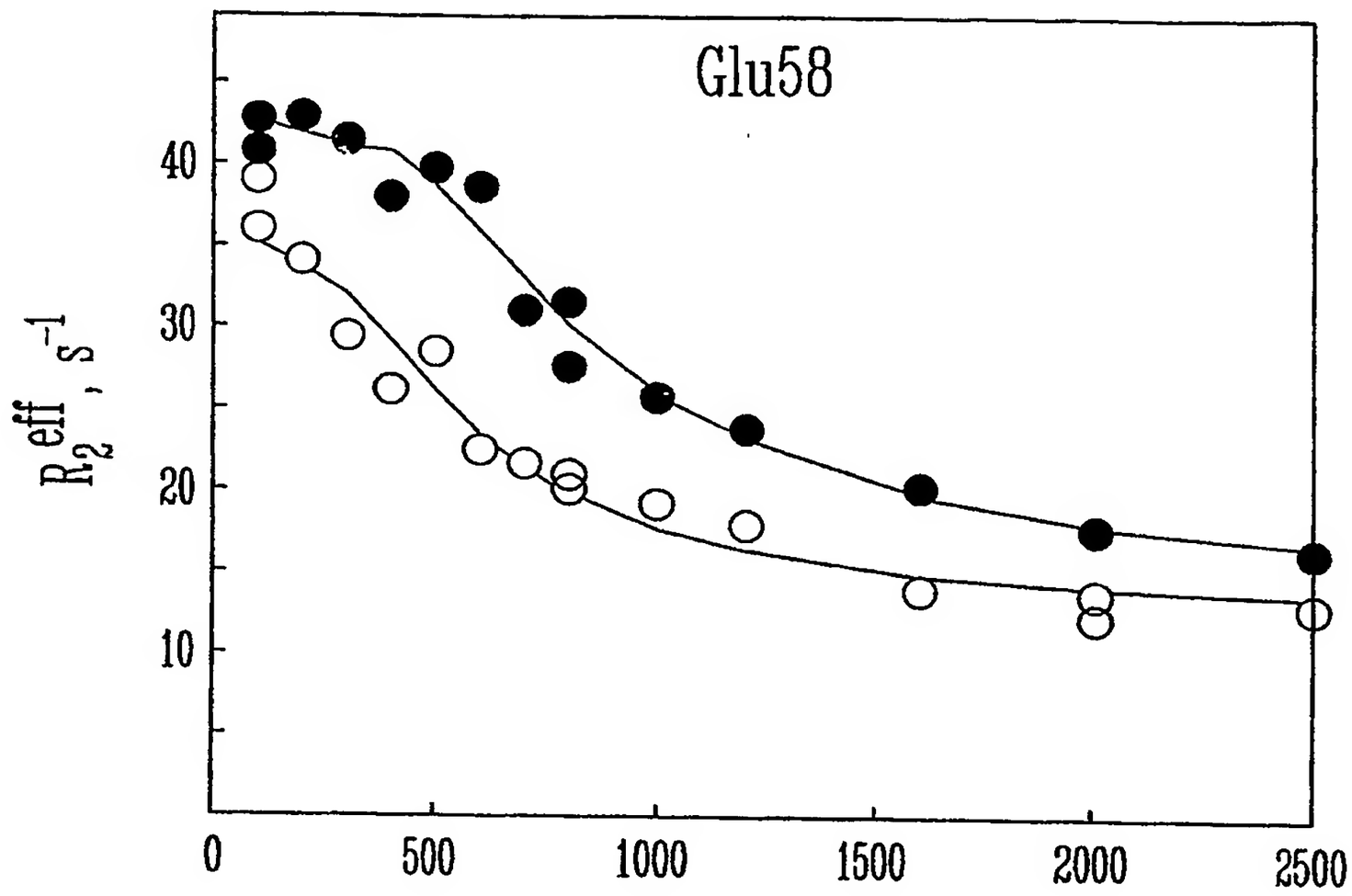
Glu58
40
30
20
10
0
500
1000
1500
2000
2500
$R_2^{eff}$, $s^{-1}$
$1/\tau_{CPMG}$, $s^{-1}$

Fig. 8C

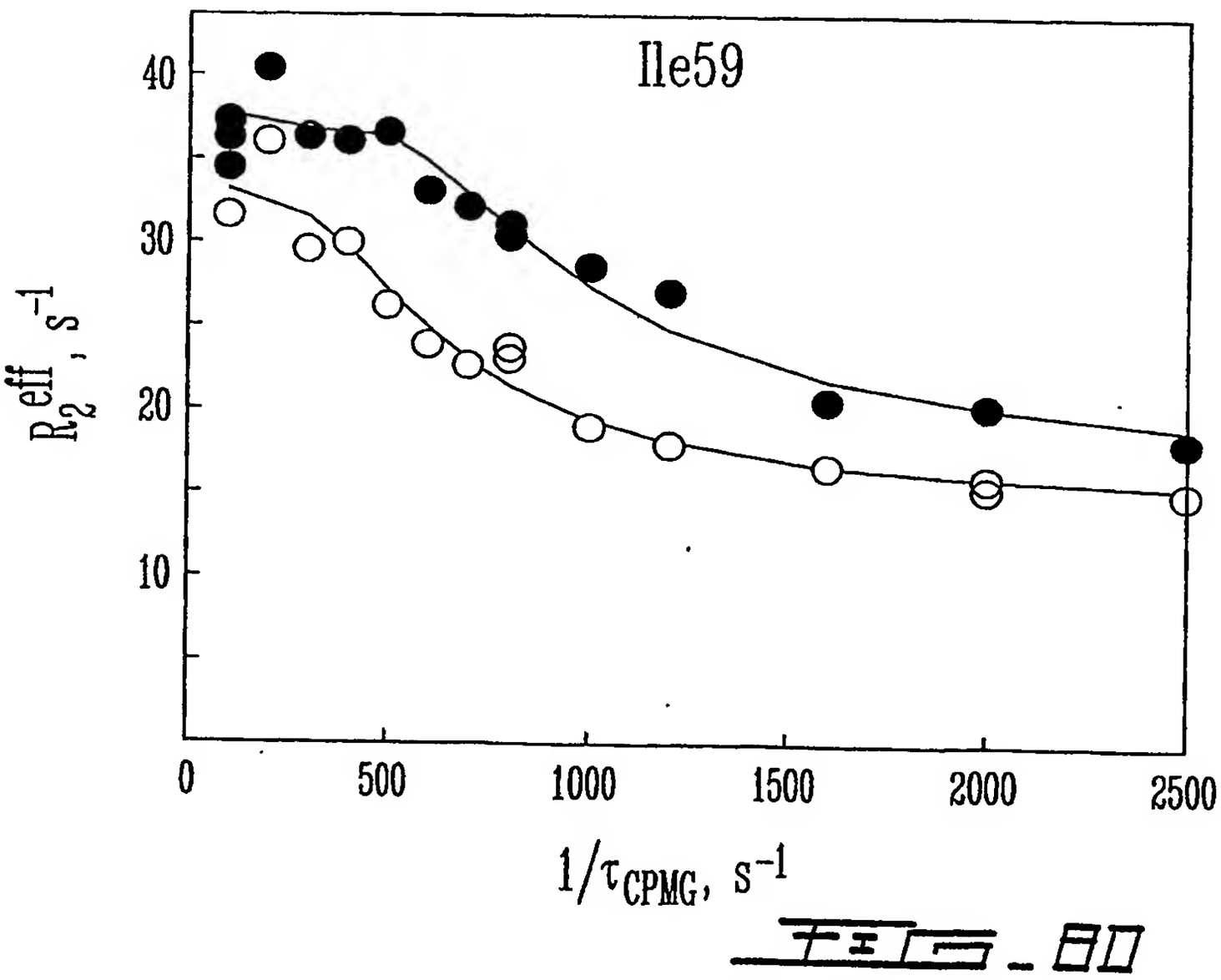
Ile59
40
30
20
10
0
500
1000
1500
2000
2500
$R_2^{eff}$, $s^{-1}$
$1/\tau_{CPMG}$, $s^{-1}$

Fig. 8D

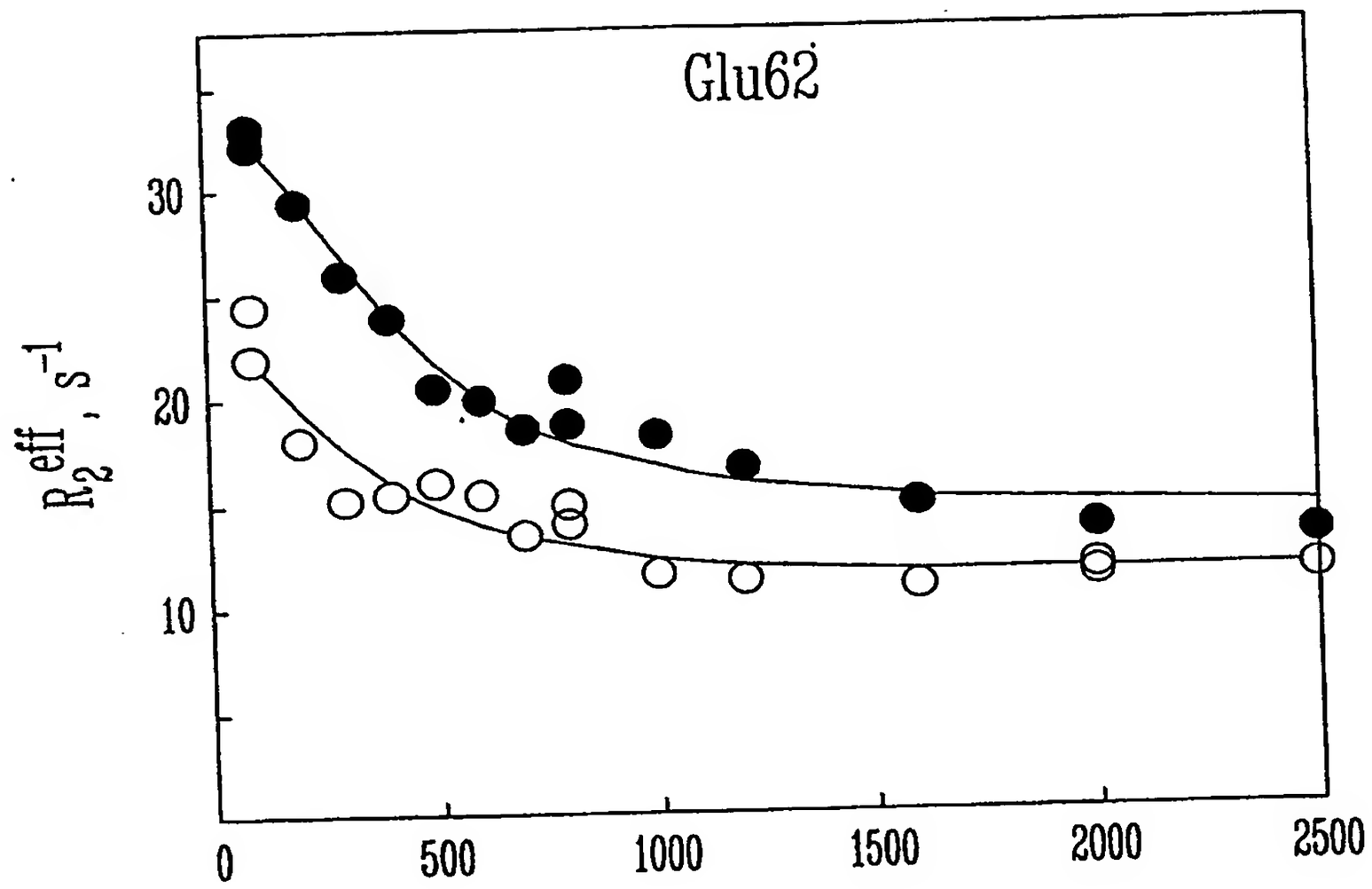
Glu62
30
20
10
0
500
1000
1500
2000
2500
$R_2^{eff}$, $s^{-1}$
$1/\tau_{CPMG}$, $s^{-1}$

FIG_8E

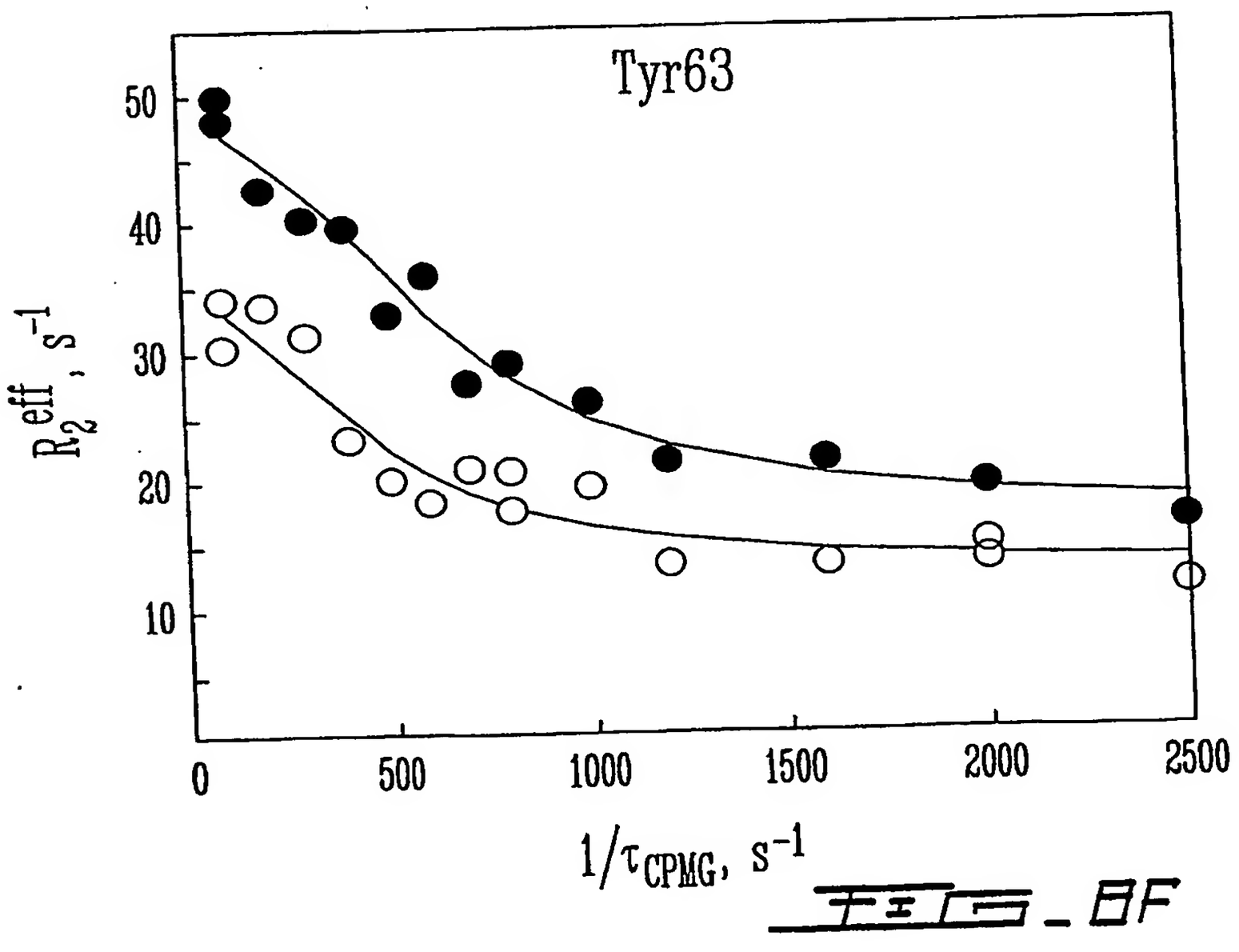
Tyr63
50
40
30
20
10
0
500
1000
1500
2000
2500
$R_2^{eff}$, $s^{-1}$
$1/\tau_{CPMG}$, $s^{-1}$

FIG_8F

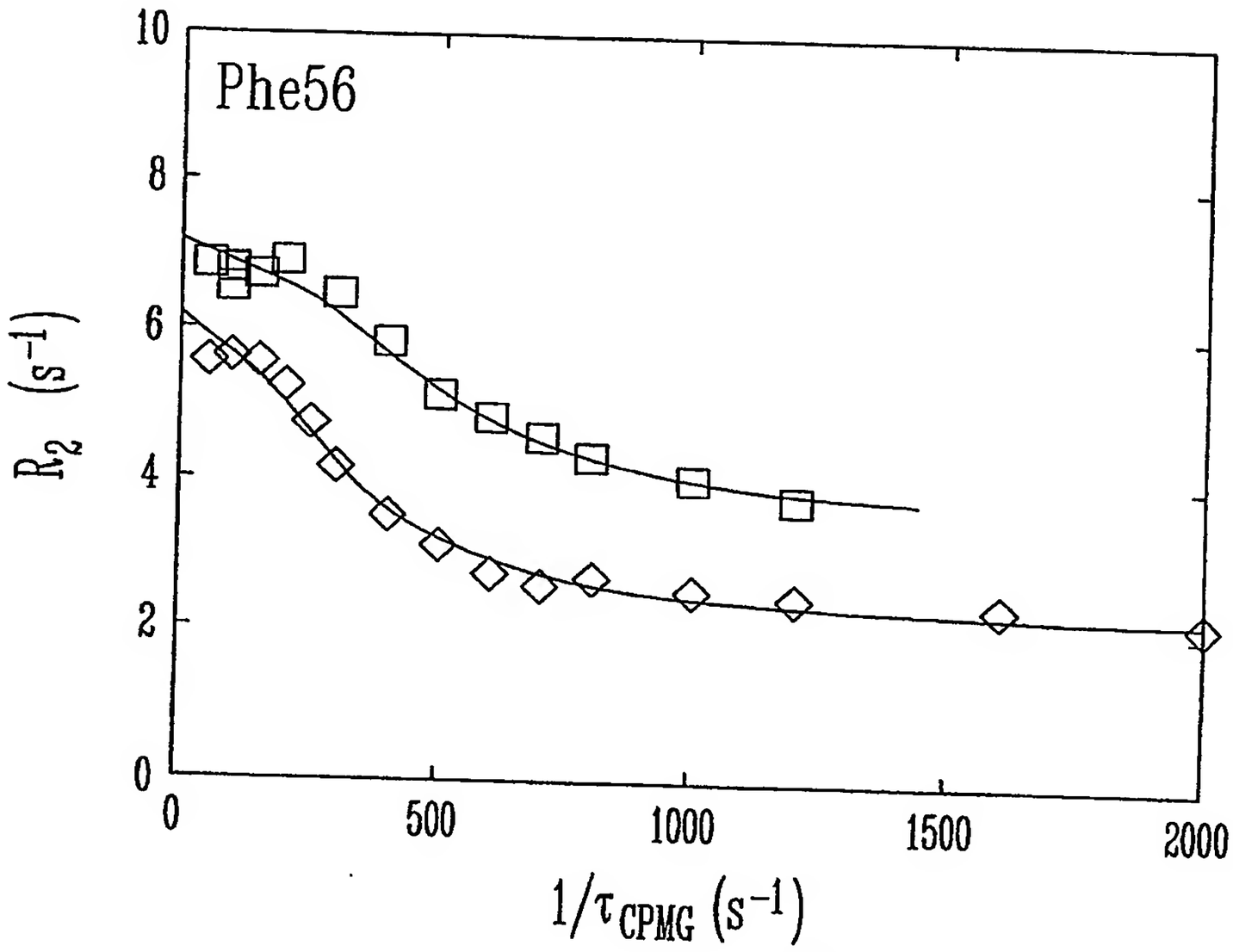
Phe56
10
8
6
4
2
0
0
500
1000
1500
2000
$R_2$ $(s^{-1})$
$1/\tau_{CPMG}$ $(s^{-1})$

Fig. 9A

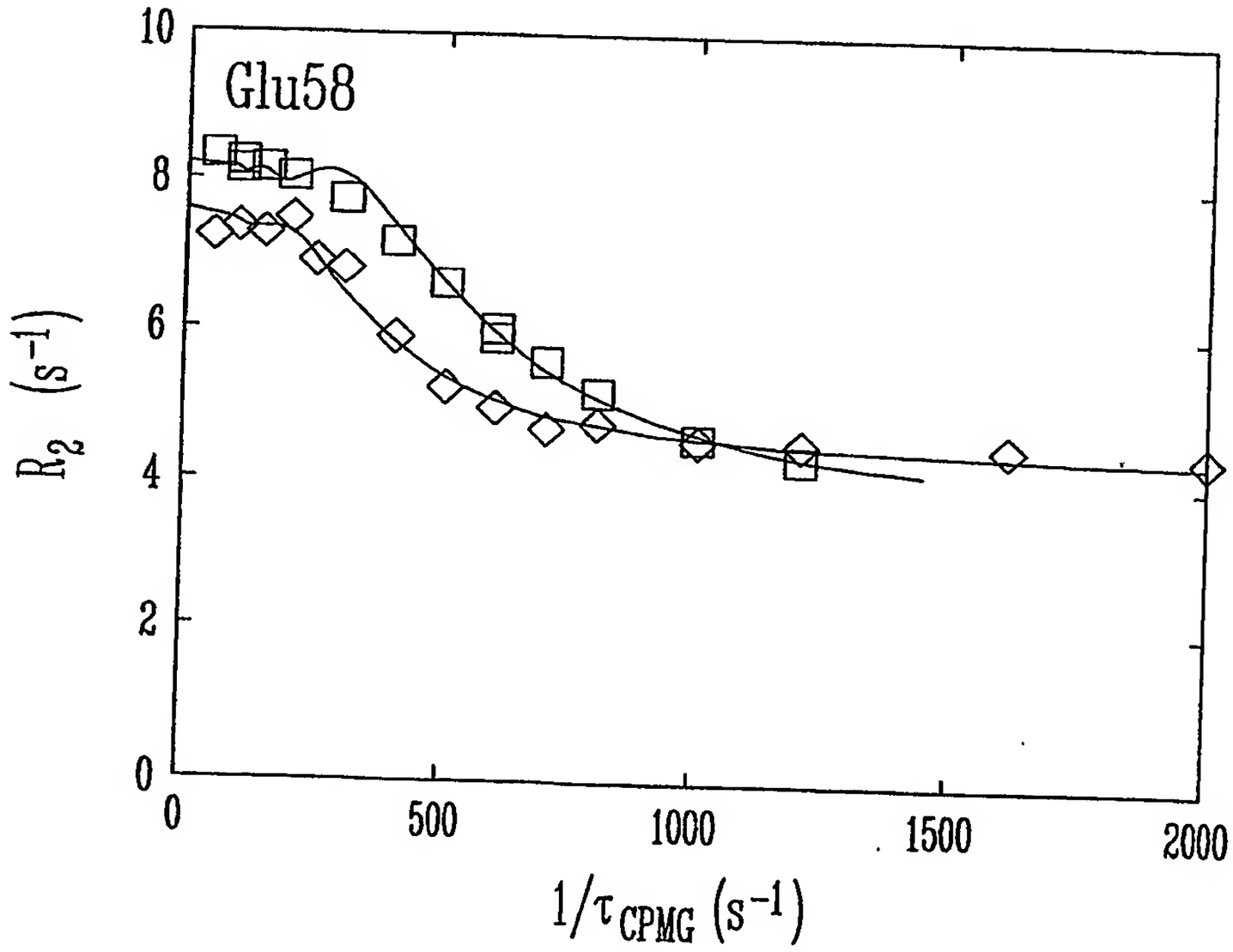
Glu58
10
8
6
4
2
0
0
500
1000
1500
2000
$R_2$ $(s^{-1})$
$1/\tau_{CPMG}$ $(s^{-1})$

Fig. 9B

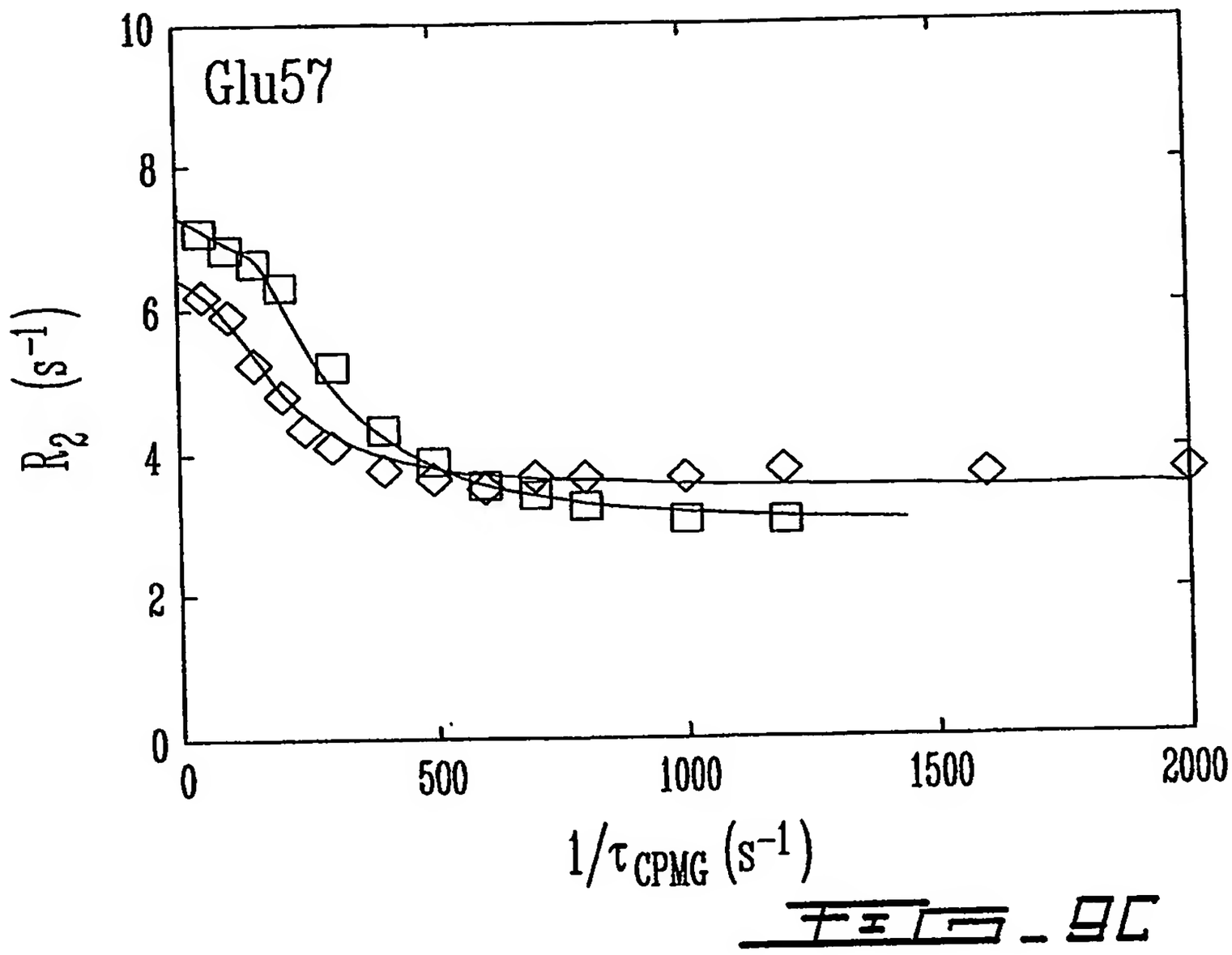
Glu57
10
8
6
4
2
0
0
500
1000
1500
2000
$R_2$ $(s^{-1})$
$1/\tau_{CPMG}$ $(s^{-1})$

FIG - 9C

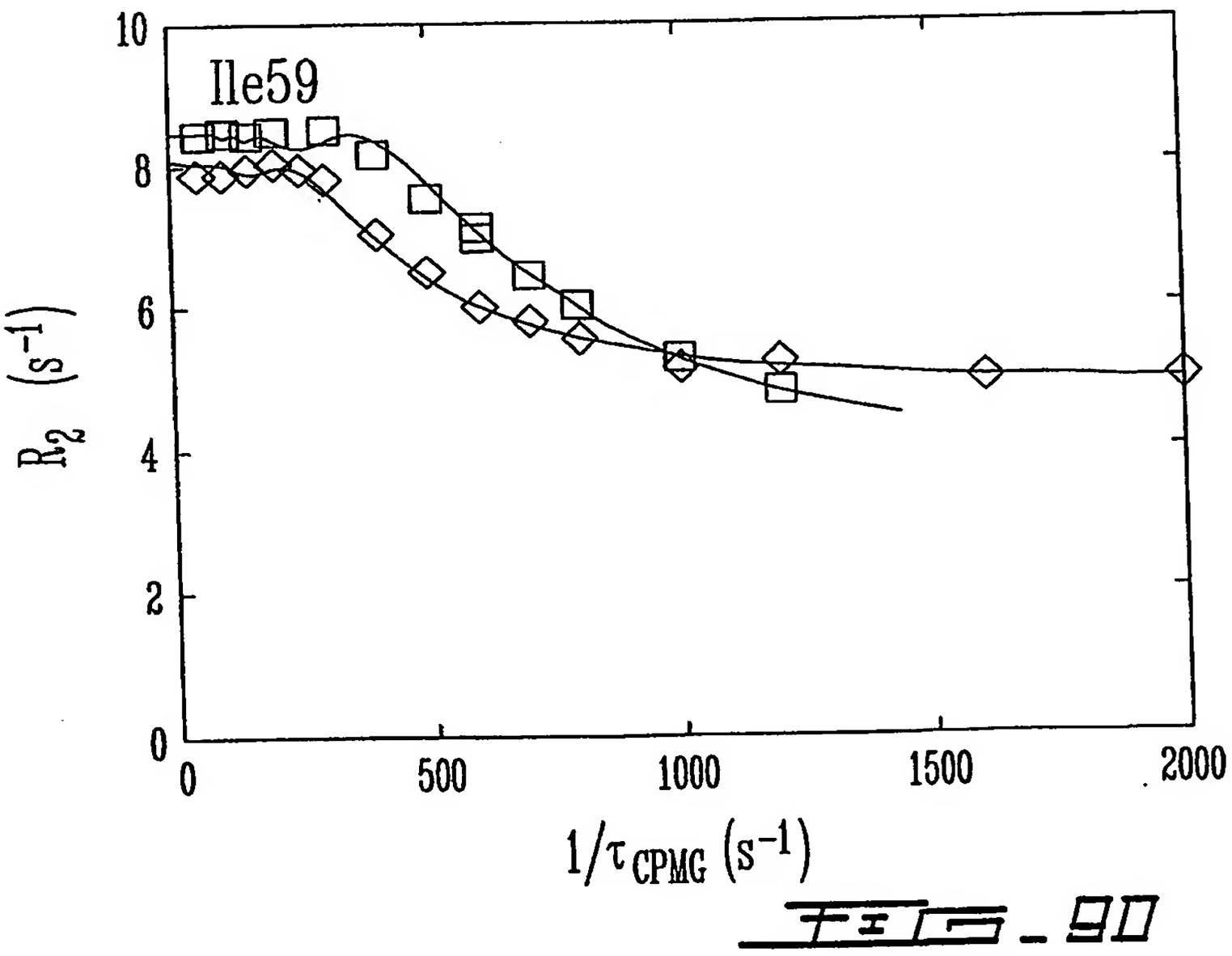
Ile59
10
8
6
4
2
0
0
500
1000
1500
2000
$R_2$ $(s^{-1})$
$1/\tau_{CPMG}$ $(s^{-1})$

FIG - 9D

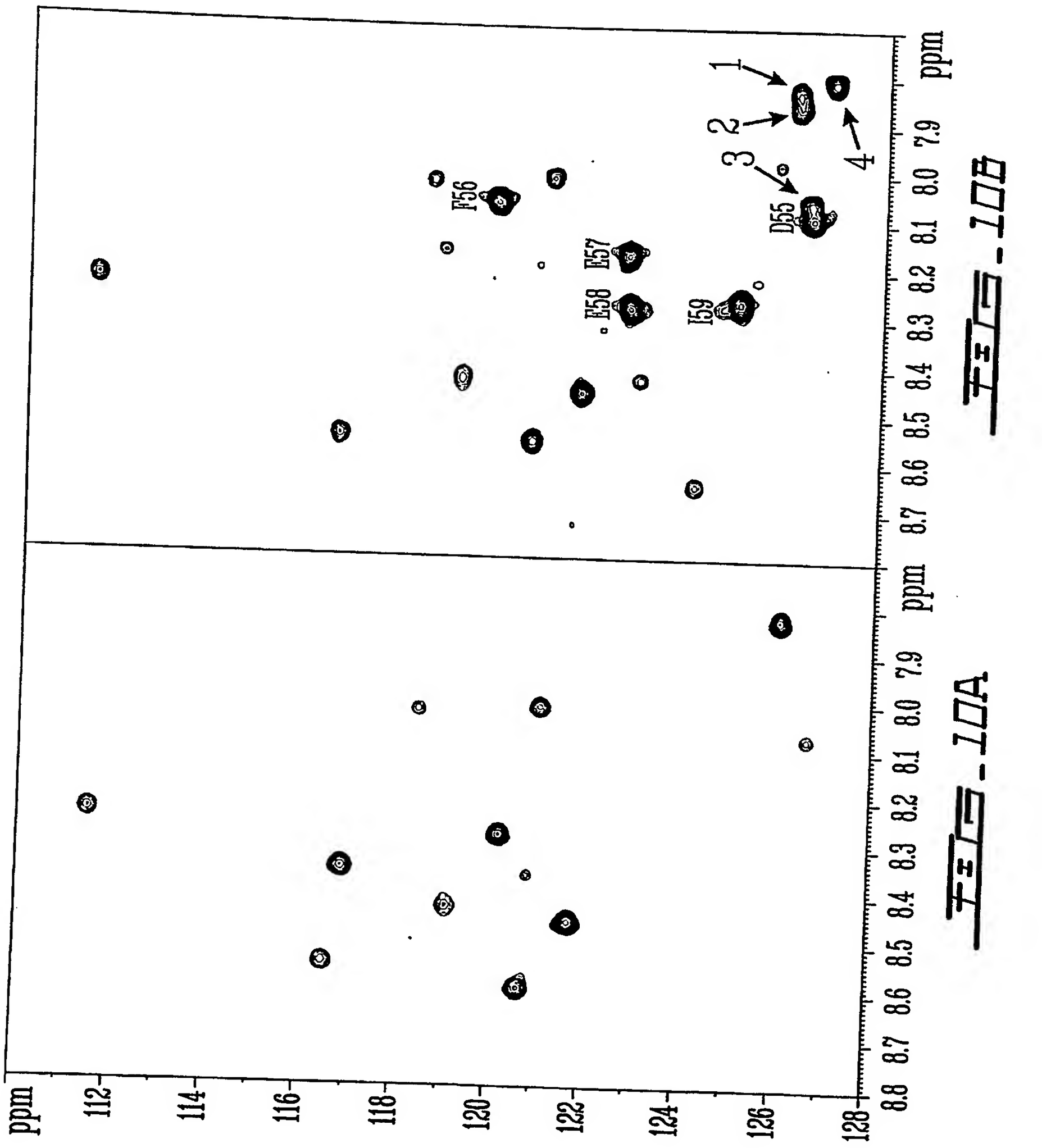


FIG-10B

FIG-10A

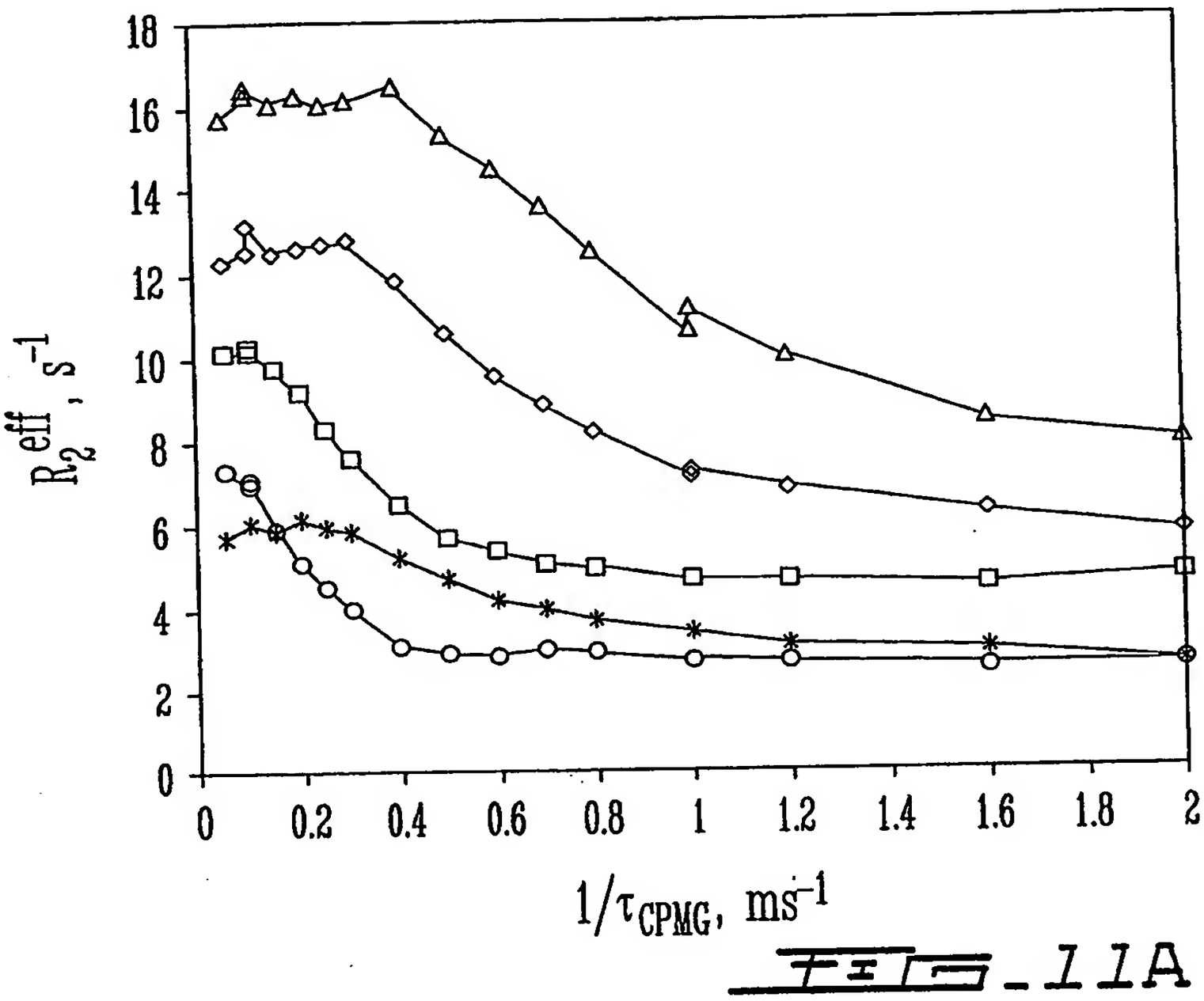


Fig_11A

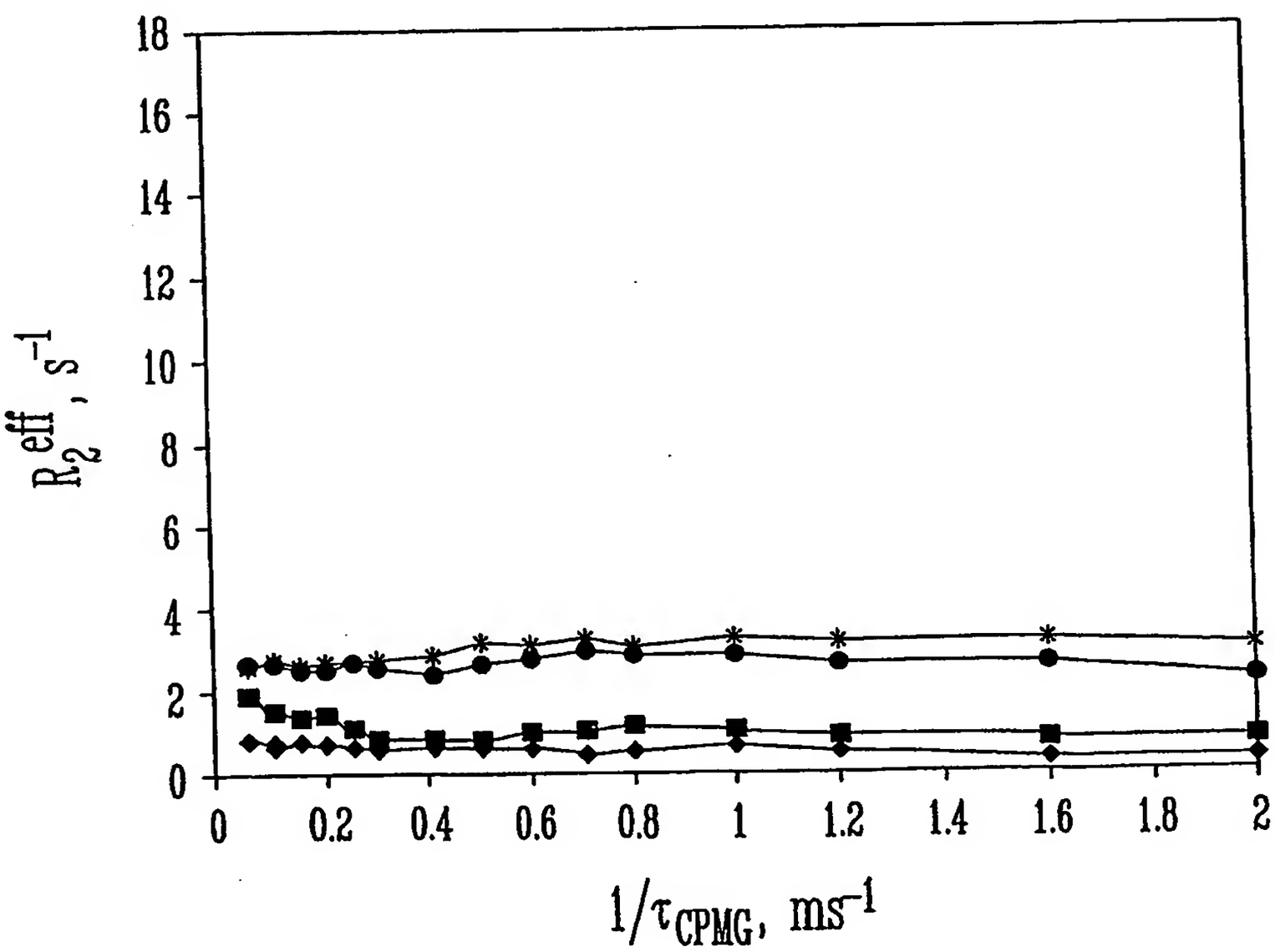


Fig_11B

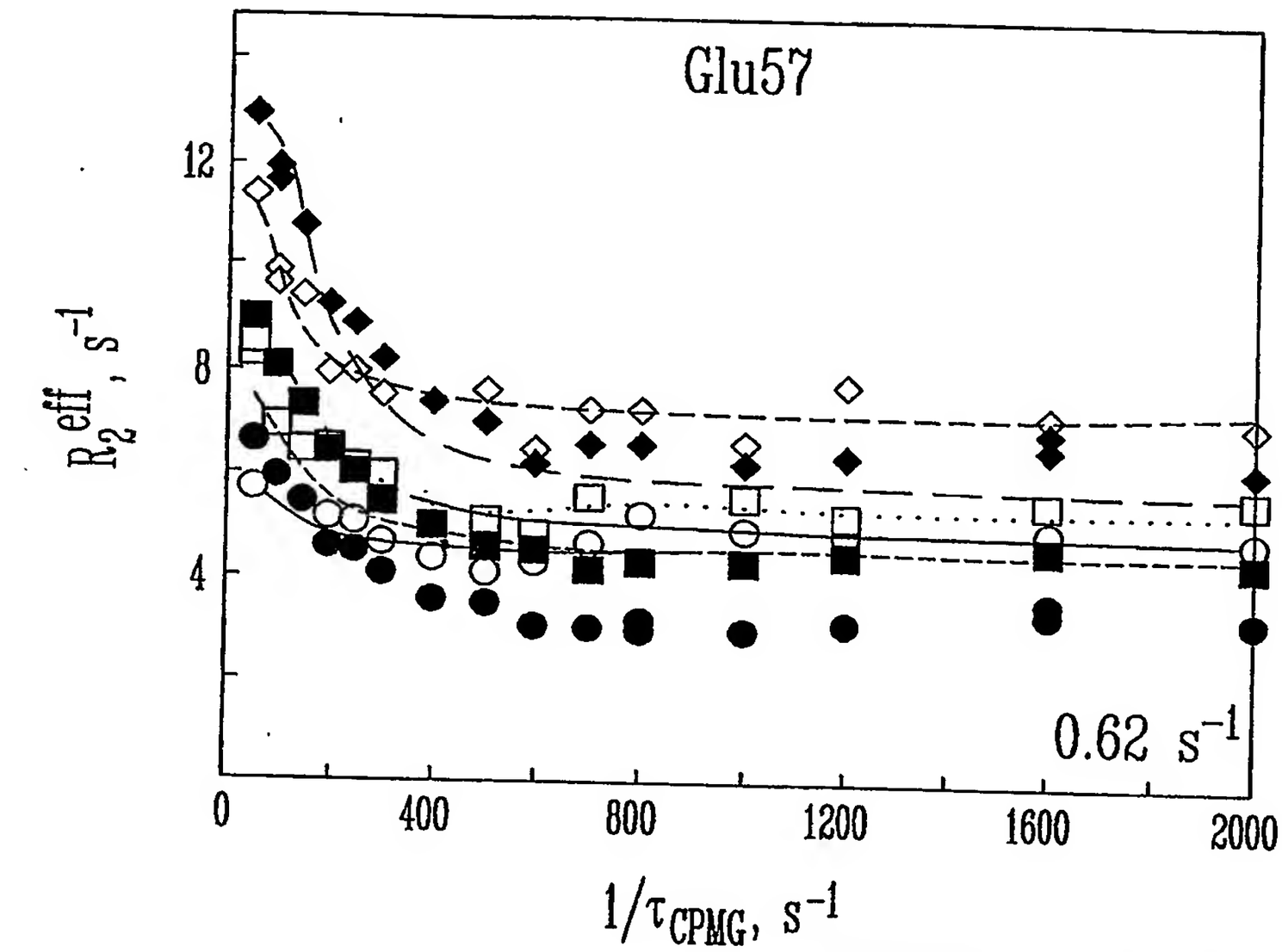


Fig. 12A

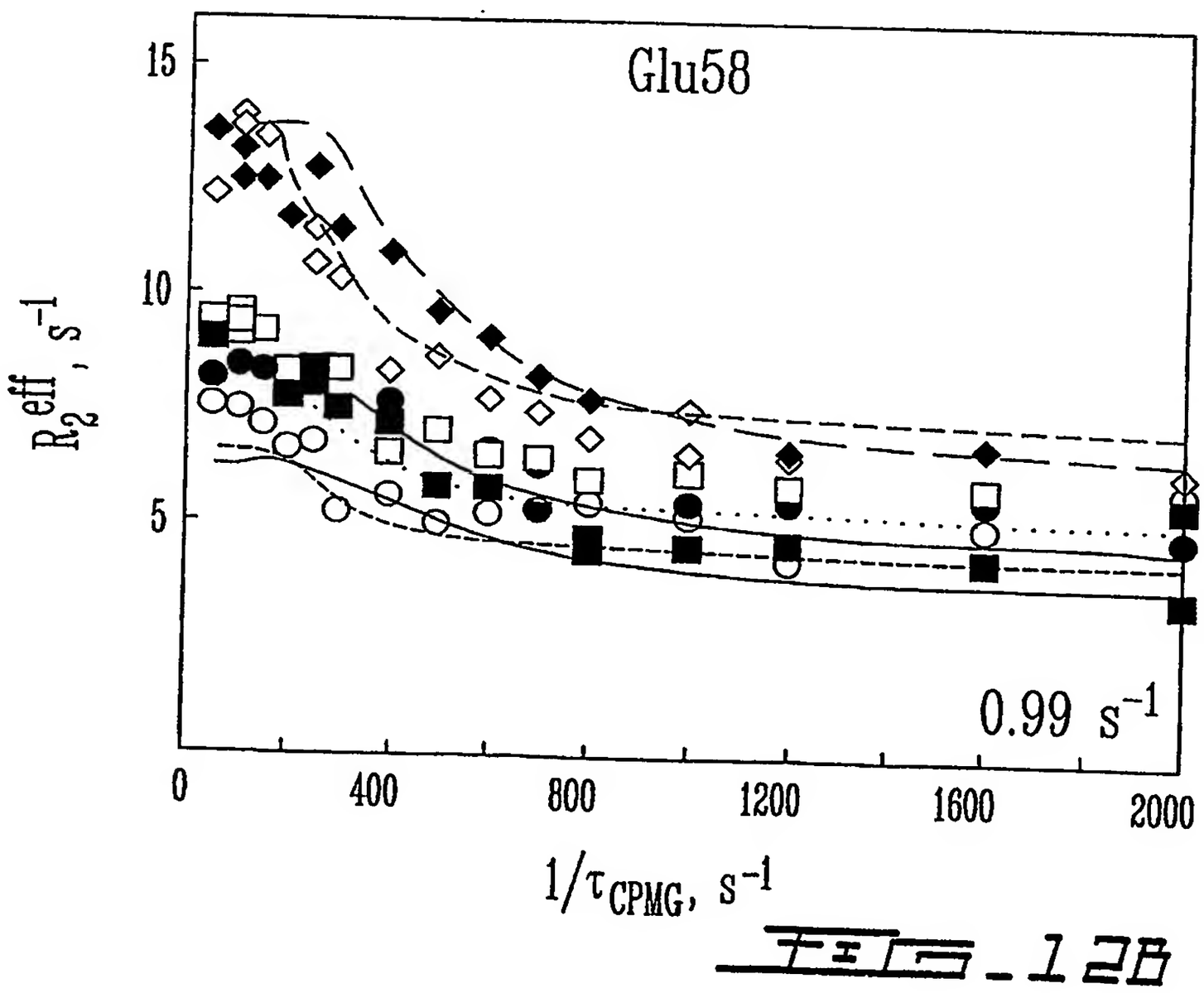


Fig. 12B

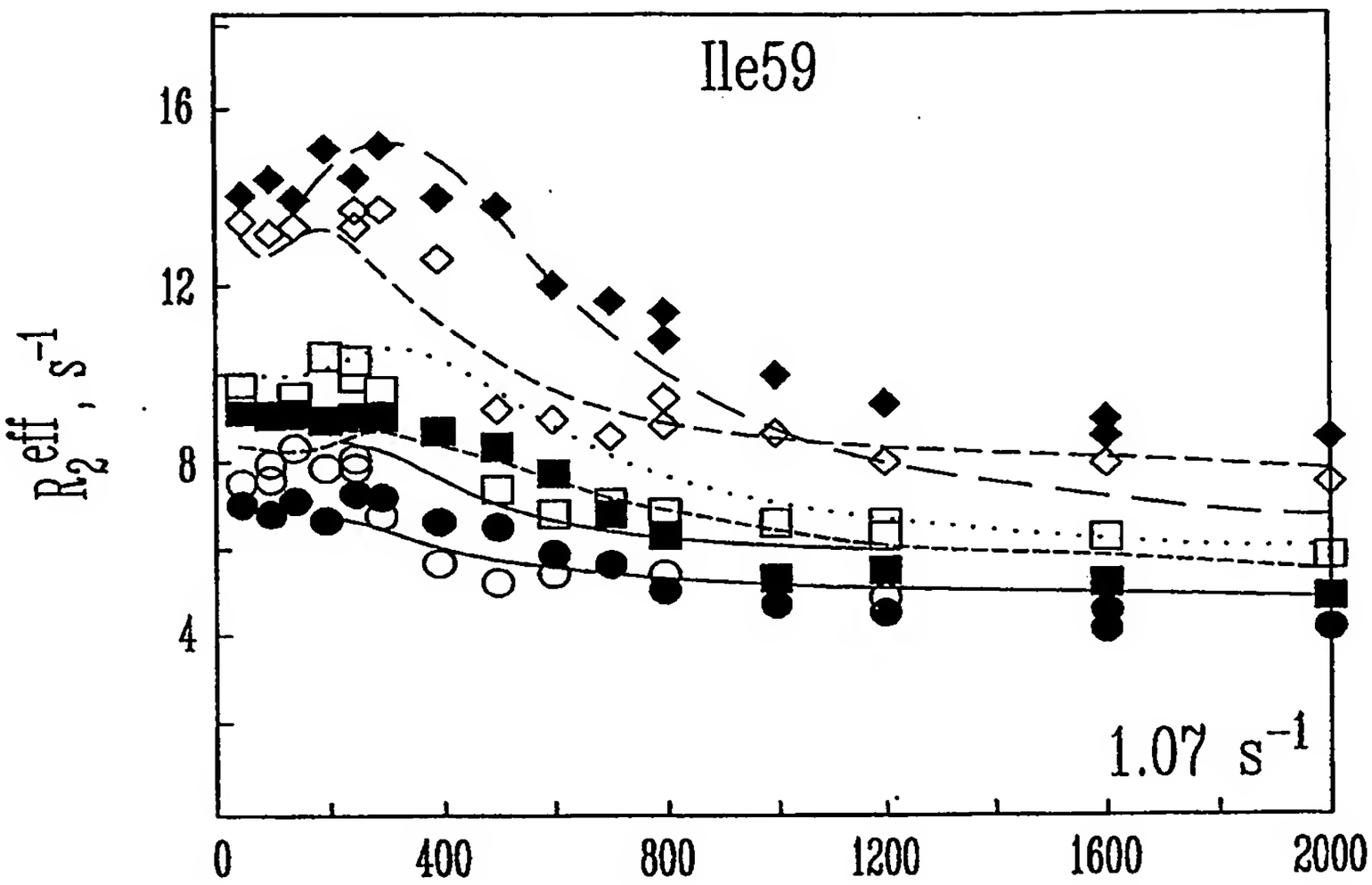


Fig-12C

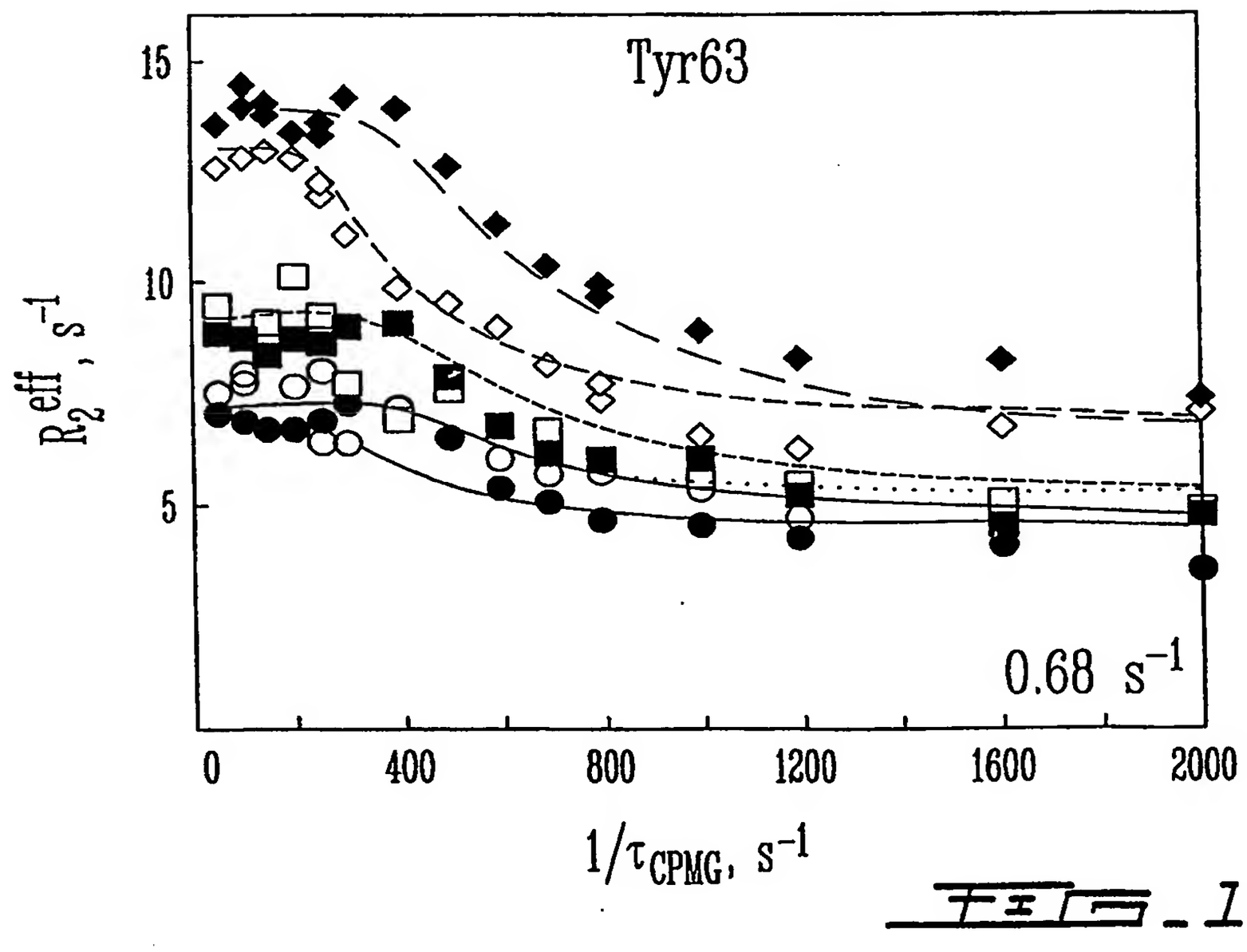


Fig-12D

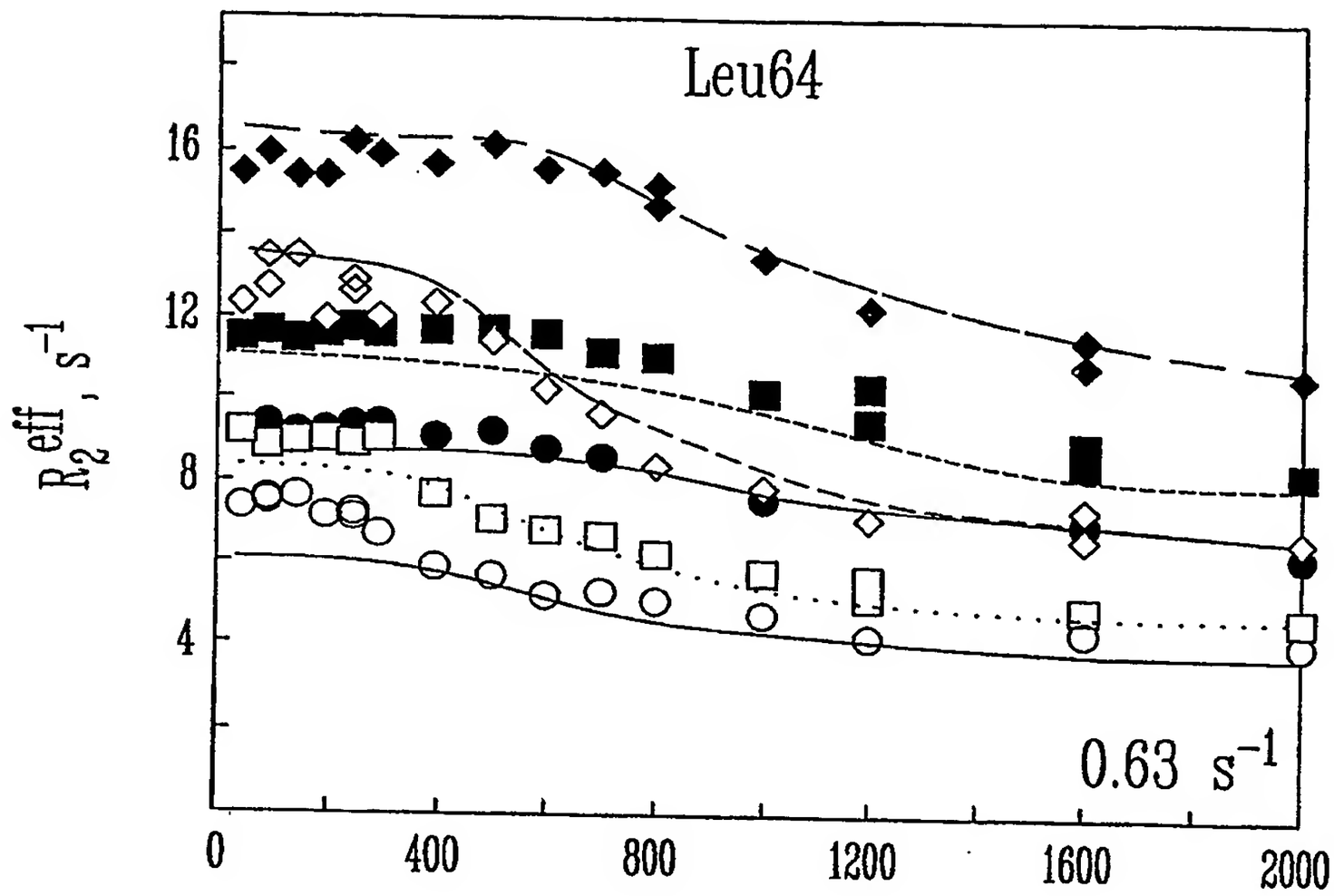


Fig 12E

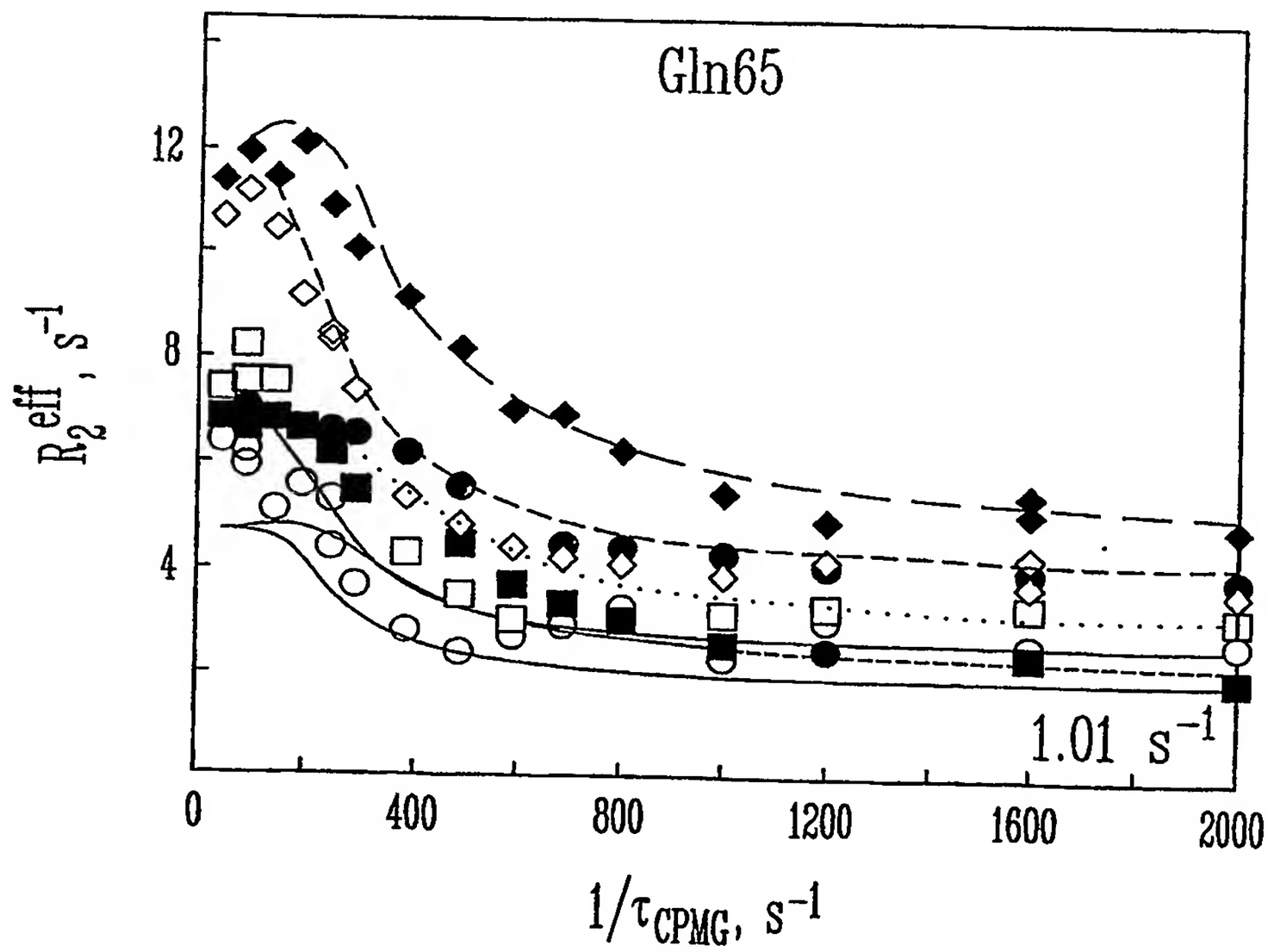


Fig 12F

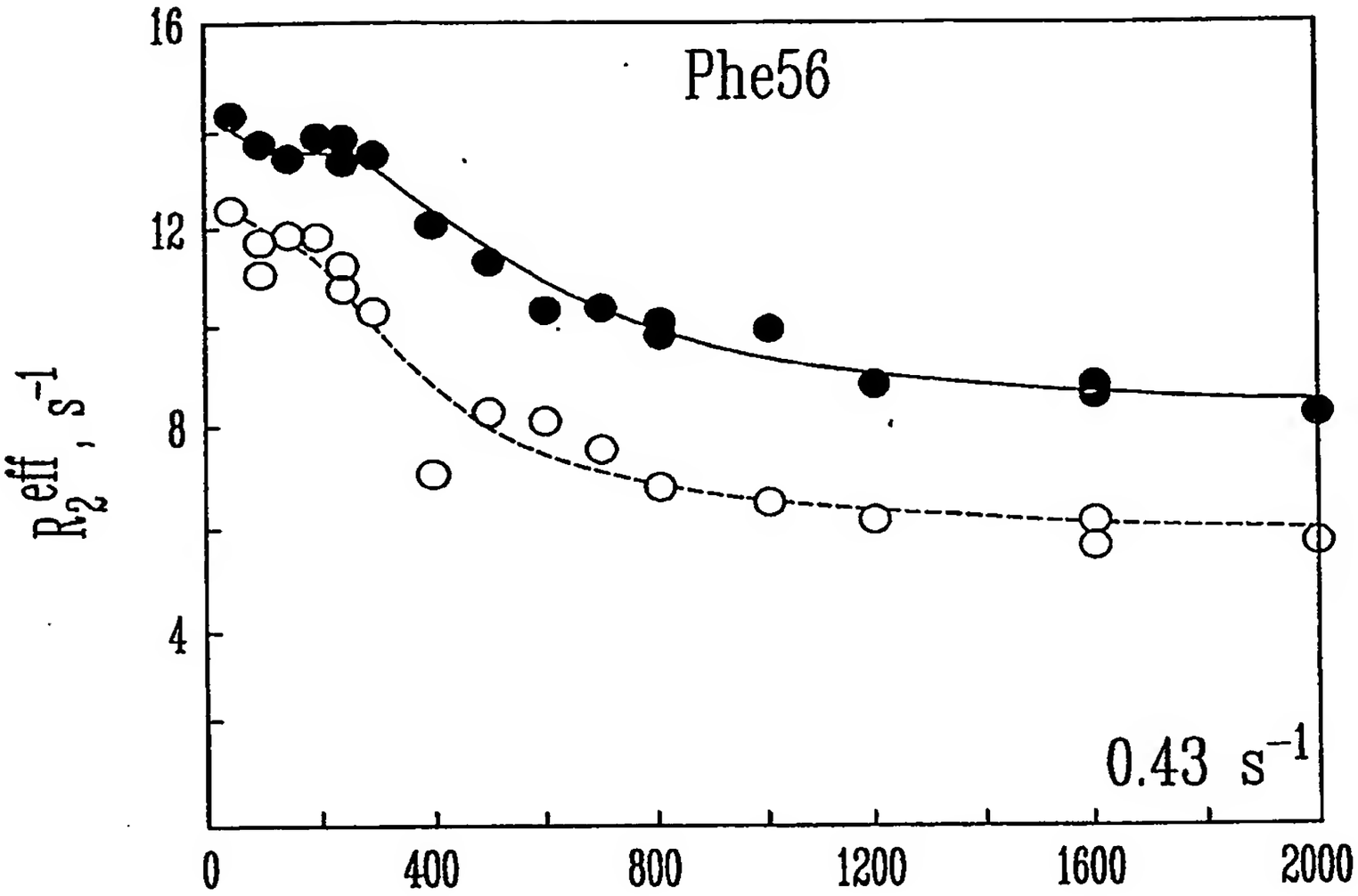


FIG_12G

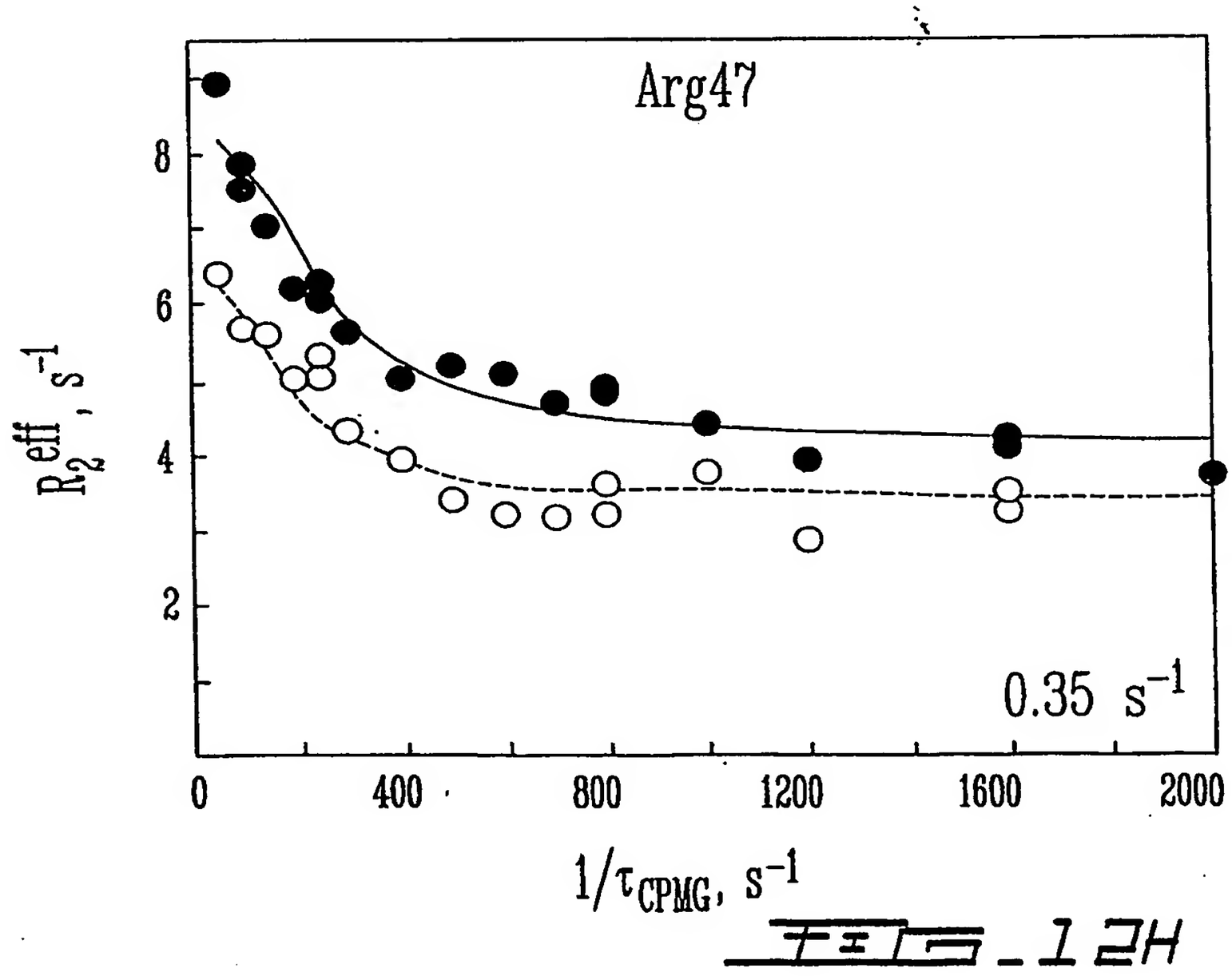


FIG_12H

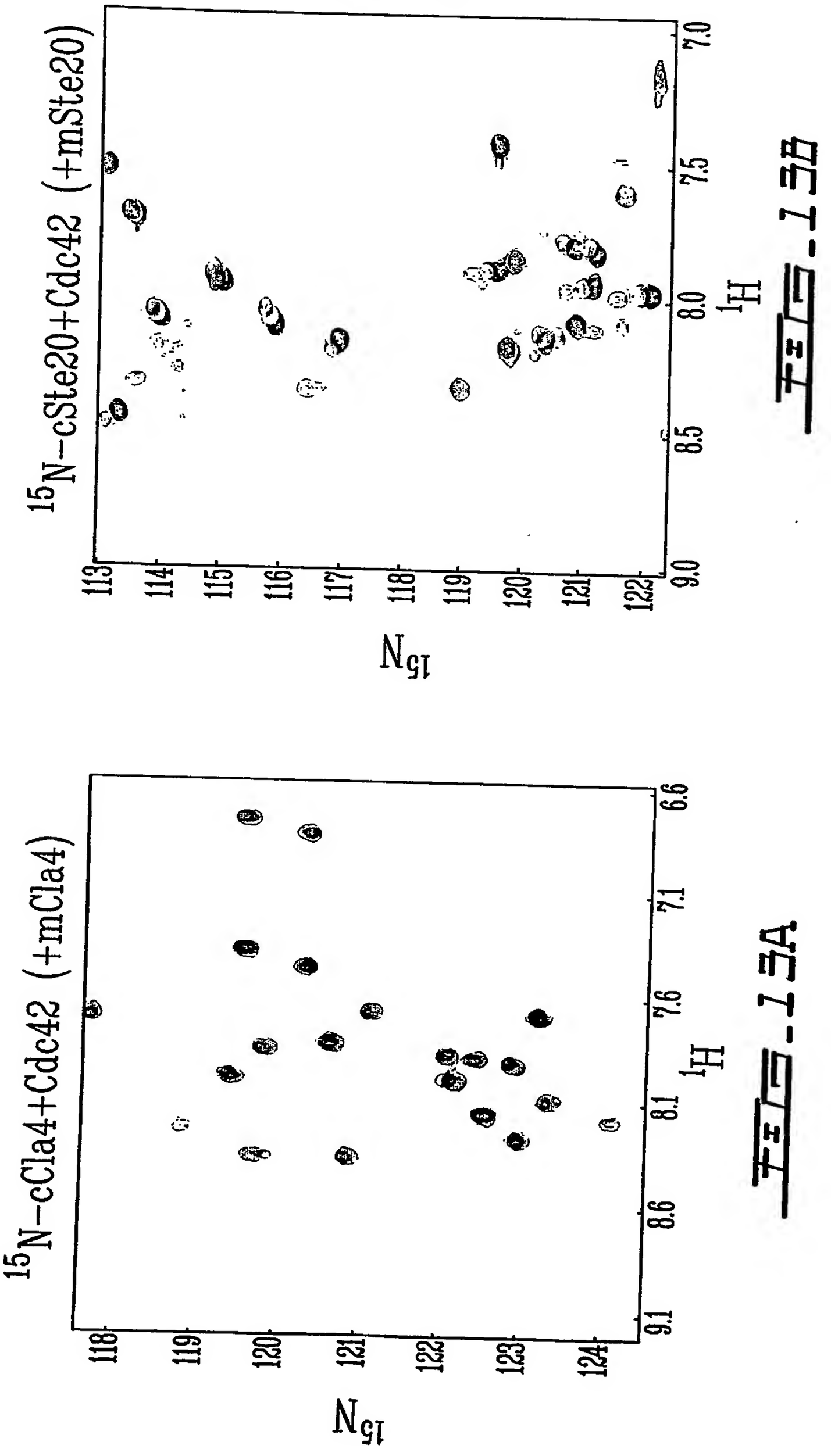


FIG. 13B




FIG. 13A

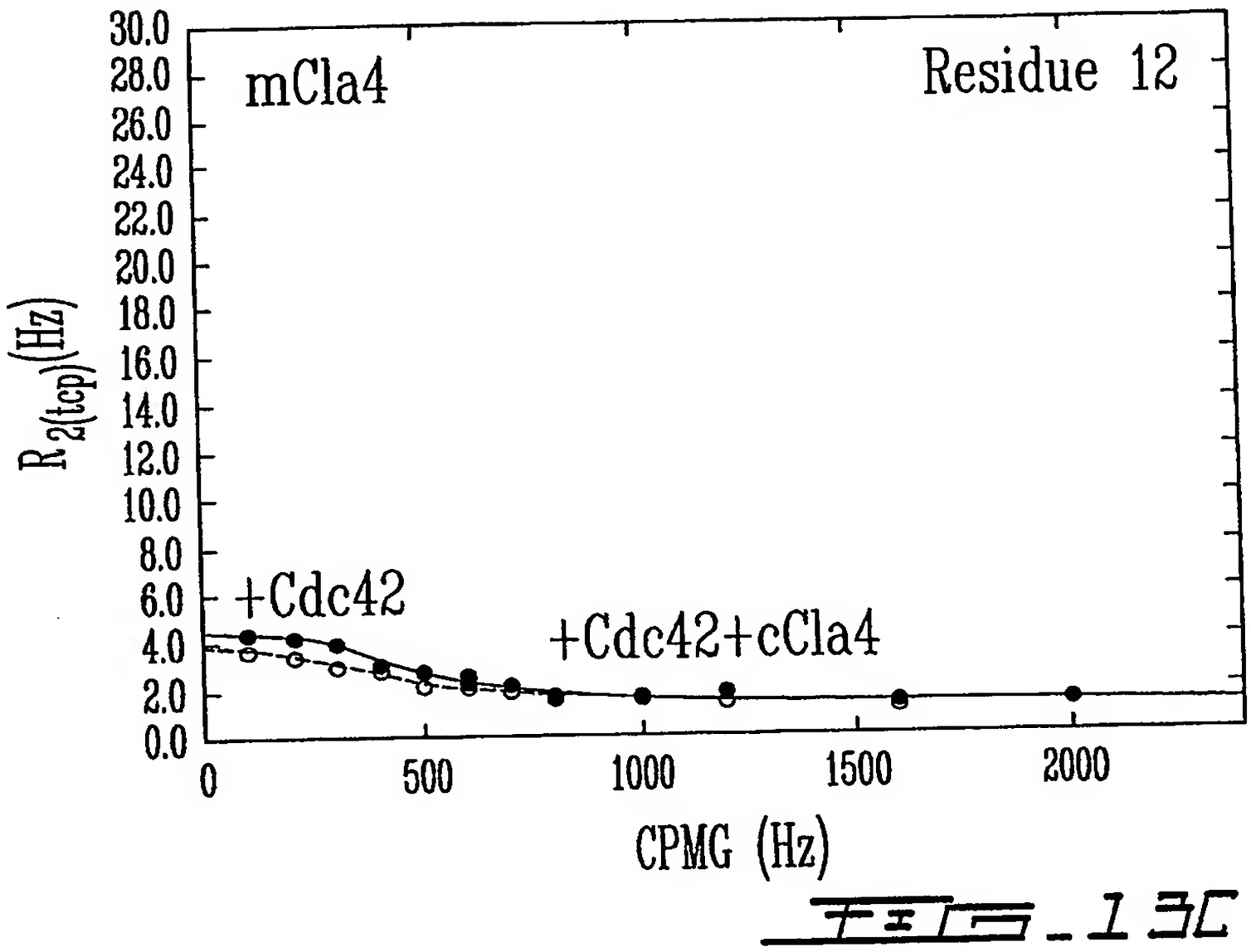


Fig_13C

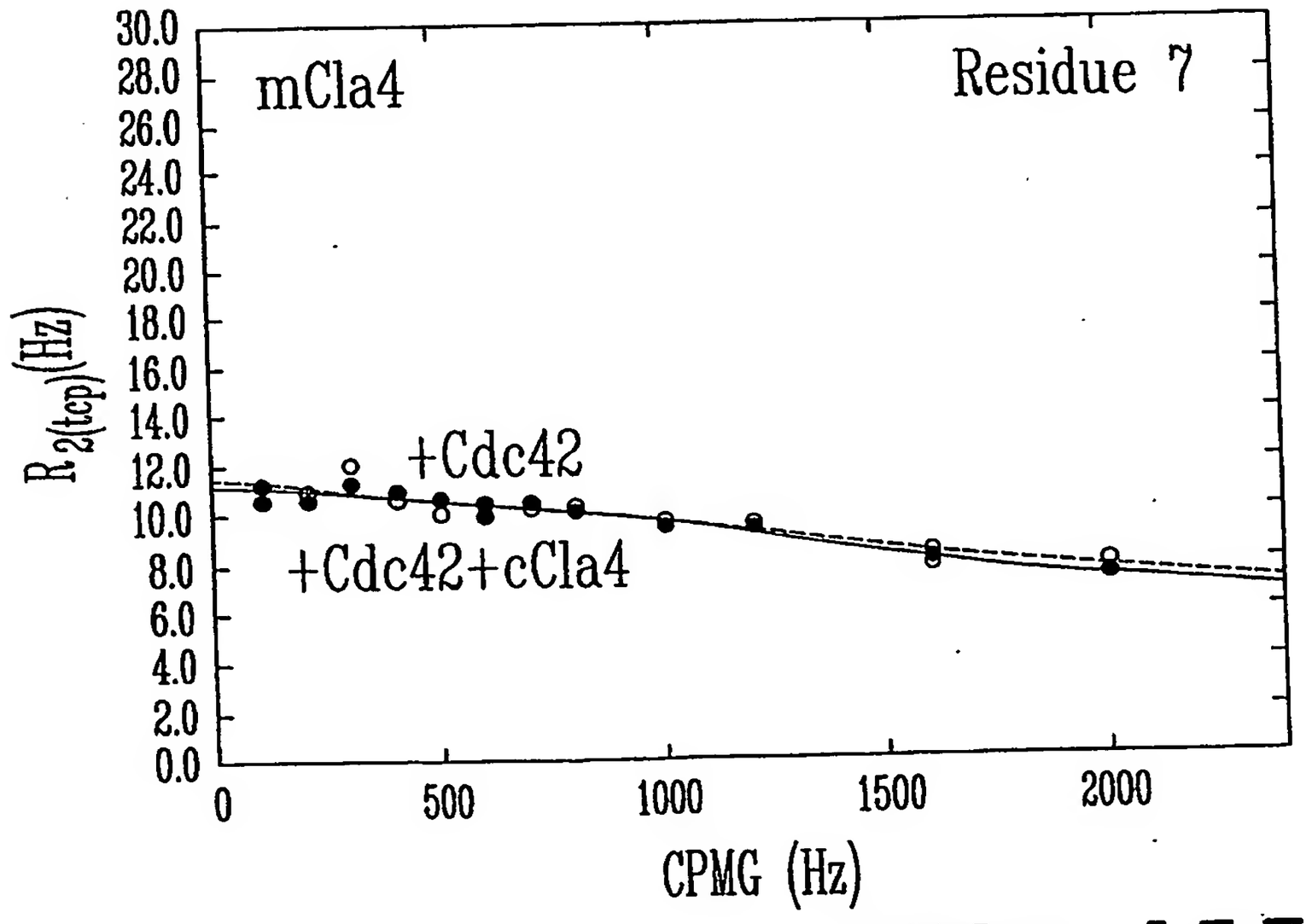


Fig_13D

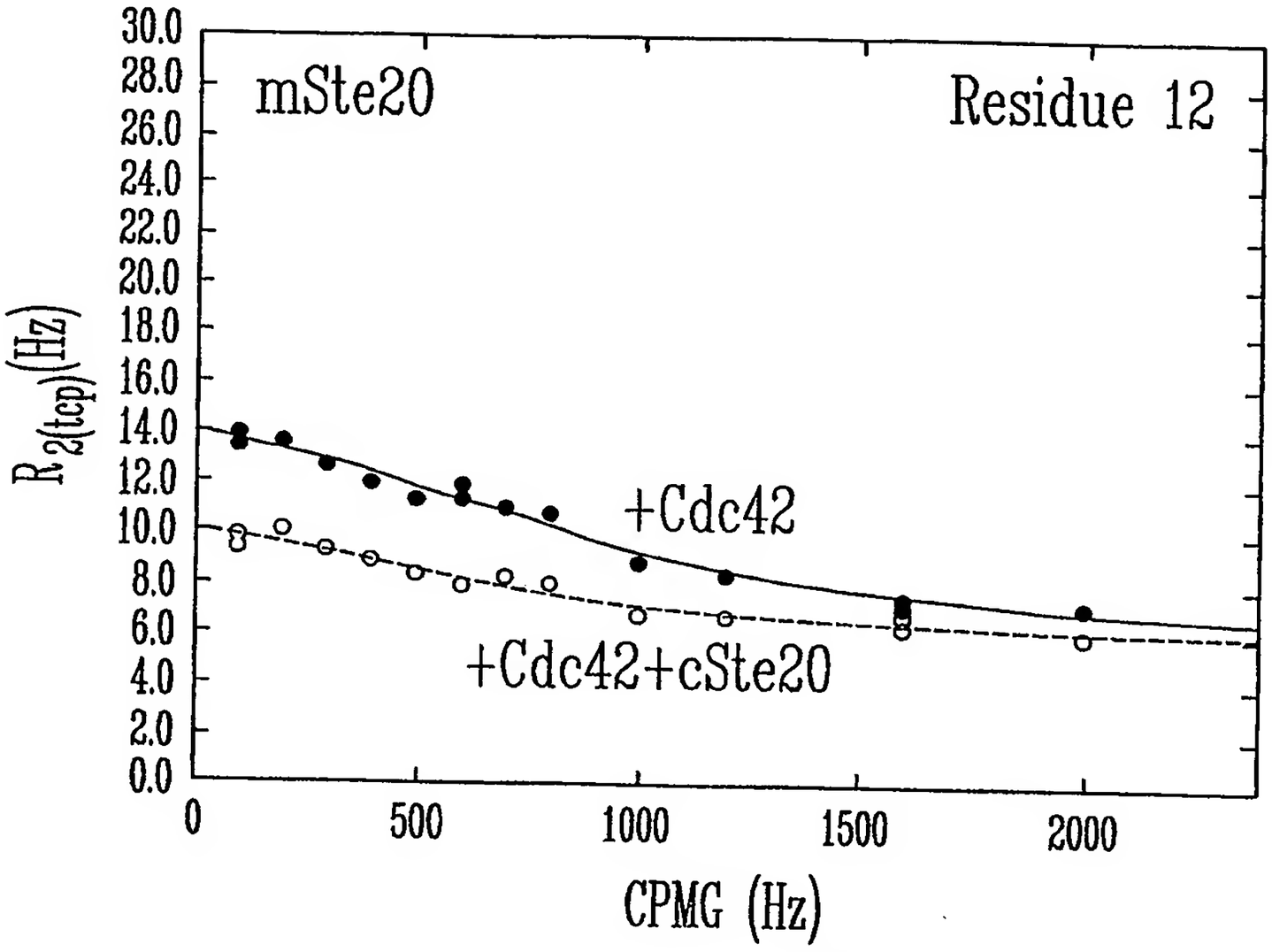


Fig_13E

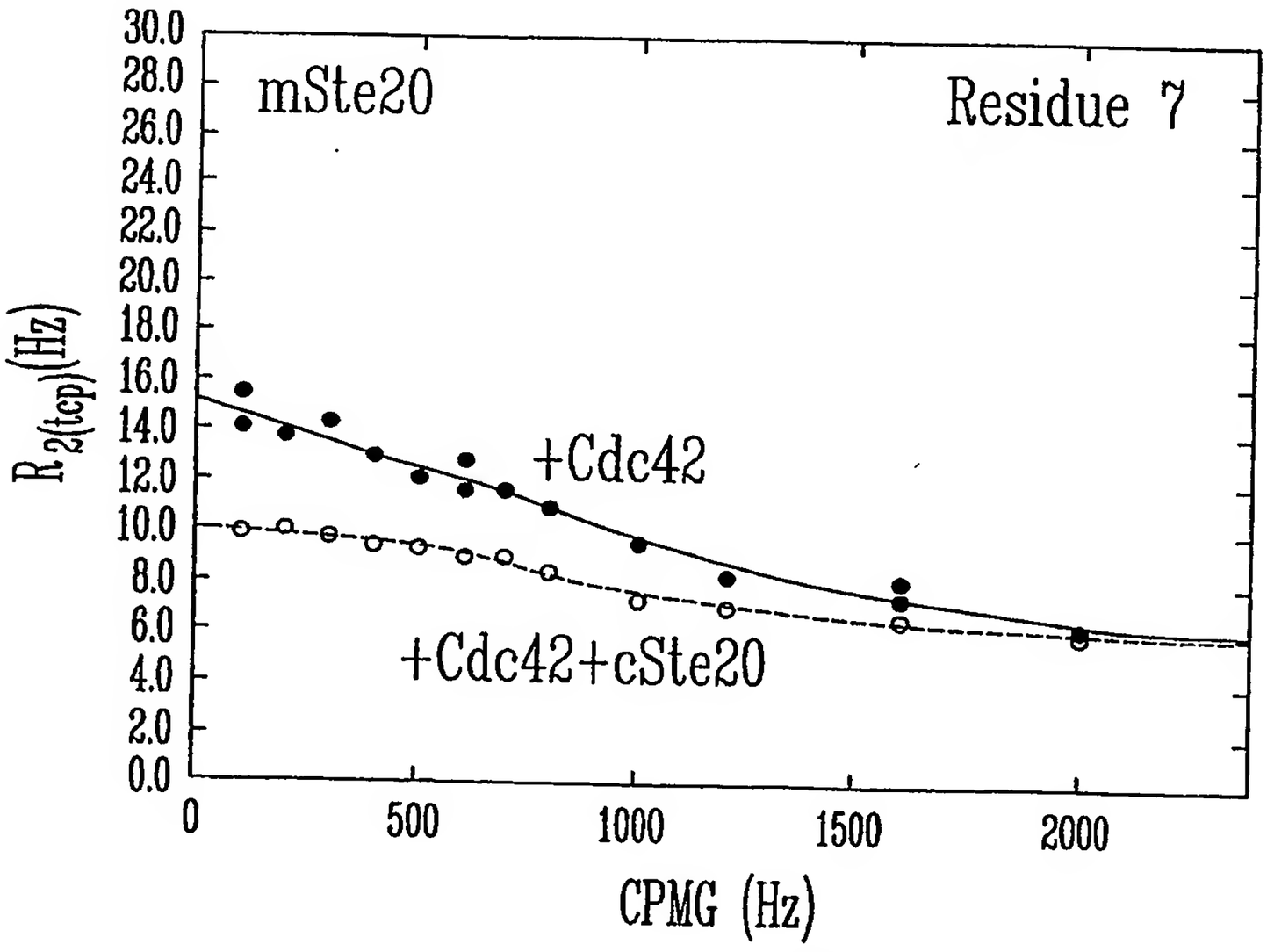


Fig_13F

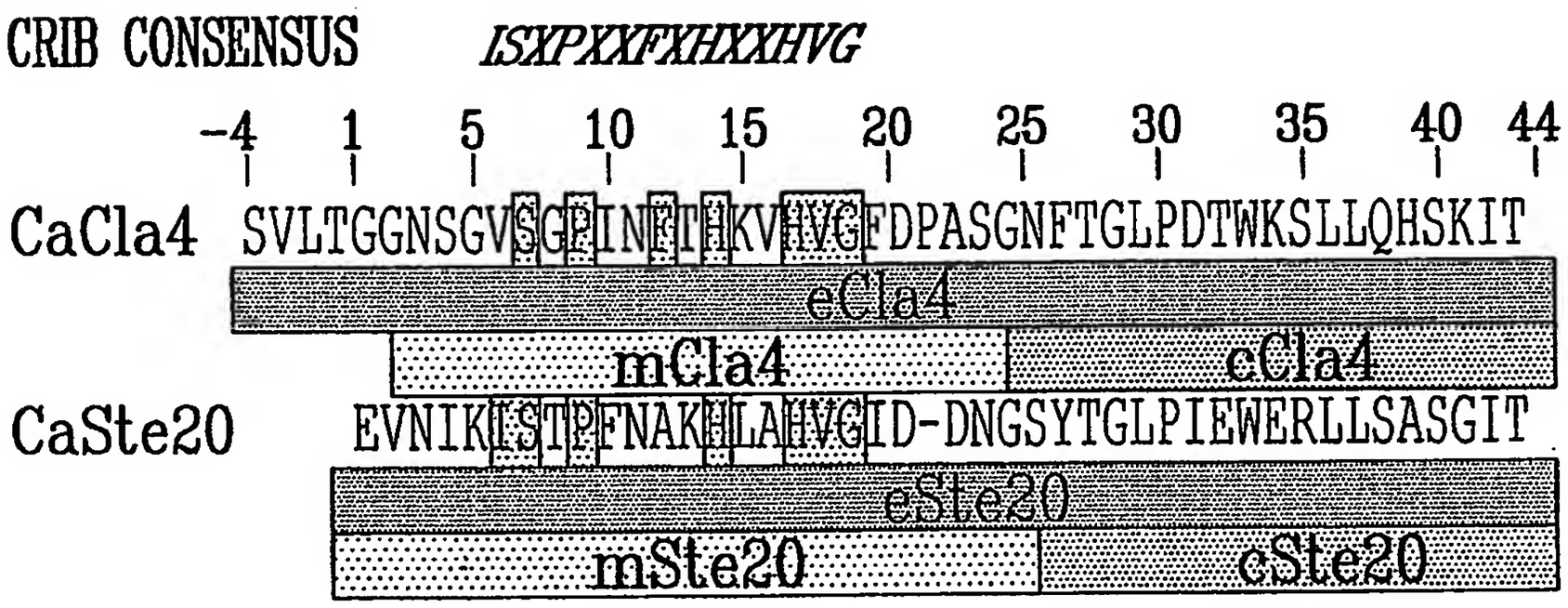
CRIB CONSENSUS ISXPXXFXHXXHVG
-4 1 5 10 15 20 25 30 35 40 44
CaCla4 SVLTGGNSGVSGPINFTHKVHVGFDPASGNFTGLPDTWKSLLQHSKIT
eCla4
mCla4
cCla4
CaSte20 EVNIKISTPFNAKHLAHVGID-DNGSYTGLPIEWERLLSASGIT
eSte20
mSte20
cSte20

FIG_14

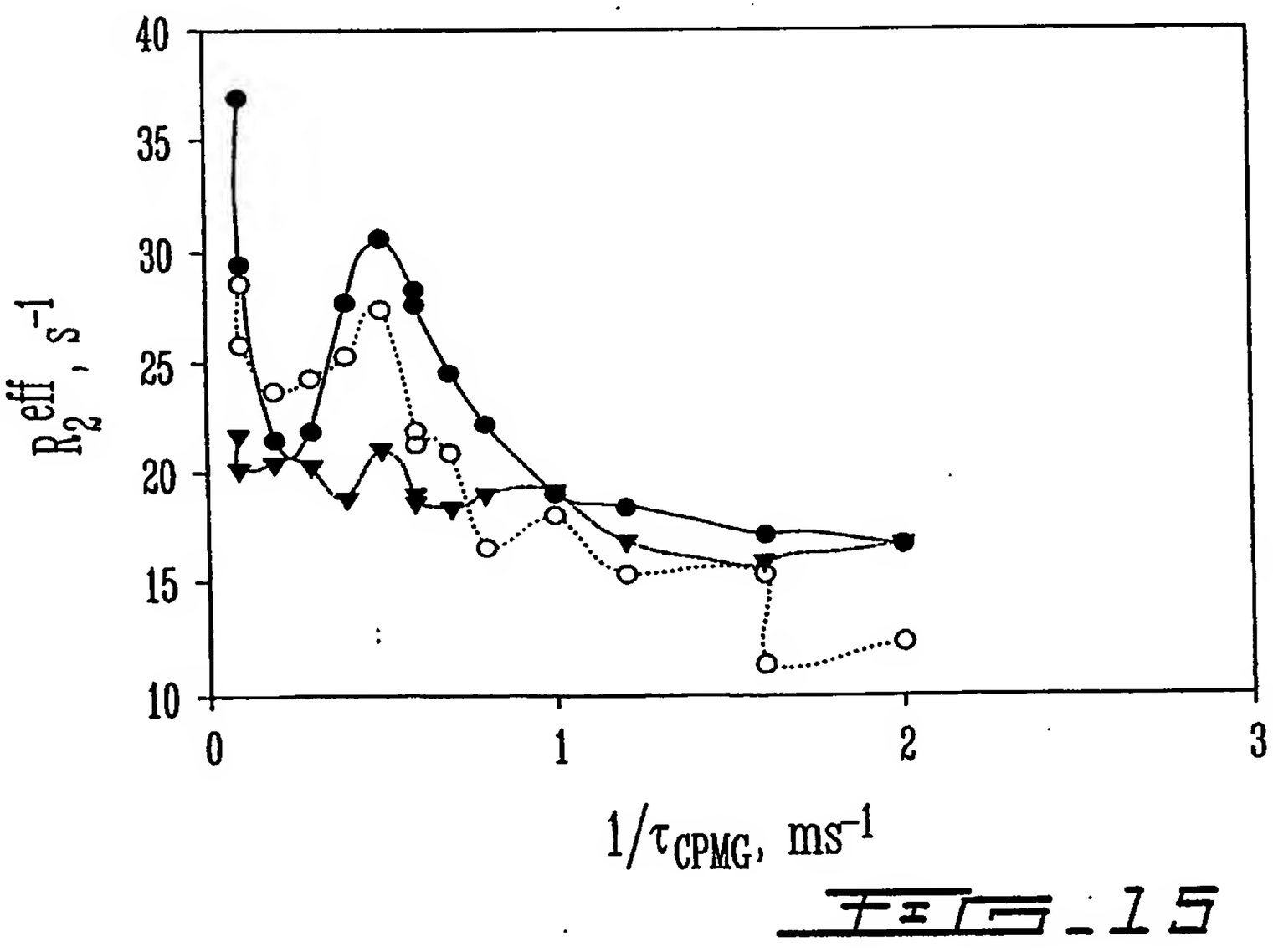
40
35
30
25
20
15
10
0
1
2
3
$R_2^{eff}$, $s^{-1}$
$1/\tau_{CPMG}$, $ms^{-1}$

FIG_15

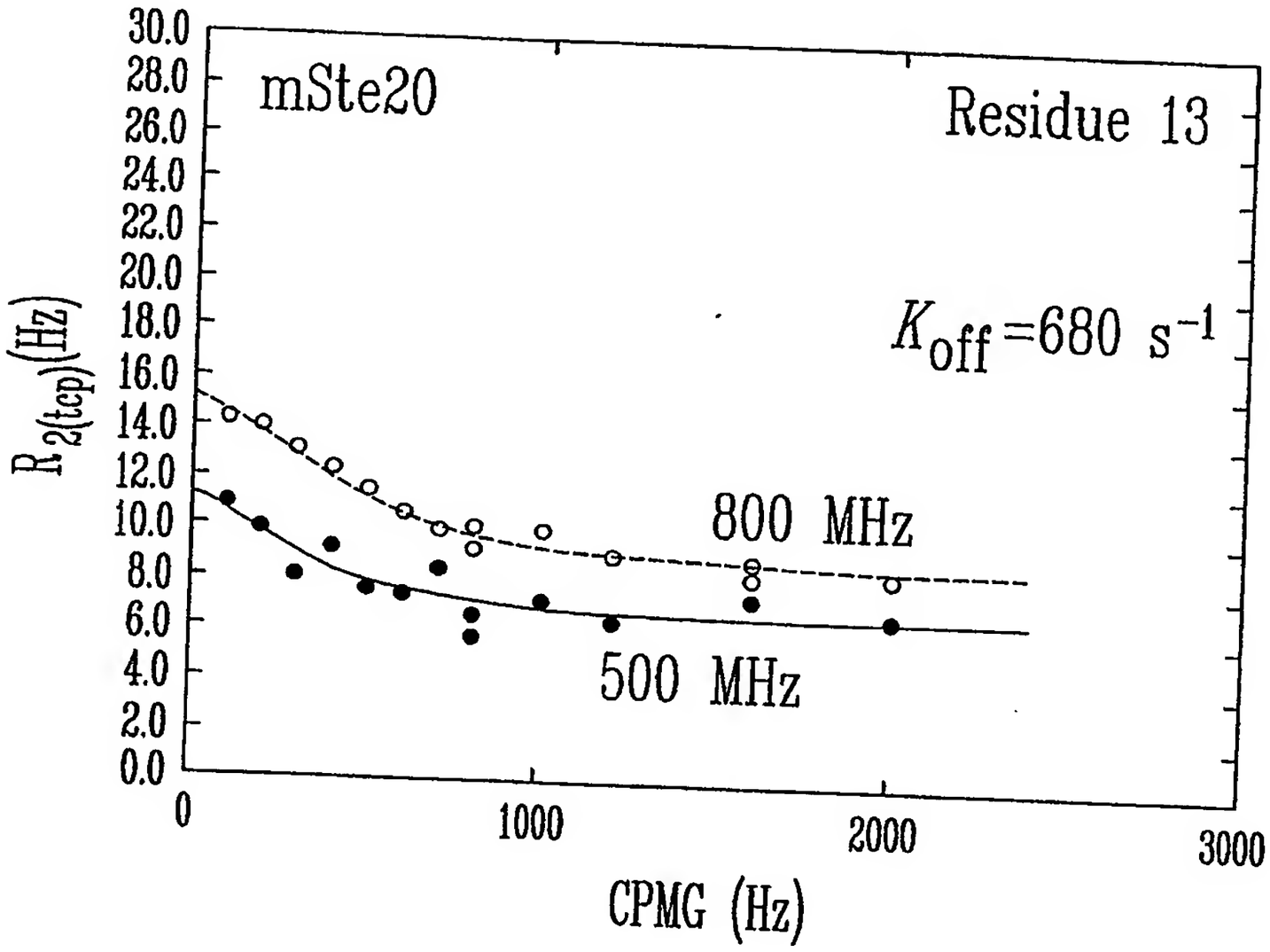


Fig 16A

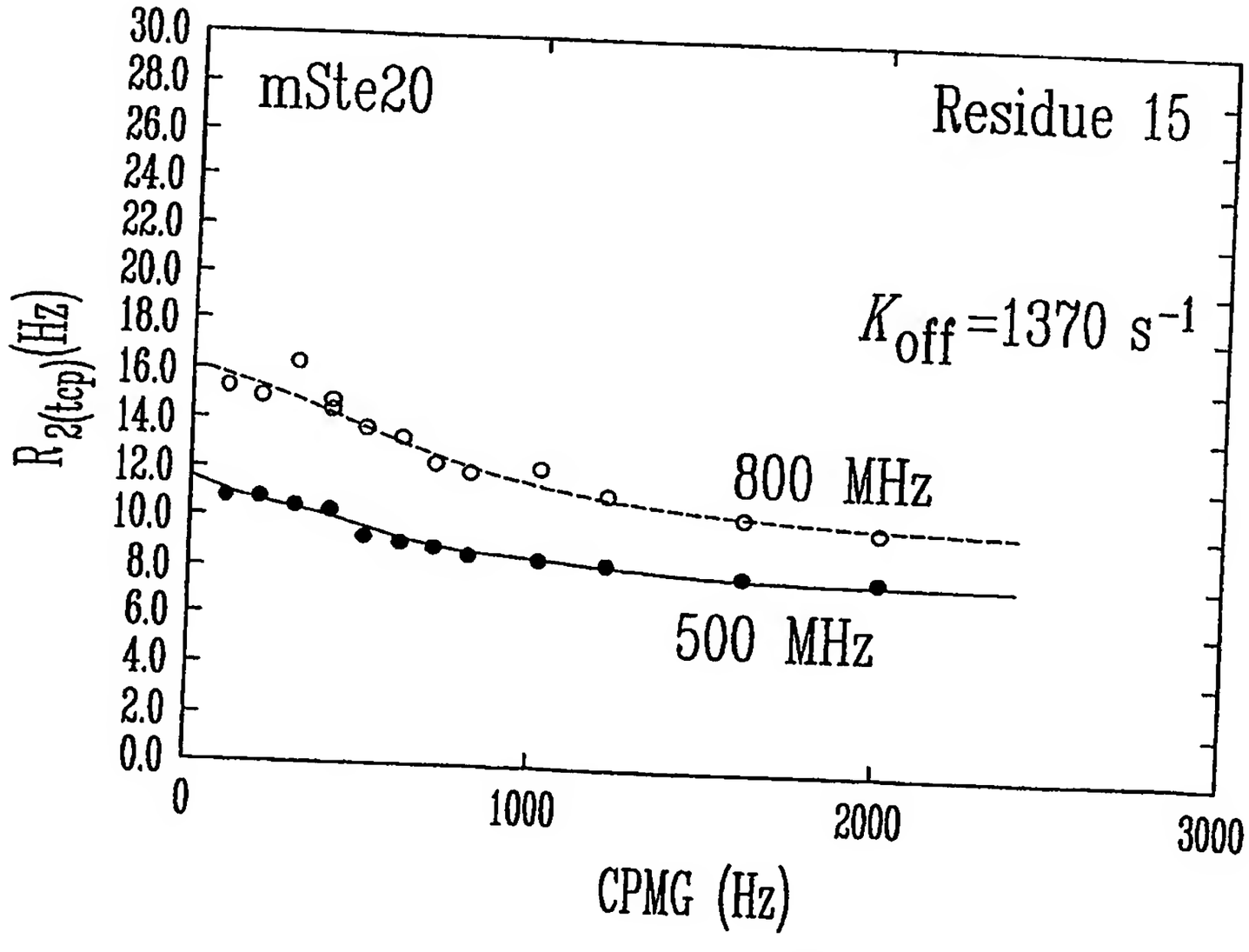


Fig 16B

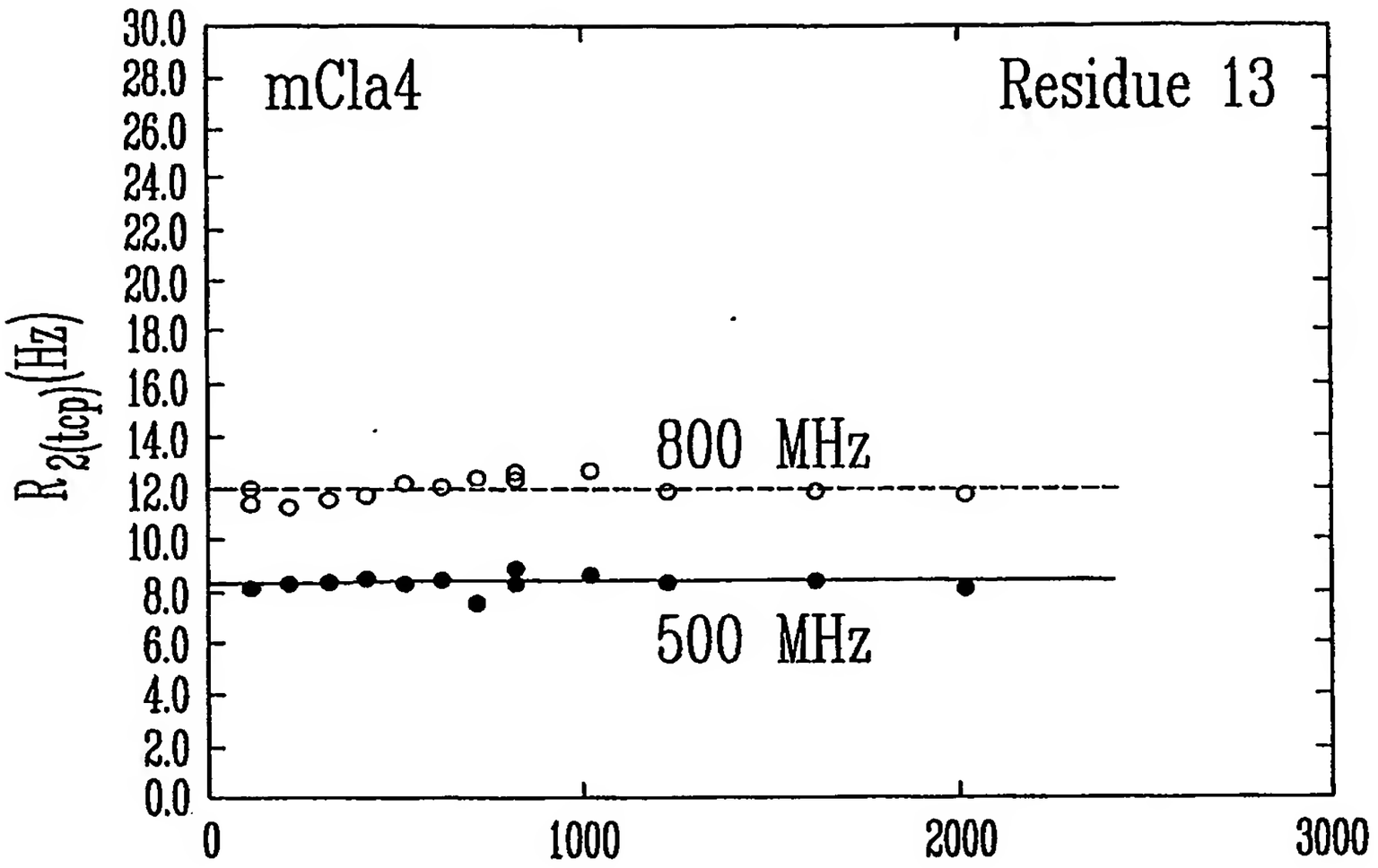


Fig_16C

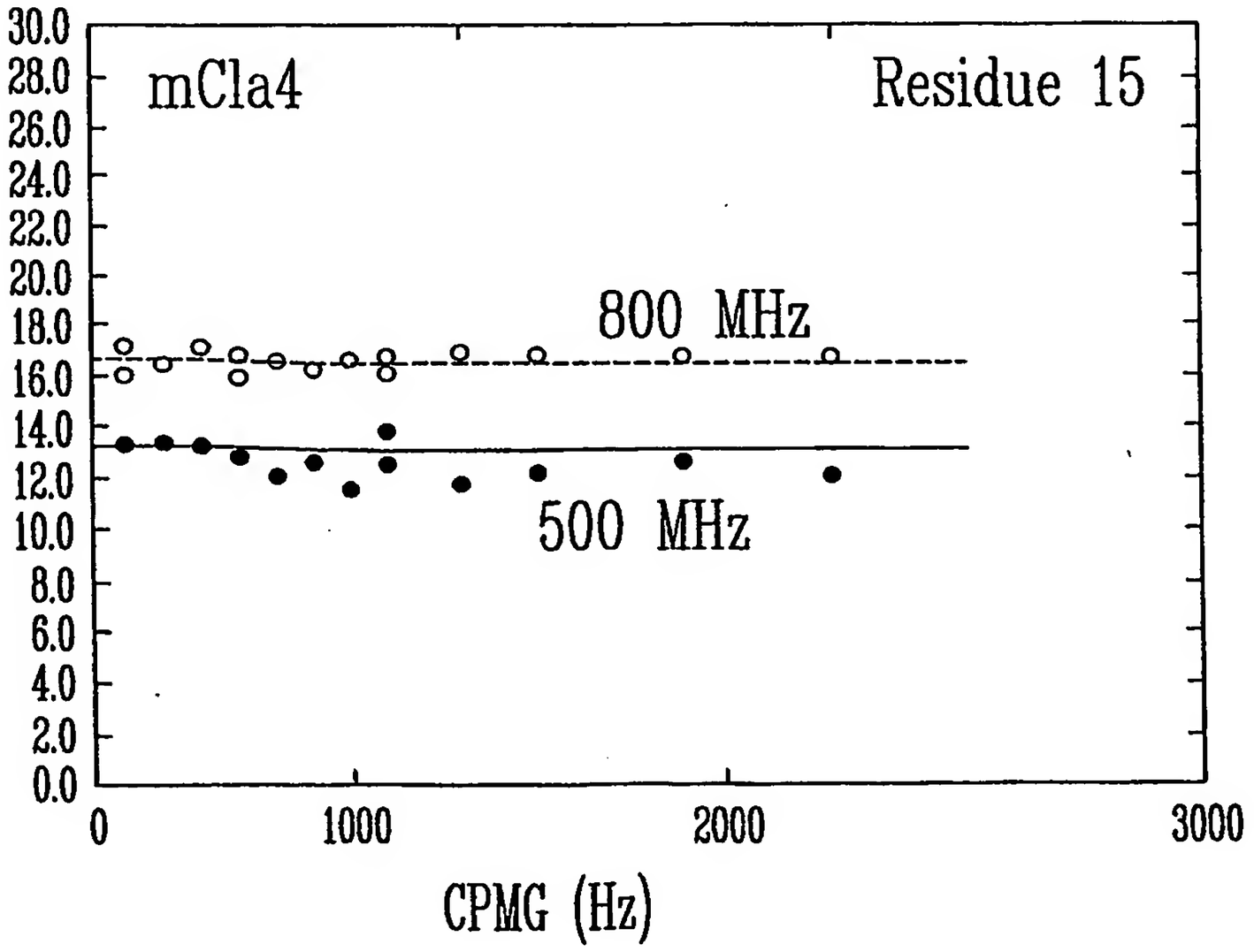


Fig_16D

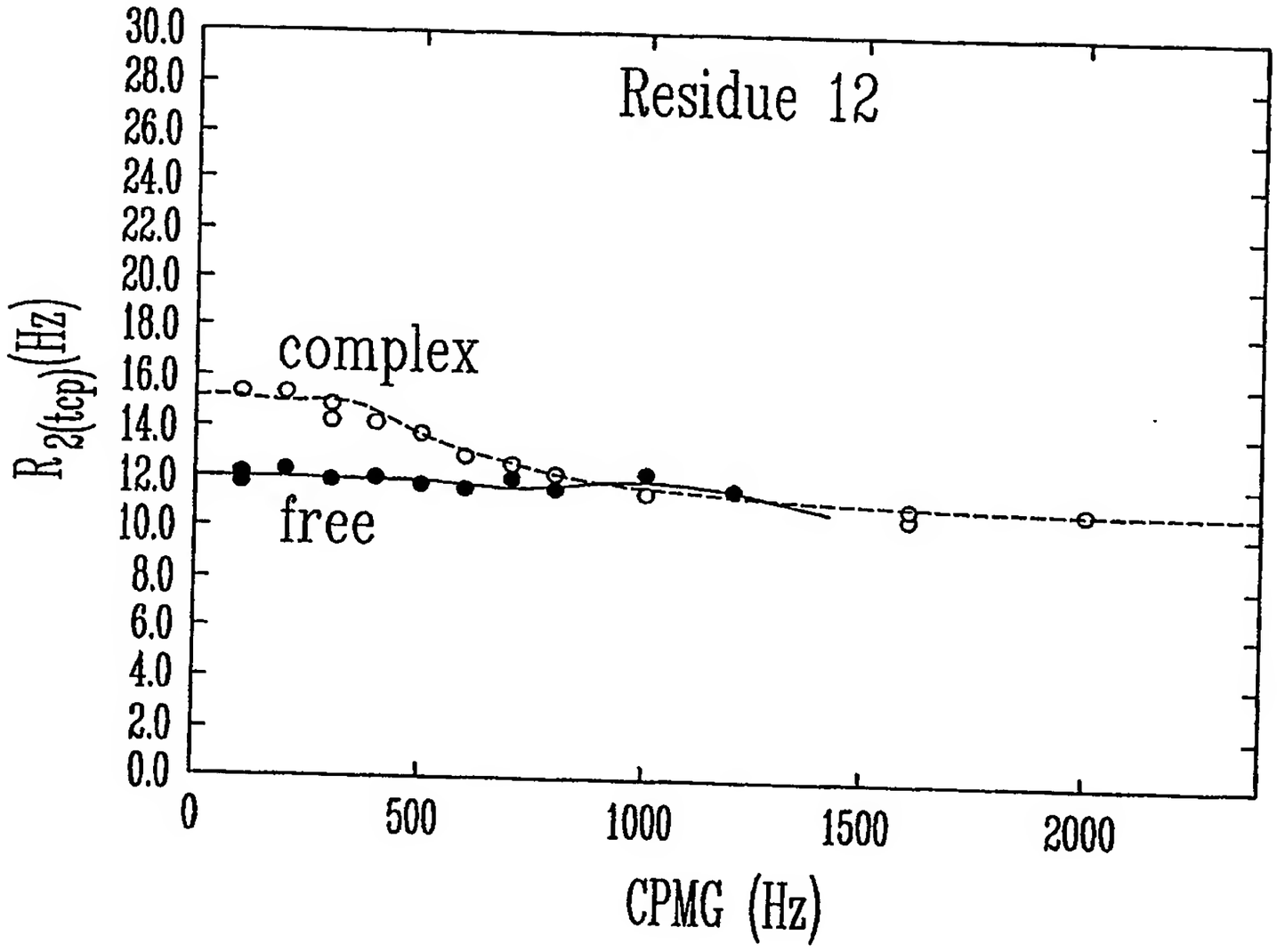


Fig_18A

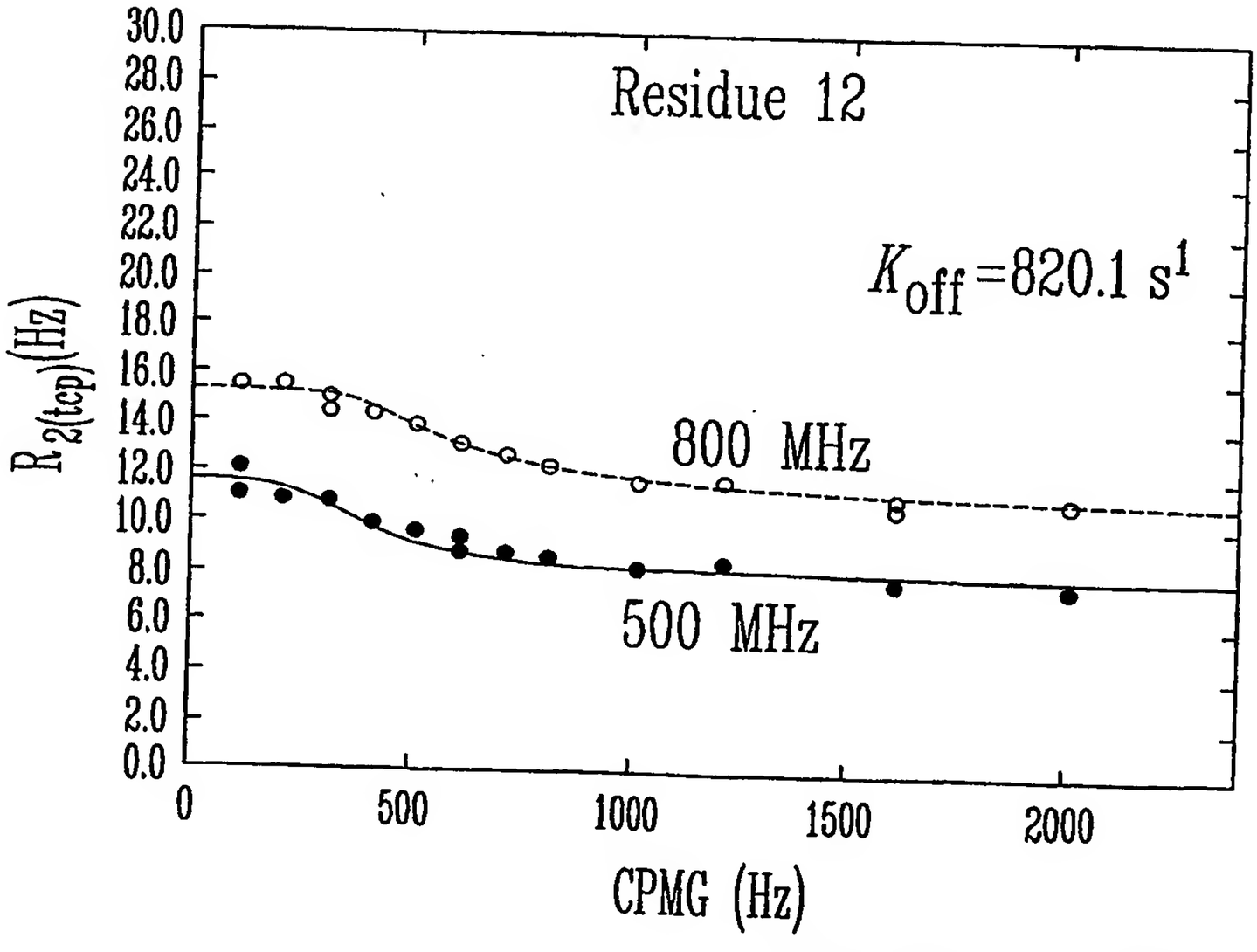


Fig_18B

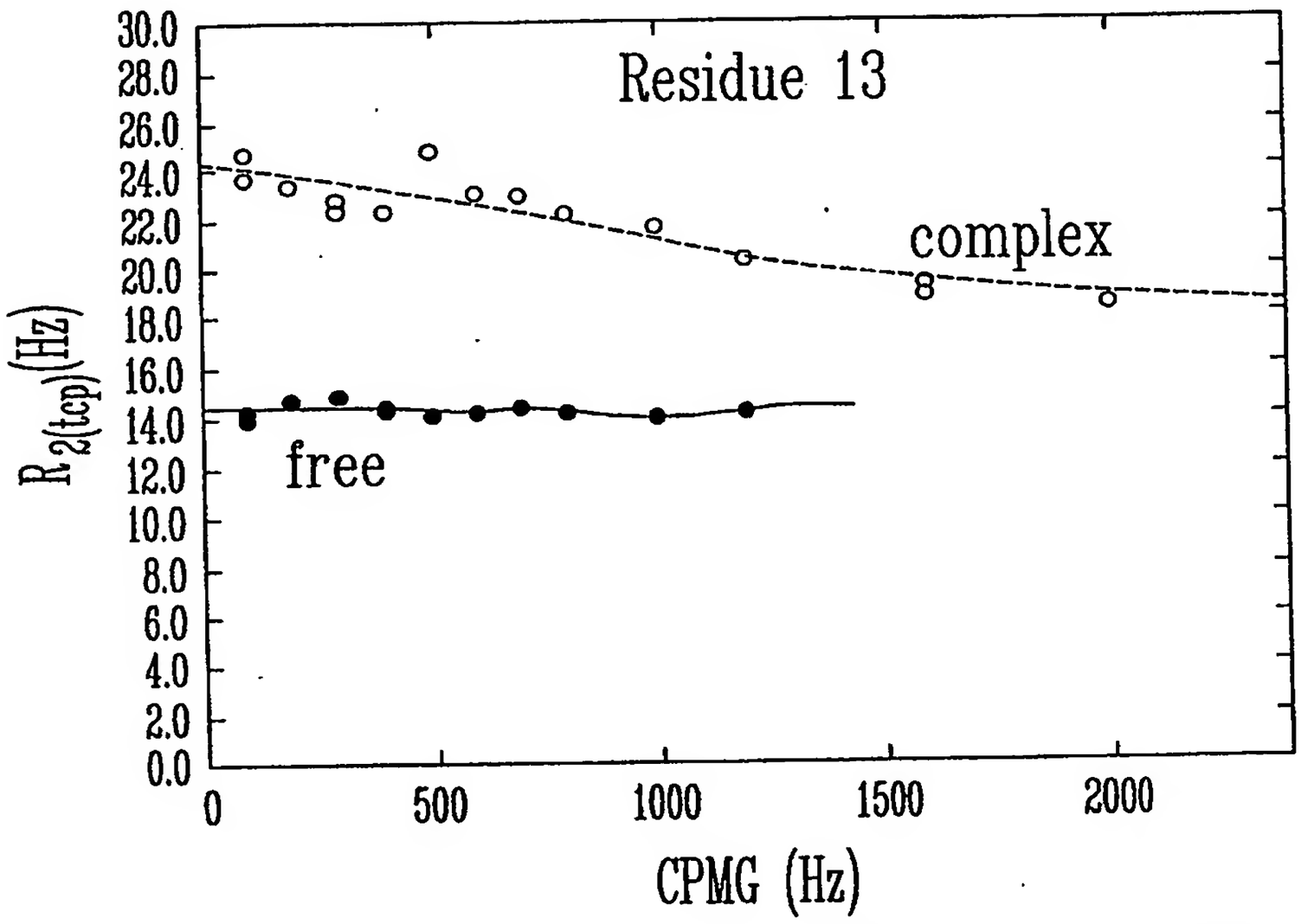


Fig_18C

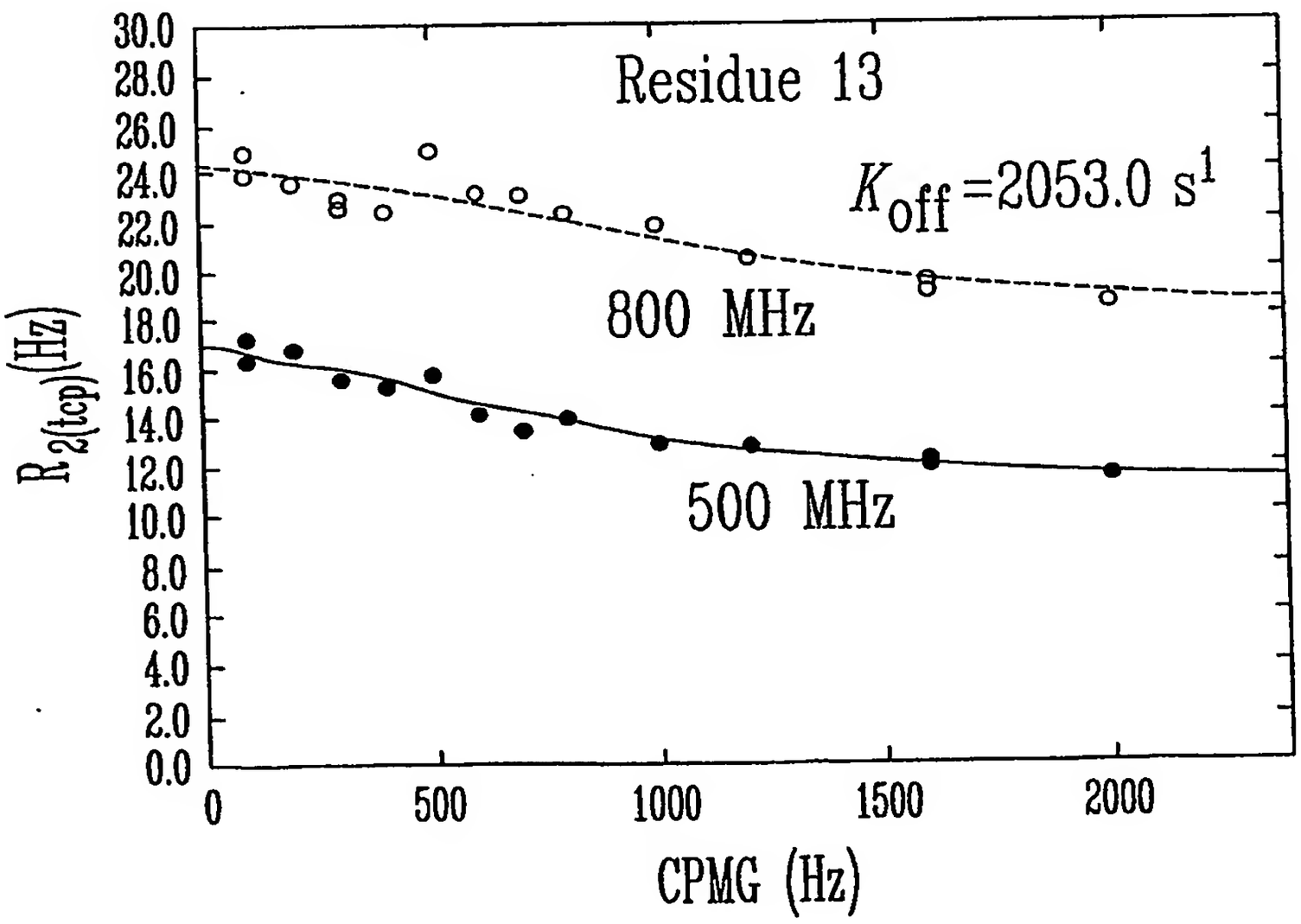


Fig_18D

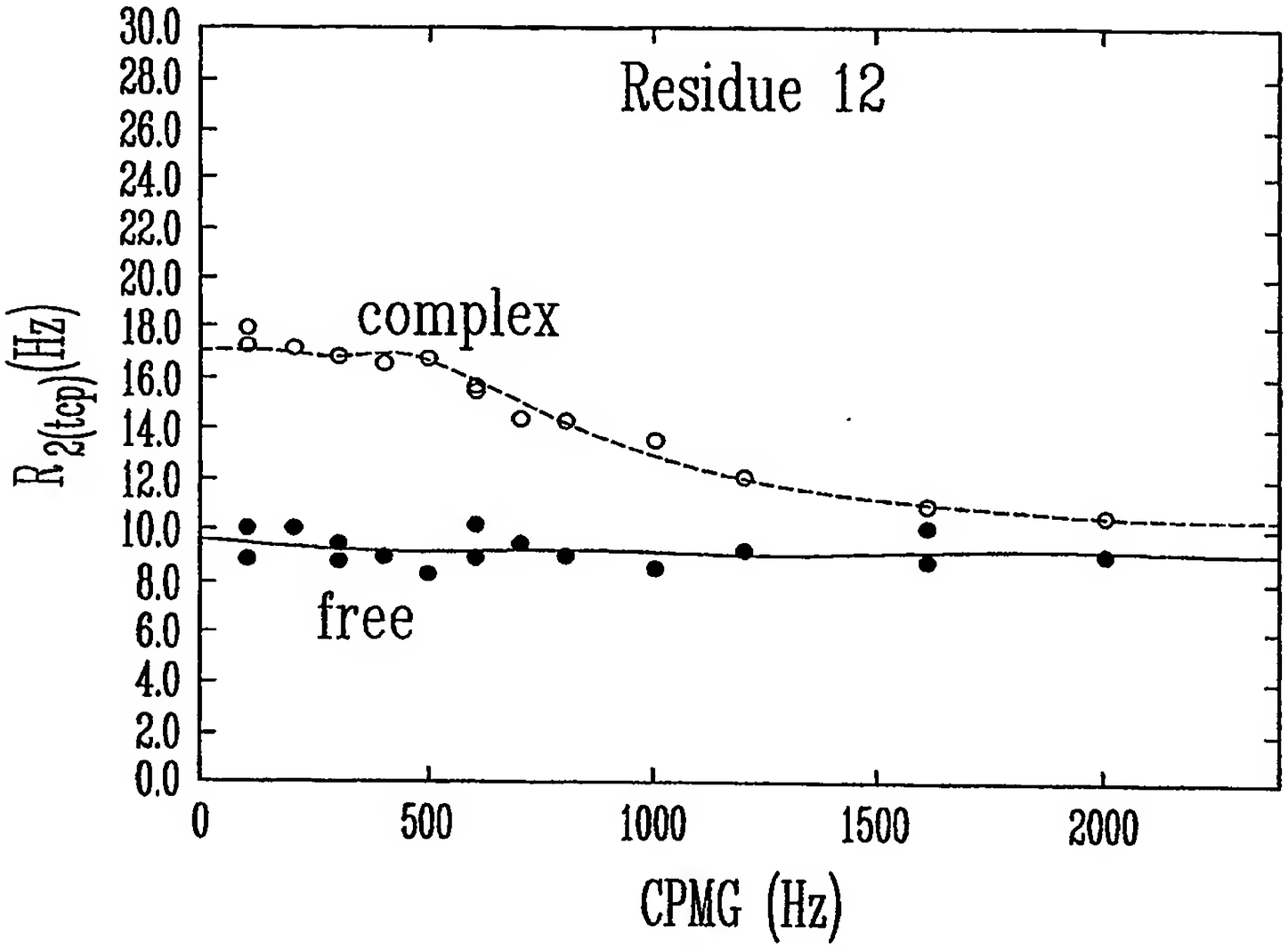


Fig_19A

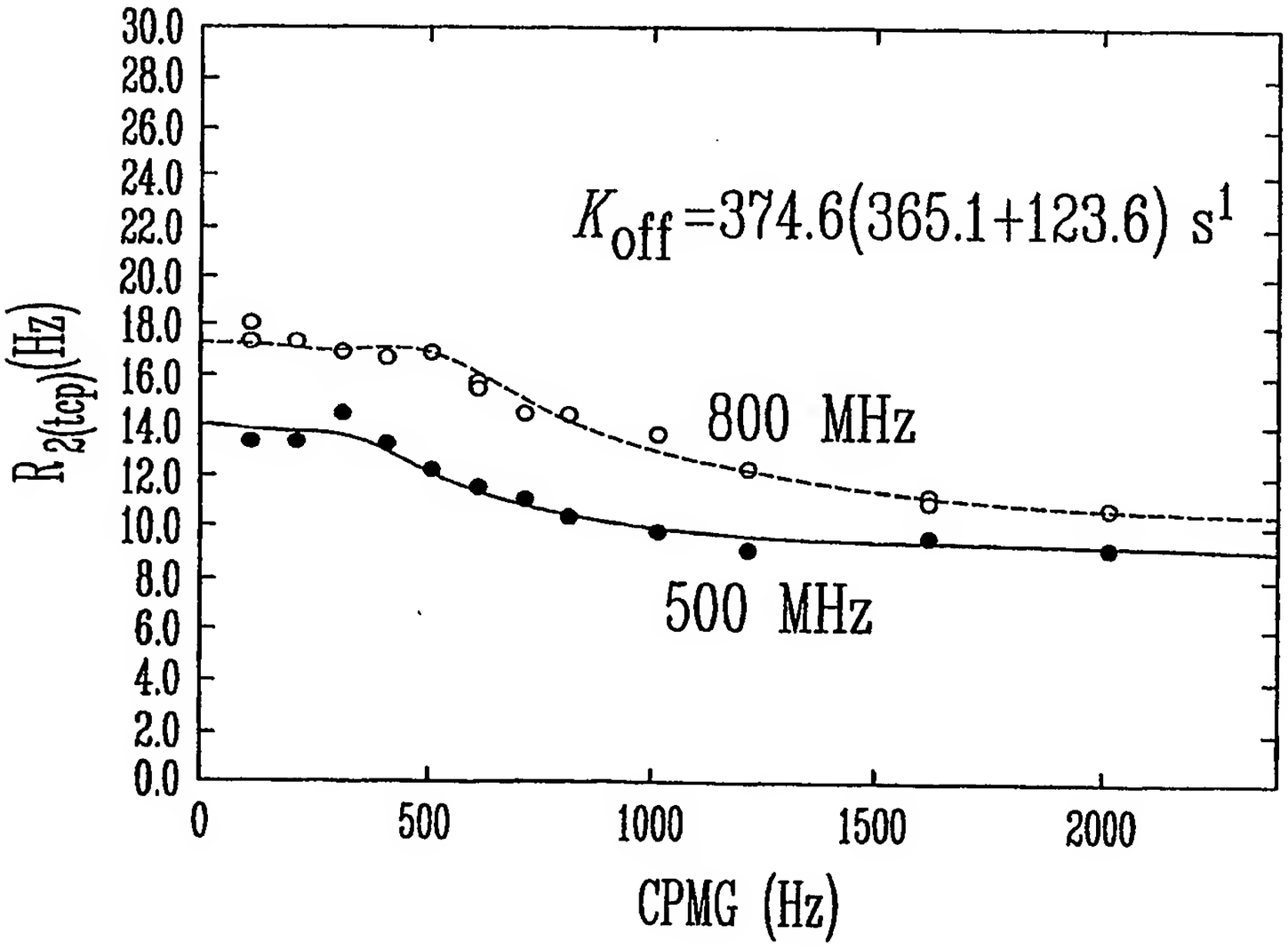


Fig_19B

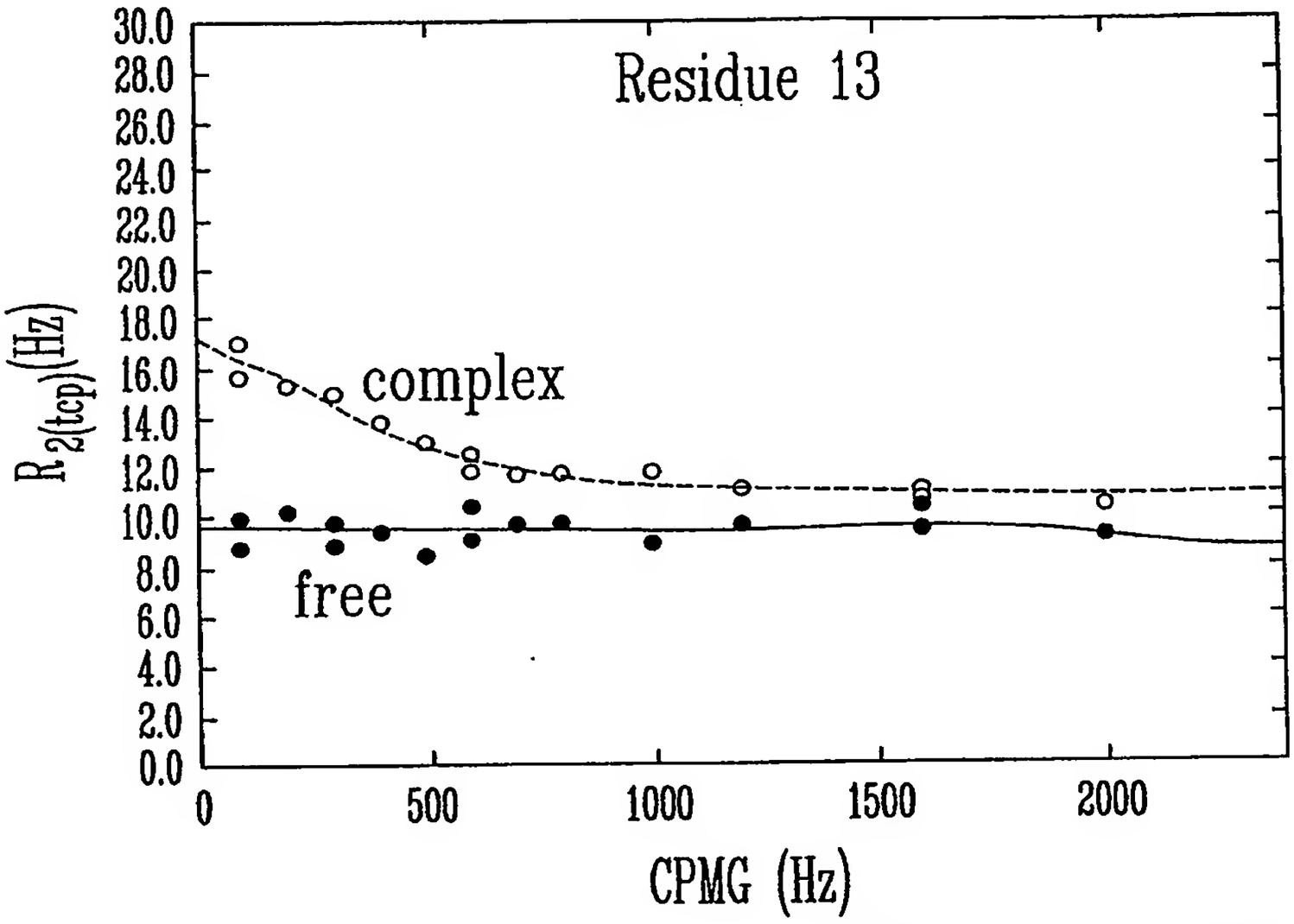


Fig_19C

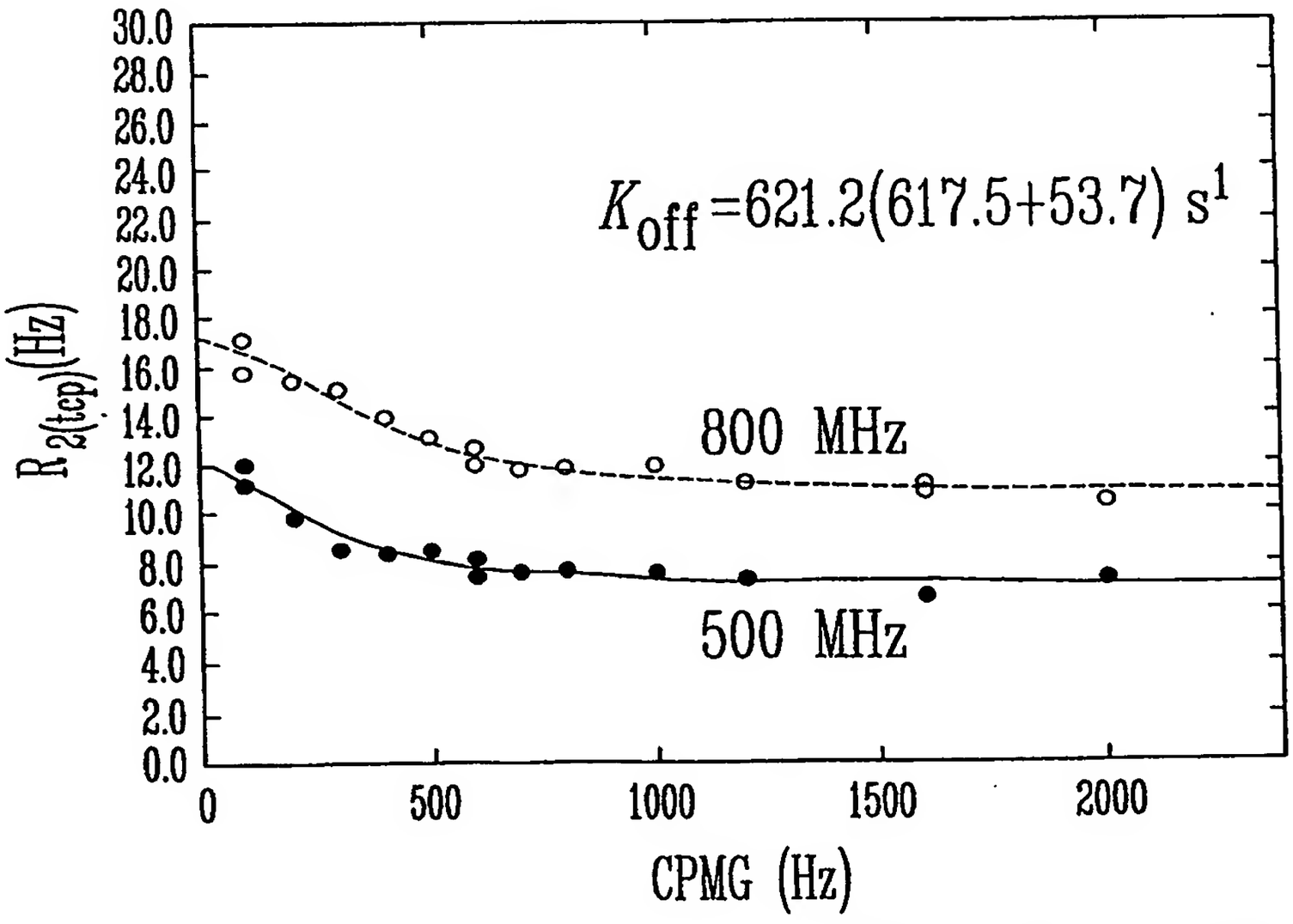


Fig_19D

NT motif CG motif

WT: RSRPSFHPVSDE L VNYVNKRNTTWQAGHNFYNVDMSYLKRLCGTFLGGPKPPQRVMFTEDLK

Mutant: RSRPSFHPVSDE L VNYVMKRNTTWQAMHNFYNVDMSYLKRLCGTFLGGPKPPQRVMFTEDLK

RSRPSFHPVSDE LVYVS"

KRNTTWQAS"

HNFYNVDS"

SYLKRLCGTFLGGPKPPQRVS"

FTEDLK

F1 F2 F3 F4 F5

FIG - 20A

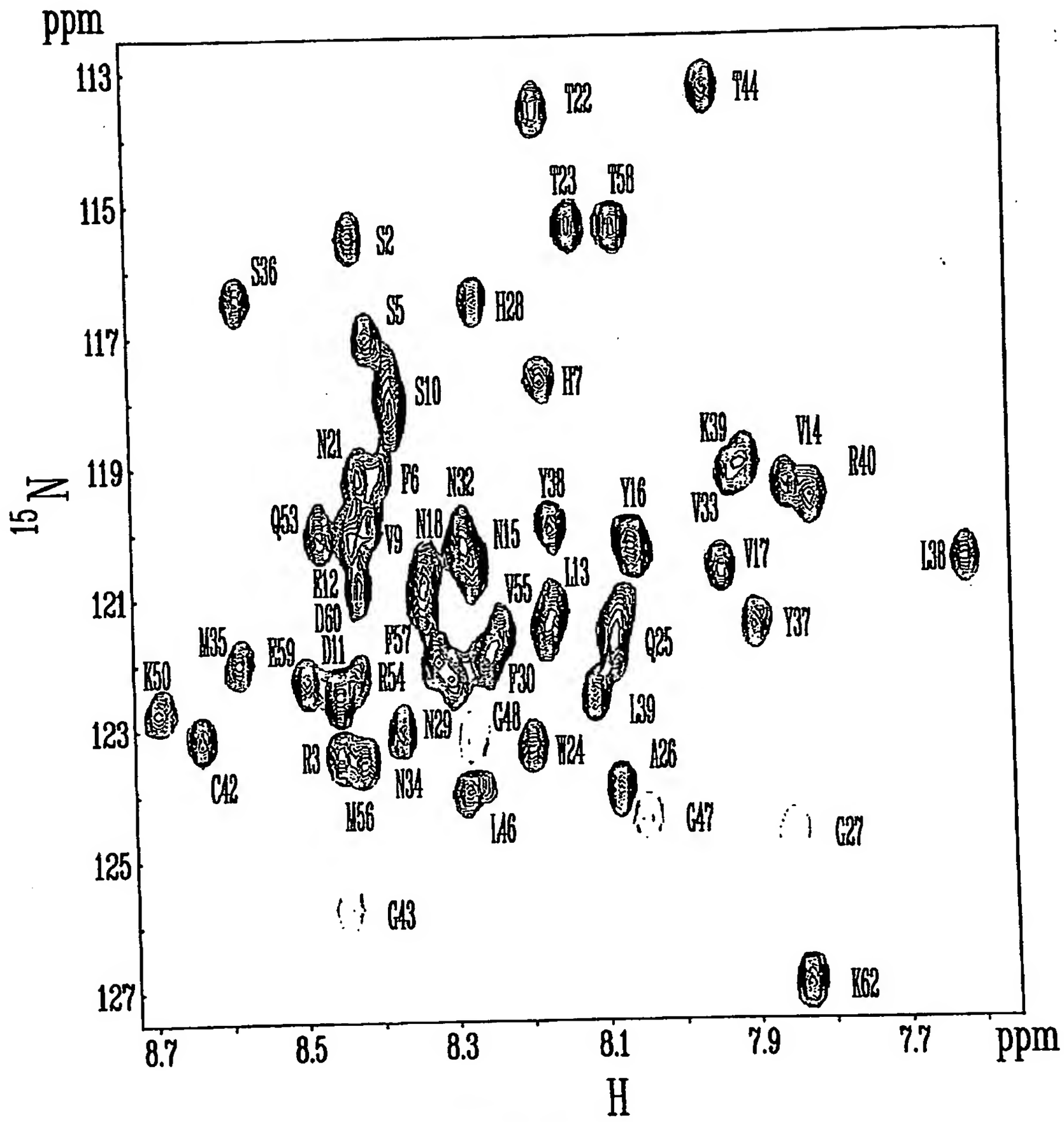
ppm
113
115
117
119
121
123
125
127
15N
T22
T44
T23
T58
S2
S36
S5
H28
S10
H7
N21
F6
N32
Y38
Y16
K39
V14
R40
V33
Q53
V9
N18
N15
V17
L38
K12
V55
L13
D60
Y37
M35
E59
D11
F57
Q25
K50
R54
F30
L39
N29
G48
W24
A26
R3
C42
N34
M56
LA6
G47
G27
G43
K62
8.7
8.5
8.3
8.1
7.9
7.7
ppm
H

FIG - 20B

<210> 3
<211> 6
<212> PRT
<213> Artificial Sequence

<220>
<223> Anti-thrombin peptide

<220>
<221> MOD_RES
<222> (6)...(6)
<223> Xaa = HomoSerine Lactone

<400> 3
Gly Phe Asn Pro Arg Xaa
1 5

<210> 4
<211> 6
<212> PRT
<213> Artificial Sequence

<220>
<223> Anti-thrombin peptide

<220>
<221> MOD_RES
<222> (6)...(6)
<223> Xaa = HomoSerine Lactone

<400> 4
Gly Pro Asn Pro Arg Xaa
1 5

<210> 5
<211> 6
<212> PRT
<213> Artificial Sequence

<220>
<223> Anti-thrombin peptide

<220>
<221> MOD_RES
<222> (6)...(6)
<223> Xaa = HomoSerine Lactone

<400> 5
Gly Phe Ser Ala Arg Xaa
1 5

<210> 6
<211> 5
<212> PRT
<213> Artificial Sequence

<220>
<223> Anti-thrombin peptide

<400> 6
Gly Val Ser Pro Arg
1 5

<210> 7
<211> 5
<212> PRT
<213> Artificial Sequence

<220>
<223> Anti-thrombin peptide

<400> 7
Gly Leu Asp Pro Arg
1 5

<210> 8
<211> 5
<212> PRT
<213> Artificial Sequence

<220>
<223> Anti-thrombin peptide

<400> 8
Gly Val Asp Pro Arg
1 5

<210> 9
<211> 5
<212> PRT
<213> Artificial Sequence

<220>
<223> Anti-thrombin peptide

<400> 9
Gly Phe Asn Pro Arg
1 5

<210> 10
<211> 5
<212> PRT
<213> Artificial Sequence

<220>
<223> Anti-thrombin peptide

<400> 10
Gly Pro Asn Pro Arg
1 5

<210> 11
<211> 5
<212> PRT
<213> Artificial Sequence

<220>
<223> Anti-thrombin peptide

<400> 11
Gly Phe Ser Ala Arg
1 5

<210> 12
<211> 13
<212> PRT
<213> Artificial Sequence

<220>
<223> Anti-thrombin peptide

<220>
<221> MOD_RES
<222> (13)...(13)
<223> Xaa = HomoSerine Lactone

<400> 12
Gly Asp Tyr Glu Glu Ile Pro Glu Glu Tyr Leu Gln Xaa
1 5 10

<210> 13
<211> 13
<212> PRT
<213> Artificial Sequence

<220>
<223> Anti-thrombin peptide

<220>
<221> MOD_RES
<222> (13)...(13)
<223> Xaa = HomoSerine Lactone

<400> 13
Gly Asp Leu Glu Glu Ile Pro Glu Glu Tyr Leu Gln Xaa
1 5 10

<210> 14
<211> 12
<212> PRT
<213> Artificial Sequence

<220>
<223> Anti-thrombin peptide

<400> 14
Gly Asp Gly Glu Glu Ile Pro Glu Glu Tyr Leu Gln
1 5 10

<210> 15
<211> 11
<212> PRT
<213> Artificial Sequence

<220>
<223> Anti-thrombin peptide

<220>
<221> ACETYLATION
<222> (1)...(1)

<400> 15
Asp Phe Glu Glu Ile Pro Glu Glu Tyr Leu Gln
1 5 10

<210> 16
<211> 35
<212> PRT
<213> Artificial Sequence

<220>
<223> six Anti-thrombin peptides in tandem

<400> 16
Gly Leu Asp Pro Arg Met Gly Val Asp Pro Arg Met Gly Phe Asn Pro
1 5 10 15
Arg Met Gly Pro Asn Pro Arg Met Gly Phe Ser Ala Arg Met Gly Val
20 25 30
Ser Pro Arg
35

<210> 17
<211> 4
<212> PRT
<213> Artificial Sequence

<220>
<223> Anti-thrombin peptide

<400> 17
Phe Asp Pro Arg
1

<210> 18
<211> 18
<212> PRT
<213> Artificial Sequence

<220>
<223> Anti-thrombin peptide

<400> 18
Pro Gln Ser His Asn Asp Gly Asp Phe Glu Glu Ile Pro Glu Glu Tyr
1 5 10 15
Leu Gln

<210> 19
<211> 12
<212> PRT
<213> Artificial Sequence

<220>
<223> Anti-thrombin peptide

<400> 19
Gly Asp Phe Glu Glu Ile Pro Glu Glu Tyr Leu Gln
1 5 10

<210> 20
<211> 22
<212> PRT
<213> Artificial Sequence

<220>
<223> Anti-thrombin peptide

<400> 20
Phe Asp Pro Arg Pro Gln Ser His Asn Asp Gly Asp Phe Glu Glu Ile
1 5 10 15
Pro Glu Glu Tyr Leu Gln
20